Nuclear mTOR in mouse embryonic stem cell pluripotency regulation

Inaugural-Dissertation
to obtain the academic degree
Doctor rerum naturalium - Dr. rer. nat.

submitted to
the Department of Biology, Chemistry, Pharmacy of
Freie Universität Berlin

by
Chieh-Yu Cheng
Berlin, 2023

The work was carried out under the supervision of Dr. Aydan Bulut-Karslioglu at the Max Planck Institute for Molecular Genetics in Berlin between 07/2019 and 06/2023.

1st Reviewer:
Dr. Aydan Bulut-Karslioglu
Department of Genome Regulation, Max Planck Institute for Molecular Genetics

2nd Reviewer:
Prof. Dr. Volker Haucke
Leibniz-Forschungsinstitut für Molekulare Pharmakologie
Department of Biology, Chemistry, Pharmacy, Freie Universität Berlin

Date of defence: 14. February 2024

Declaration of Independence

Herewith, I certify that I have prepared and written my thesis independently and that I have not used any sources and aids other than those indicated by me.
This dissertation has not yet been presented to any other examination authority in the same or a similar form and has not yet been published.

Summary

Pluripotency, where cells have the capacity to differentiate into all types of cells in the embryo, is a transient state in early embryonic development. Normally, it lasts for 2-3 days, but many animal species can undergo diapause to halt the development and retain pluripotency under unfavourable conditions. One way to induce the paused state is through inhibition of mechanistic target of rapamycin (mTOR). mTOR is a protein kinase that plays a central role in regulating cellular processes such as growth, metabolism, and autophagy with environmental inputs. Mouse embryos lacking mTOR failed to develop beyond the blastocyst stage. Overall, these indicate that mTOR plays a vital role in pluripotency regulation. However, the mechanisms remain unknown.

In this study, I established and applied various biochemical, genetic and NGS technologies to investigate the role of nuclear mTOR in embryonic stem cells (mESCs). mTOR kinase activity was found to be essential for mESC differentiation and mTOR nuclear and chromatin localisation were observed. ChIP-seq experiments revealed that mTOR associates with the promoters of developmental genes at the chromatin in mESCs. *In vitro* kinase assay showed that mTOR is a histone H2A kinase, phosphorylating H2A at threonine 120 (H2AT120ph). Using integrative analyses of CUT&Tag and TT-SLAM-seq, I found that the level of H2AT120ph at mTOR-associated promoters and their nascent transcription transiently increases during pluripotency exit. These promoters had a high presence of polycomb repressive complex 1 (PRC1) and correlated with the polycomb histone marks, suggesting mTOR works closely with PRC to regulate gene expression.

The results reveal a novel mechanism through which mTOR can regulate gene expression and may have implications in other developmental and disease contexts.

Zusammenfassung

Die Pluripotenz, bei der Zellen die Fähigkeit haben, sich in alle Zelltypen im Embryo zu differenzieren, ist ein vorübergehender Zustand in der frühembryonalen Entwicklung. Normalerweise dauert sie 2-3 Tage, aber viele Tierarten können eine Diapause durchlaufen, um die Entwicklung anzuhalten und die Pluripotenz unter ungünstigen Bedingungen aufrechtzuerhalten. Eine Möglichkeit, diesen pausierten Zustand herbeizuführen, ist die Hemmung des mechanistic target of rapamycin (mTOR). mTOR ist eine Proteinkinase, die eine zentrale Rolle bei der Regulation von zellulären Prozessen wie Wachstum, Stoffwechsel und Autophagie unter Einfluss von Umweltbedingungen spielt. Mäuseembryonen ohne mTOR entwickeln sich nicht über das Blastozystenstadium hinaus. Dies deutet insgesamt darauf hin, dass mTOR eine wichtige Rolle bei der Regulation der Pluripotenz spielt. Die genauen Mechanismen bleiben jedoch unbekannt.

In dieser Studie habe ich verschiedene biochemische, genetische und NGS-Technologien etabliert und angewendet, um die Rolle von nukleärem mTOR in embryonalen Stammzellen (mESCs) zu untersuchen. Es stellte sich heraus, dass die Kinaseaktivität von mTOR für die Differenzierung von mESCs essentiell ist und mTOR eine nukleäre und chromatinale Lokalisation aufweist. ChIP-seq-Experimente ergaben, dass mTOR mit den Promotoren von Entwicklungs-Genen am Chromatin in mESCs assoziiert ist. In einem In-vitro-Kinase-Assay wurde festgestellt, dass mTOR eine Histone H2A-Kinase ist, die H2A am Threonin 120 phosphoryliert (H2AT120ph). Durch die Integration von CUT&Tag- und TT-SLAM-seq-Analysen konnte ich feststellen, dass der H2AT120ph-Spiegel an den mTOR-assoziierten Promotoren und ihrer neu synthetisierten Transkription während des Austritts aus der Pluripotenz vorübergehend ansteigt. Diese Promotoren wiesen eine hohe Präsenz des Polycomb-Repressive Complex 1 (PRC1) auf und korrelierten mit den Polycomb-Histonmarkierungen, was darauf hindeutet, dass mTOR eng mit PRC zusammenarbeitet, um die Genexpression zu regulieren.

Die Ergebnisse enthüllen einen neuen Mechanismus, durch den mTOR die Genexpression regulieren kann, und könnten Auswirkungen auf andere Entwicklungs- und Krankheitszusammenhänge haben.

Contents

1. Introduction

1.1. Pluripotency - a transient state in early embryonic development

Pluripotency is a state of cells that has great significance and promise in the field of developmental and regenerative biology. Pluripotent cells are characterised by 2 key features, the capacity to give rise to all cell types found in an adult animal and the ability to self-renew indefinitely. This unique state is transient and occurs during early embryonic development[1]. Shortly after fertilisation, the zygote, a totipotent single cell, initiates a series of rapid mitotic divisions, leading to the formation of morula at approximately embryonic day 3 (E3) in mouse development. Subsequently, the first cell fate decision takes place, leading to the formation of a pre-implantation blastocyst. The blastocyst comprises two distinct cell populations: the outer trophectoderm (TE) cells, which will ultimately contribute to the development of the placenta, and the inner cell mass (ICM), which harbours the pluripotent cells. Of note, totipotent cells and pluripotent cells are different in their developmental potential. While pluripotent cells possess the capacity to generate all cell types within the adult organism, totipotent cells exhibit an even greater potential by having the ability to give rise to extraembryonic tissues. As development continues, the ICM undergoes further segregation, differentiating into the pluripotent epiblast stem cells and the primitive endoderm. The primitive endoderm subsequently contributes to the development of the extraembryonic endoderm, while the pluripotent epiblast stem cells maintain their pluripotent state (**Fig. 1**)[2]. The blastocyst then implants into the uterus at around E4.5-E5 and enters gastrulation at about E6.5. During gastrulation, the pluripotent epiblast undergoes extensive differentiation, ultimately giving rise to the three germ layers — endoderm, mesoderm, and ectoderm — accompanied by the gradual loss of pluripotency[3].

Pluripotency can be effectively modelled in vitro by culturing pluripotent stem cells (PSCs) using specific culturing conditions. These PSCs can be obtained either directly from embryos as embryonic stem cells (ESCs) or through the reprogramming of somatic cells into induced pluripotent stem cells (iPSCs)[4,5]. A wide range of PSCs derived from mice representing different pluripotent states have been reported and have provided insights into the mechanism of pluripotency regulation. They can be

categorised into 2 main pluripotent states, naive and primed, corresponding to the pre- and post- implantation mouse embryos.

Mouse embryonic stem cells (mESCs) were first derived from the ICM of pre-implantation mouse embryos and traditionally cultured in media supplemented with serum and feeder cells. These mESCs fully demonstrate all functional assays of pluripotency, including differentiation into all three germ layers in vitro, teratoma formation in vivo, chimaera formation upon blastocyst injection and tetraploid complementation. It is considered to be in the “naive” pluripotent state[6–10]. On the other hand, PSCs can also be derived from the epiblast of post-implantation mouse embryos known as epiblast stem cells (EpiSCs)[11,12].

The EpiSCs possess the ability to differentiate into all three germ layers in vitro. Unlike mESCs, EpiSCs have a limited capacity for chimaera formation. EpiSCs can contribute to chimeric animals upon injection into post-implantation epiblasts. However when EpiSCs were injected into pre-implantation epiblast, chimeric animals rarely form. This distinction suggests that EpiSCs are at a more developmentally advanced state and thus EpiSCs are considered to be in the "primed" state of pluripotency[13,14]. These distinct PSC models are useful tools to investigate the mechanisms underlying pluripotency and its regulation during different stages of embryonic development.

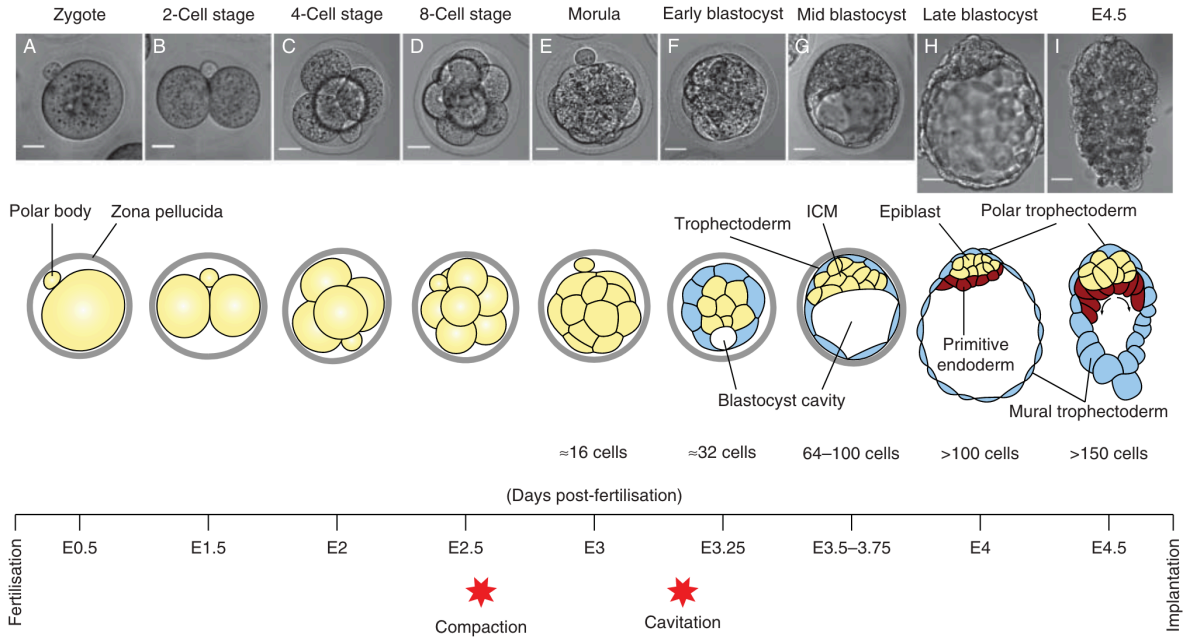

Figure 1 | Mouse pre-implantation development[2]**.** The top panel shows the bright field microscopy images of mouse embryos at the indicated stages. The middle panel shows cartoon illustrations of the embryo structure of the corresponding stages. The bottom panel shows a timeline indicating embryonic days (E). ICM, inner cell mass. Timeline not to scale. Scale bars: 20 μm.

1.2. Naive pluripotency *in vitro* - serum/LIF and 2i mESCs

As *in vivo* pluripotency is a transient state, indefinite self-renewal is not an inherent feature. Therefore, it is necessary to develop specialised culture conditions to maintain indefinite pluripotency *in vitro*.

The core pluripotency transcription factors (TFs) OCT4 (also known as POU5F1), SOX2 and NANOG co-occupy hundreds of genomic loci to integrate external signals and regulate pluripotent state[15,16]. However, OCT4 and SOX2 also activate the expression of FGF4, which acts as an autocrine factor promoting differentiation. FGF4 feeds back through the MEK/ERK signalling pathway to promote differentiation and lineage commitment[17,18]. In order to maintain indefinite pluripotency in vitro, special culture conditions are needed to counteract the spontaneous differentiation propensity of the mESCs. Conventionally, the most common way to culture naive mESCs is to supply leukaemia inhibitory factor (LIF) and bone morphogenetic protein 4 (BMP4) in the form of serum to the culture, hence the name serum/LIF[6,7]. Mechanistically, LIF leads to the activation of a TF, STAT3, through a series of signalling transduction[19]. Downstream targets of STAT3 include *Klf4* and *Tfcp2l1* which eventually promote mESC self-renewal[20,21]. BMP4 activates the transcription factor, SMAD, to induce the expression of Inhibitor of Differentiation genes preventing differentiation[22]. Later study reveals that naive mESCs can also be cultured in the presence of 2 small molecule inhibitors (2i), the MEK inhibitor PD0325901 and GSK3 inhibitor CHIR99021[23]. PD0325901 counteracts the FGF4 signalling pathway by inhibiting FGF4 downstream target MEK. Inhibition of the MEK/ERK signalling pathway suppresses differentiation. On the other hand, CHIR99021 reinforces the pluripotency gene network by activation of the WNT signalling pathway[24].

mESCs cultured in both serum/LIF and 2i conditions are naive pluripotent cells as they are able to contribute to chimaera animals when injected into the ICM of a blastocyst. However, key differences between the 2 cell lines indicate that they are in different pluripotent states. Morphologically, the serum/LIF mESCs culture is composed of heterogeneous colonies compared to the uniform 2i culture. Single-cell RNA-seq study reveals that indeed there are 2 subpopulations of cells under serum/LIF culture. One has a transcriptome similar to the ICM, while the other resembles a more mature epiblast[25]. Other differences at the transcriptome level

include that serum/LIF mESCs exhibit mosaic expression of pluripotency factors, such as Nanog and Rex1, and show higher levels of lineage priming[26–29]. In addition, serum/LIF mESCs show higher levels of DNA methylation, repressive histone mark H3K27me3 at developmental genes and RNA polymerase pausing[29]. Therefore, 2i mESCs are considered to be at the “ground” state of pluripotency, while serum/LIF mESCs are at a metastable, sometimes referred to as “confused”, state of pluripotency (**Fig. 2**)[30].

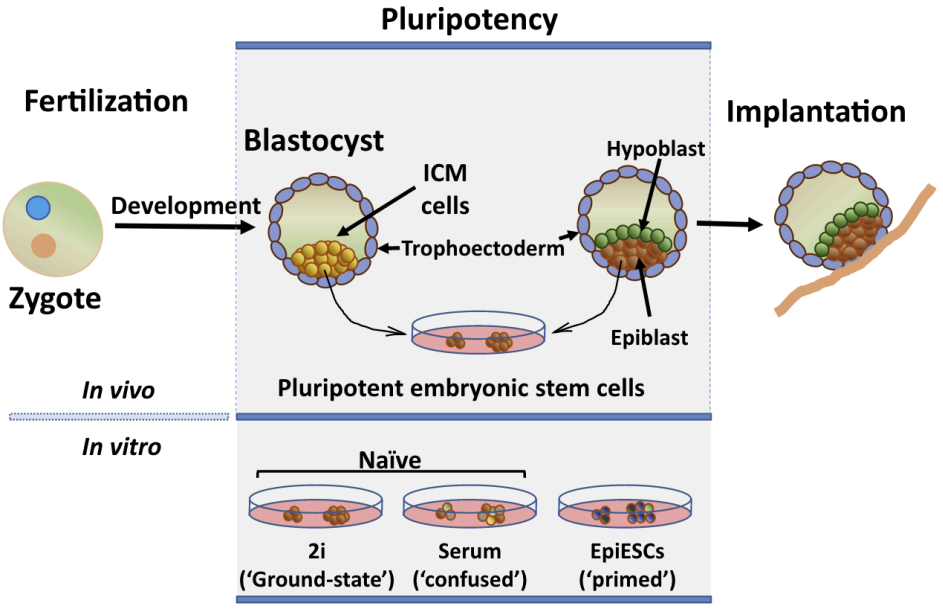

Figure 2 | Illustration showing *in vitro* mESCs and their corresponding *in vivo* stages[30].

1.3. Polycomb repressive system - a key gene repressive mechanism during development

To ensure proper development of multicellular organisms, gene expression is tightly controlled during development. Among complex layers of transcription regulation, the state of chromatin and histone modification are known to play a crucial role. The Polycomb repressive system represents an important gene repressive mechanism during development[31,32]. Polycomb group (PcG) proteins were initially discovered in Drosophila melanogaster. Mammalian orthologous counterparts have later been discovered. The PcG proteins form 2 multiprotein complexes, Polycomb repressive complex 1 and 2 (PRC1 and PRC2), to regulate gene expression by depositing repressive histone modifications, monoubiquitylation of histone H2A at K119 (H2AK119ub) and trimethylation of histone H3 at lysine 27 (H3K27me3) respectively (**Fig. 3**). Polycomb repressive complexes have been extensively studied. However, the mechanisms by which they affect transcriptional repression remain unclear[31,32].

PRC1 is an E3 ubiquitin ligase, catalysing H2AK119ub[33,34]. The catalytic core of PRC1 consists of RING1B or RING1A and one of six Polycomb group RING finger (PCGF1-6) proteins. Through their RING domains, RING1 and PCGF proteins form dimers[35,36]. The specific PCGF component determines the incorporation of auxiliary subunits into PRC1 complexes. These complexes are classified as canonical PRC1 (cPRC1) or variant PRC1 (vPRC1)[37,38]. cPRC1 complexes are formed around PCGF2/4 and consist of one of the chromobox proteins (CBX2/4/7/8), along with a Polyhomeotic subunit (PHC1/2/3)[37,39]. On the other hand, vPRC can assemble around any of the six PCGF proteins (PCGF1–6) and include RING1 and YY1-binding protein (RYBP) or its paralogue YAF2, along with additional subunits that vary depending on the specific PCGF component present in the complex (**Fig. 3**)[38,40]. PRC1 is highly dynamic and only a small fraction binds stably to chromatin[41]. Notably, vPRC1 exhibits significantly higher catalytic activity than cPRC1 and contributes to most H2AK119ub *in vivo*[42,43].

PRC2 consists of four core proteins: EZH1/2, EED, SUZ12, and RBBP4/7[44,45]. The assembly of this core complex is essential for the catalytic function of PRC2. Structural studies have provided details on the mechanism by which PRC2 catalyses H3K27me3. PRC2 can be divided into two functional lobes: the catalytic lobe and the regulatory lobe[31,32]. In the catalytic lobe, the interaction between EZH1/2, EED, and

SUZ12 relieves the autoinhibition of EZH1/2 and activates its methyltransferase activity[46,47]. EZH1/2 also interacts with the N-terminal tail of H3 and facilitates the deposition of methyl groups at lysine 27. In the regulatory lobe, different auxiliary subunits are incorporated and define different variants of PRC2. PRC2.1 complexes contain a PCL protein (PCL1/2/3) and PALI1/2 or EPOP[48,49]. On the other hand, PRC2.2 complexes contain JARID2 and AEBP2[50]. These subunits are known to affect PRC2 methyltransferase activity.

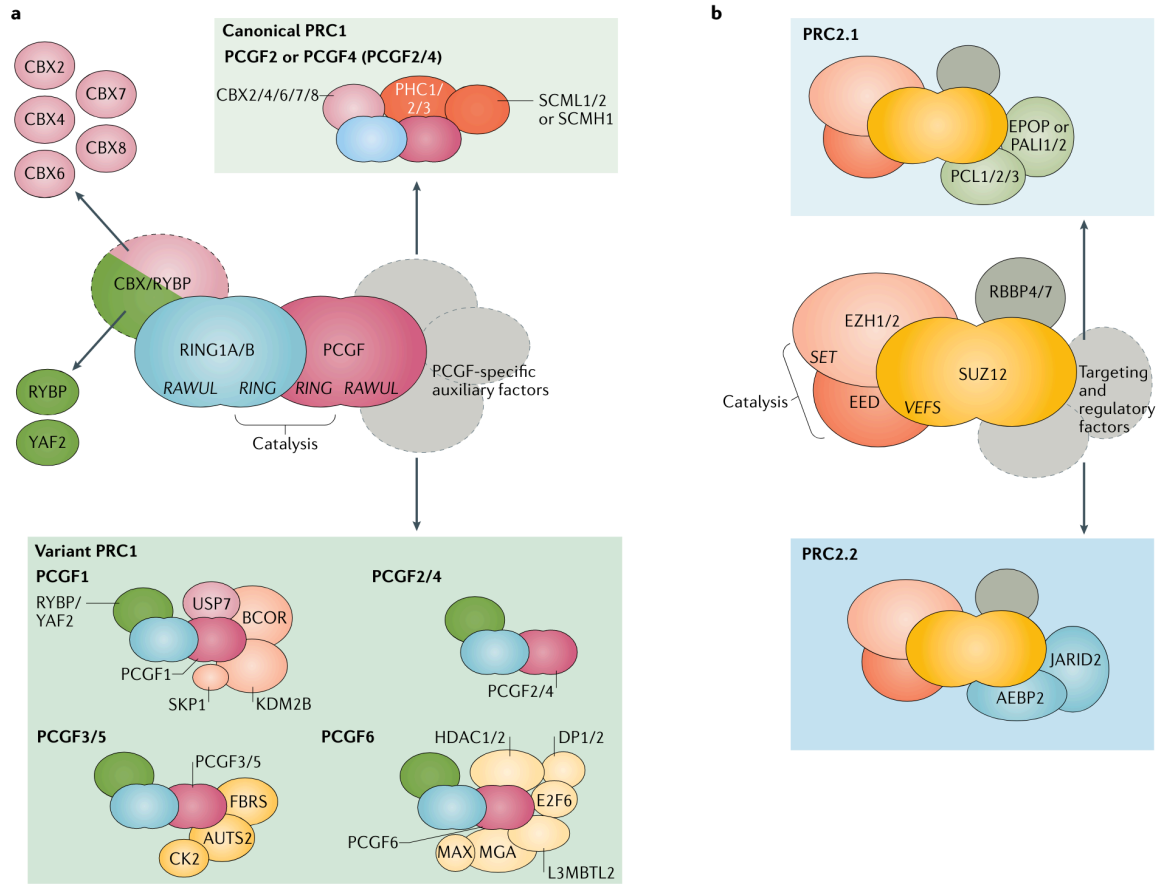

Figure 3 | Schematic overview of protein compositions of PRC1 and PRC2[31]**. a.** The core of PRC1 is a dimer composed of RING1A/B and one of PGCF proteins. Other auxiliary protein subunits defining canonical and variant PRC1 are depicted. **b.** The core proteins of PRC2 are SUZ12, EZH1/2 and EED. Other auxiliary protein subunits giving rise to PRC2.1 and PRC2.2 are shown.

1.4. Prolonged pluripotency by mTOR inhibition

More than 130 mammalian species are known to use embryonic diapause to adjust the proper timing of the birth of the offspring[51,52]. In mammals, embryonic diapause usually happens in pre-implantation blastocysts with a few exceptions like cows, where gastrulation begins before implantation[53,54]. Diapause embryos are characterised by minimal cell proliferation, reduced metabolism, and delayed development. Importantly, diapause embryos preserve the full capacity to develop into healthy animals once reactivated[52]. Diapause is either obligate (also known as seasonal) or facultative (also known as lactational)[55,56]. In obligate diapause, developmental suspension is induced in every gestation to synchronise the birth and favourable environmental conditions. For example, the embryos of the American mink (*Neovison vison*) undergo diapause during the mating season and resume development once the daylight increases[52,55,57]. Facultative diapause is best studied in mice. Mouse blastocysts enter diapause in the presence of suckling young. The suckling causes an increase in prolactin and prevents the surge of oestrogen, causing the blastocysts to diapause[52]. Indeed, ovariectomy or injection of oestrogen antagonists at 3.5 days of pregnancy induces diapause[55,58].

Due to the prolonged pluripotency, diapaused mouse blastocyst provides a great opportunity to study pluripotency regulation. Several methods have been reported to induce a paused state in mouse blastocyst *ex vivo*, such as mTOR inhibition, Myc inhibition and microRNA let-7 overexpression. Among them, mTORi results in the longest pause (up to 22 days) followed by let-7 overexpression (up to 14 days), whereas Myc inhibition only marginally prolongs the survival to 24 hours[59–61]. Let-7 is upstream of mTOR and c-myc. Its overexpression leads to mTOR and Myc suppression[61]. The transcriptomes of the paused blastocysts induced by mTOR inhibition and let-7 overexpression resemble the one of *in vivo* diapause embryos[59,61]. Importantly, translation inhibition does not induce a pause state in mouse blastocyst[59]. This suggests that a global metabolic shutdown by mTOR inhibition is not sufficient to prolong pluripotency. Other mTOR functions are likely to be involved. Overall, this evidence suggests that mTOR is critical for pluripotency regulation but the full mechanisms remain unclear.

Like in blastocyst, mTOR inhibition also induces a paused pluripotent state in serum/LIF mESCs. The paused mESCs show reductions in cellular growth,

proliferation, metabolic rate, transcription and translation. The paused mESCs contribute to chimaera formation after being released from 7-day pausing, indicating that they remain fully pluripotent. The transcriptome of paused mESCs is also similar to the one of diapause epiblast[59]. The *in vitro* serum/LIF mESCs culture is a useful model as it provides relatively low material limitation and greater manipulation possibility.

1.5. mTOR functions in mESCs

1.5.1. Canonical mTOR functions in mammalian cells

mTOR coordinates cellular growth with the environmental inputs, such as nutrient levels and growth factors, in eukaryotic cells[62]. In mammals, mTOR is encoded by 1 gene, *MTOR*, and functions as the catalytic subunit of 2 distinct protein complexes, mTORC1 and mTORC2. The core components of mTORC1 are mTOR, Raptor and mLST8 while the core of mTORC2 is composed of mTOR, Rictor and mLST8 (**Fig. 4**)[63–66]. Structural study reveals that mTORC1 is rapamycin sensitive as the rapamycin-FKBP12 complex inhibits mTORC1 by narrowing the catalytic cleft and hindering substrate access[67]. In contrast, mTORC2 is insensitive to acute rapamycin treatment since rapamycin-FKBP12 is not part of the complex. Prolonged rapamycin treatment affects mTORC2 signalling by depleting available mTOR to form new mTORC2[68,69].

mTORC1 and mTORC2 regulate distinct downstream cellular processes (**Fig. 4**). mTORC1 primarily regulates protein, lipid, and nucleotide synthesis, autophagy, lysosome biogenesis and cell growth[62,70]. It promotes protein synthesis by phosphorylating S6K and 4EBP1, which in turn promotes mRNA translation initiation[71]. mTORC1 also suppresses catabolism by inhibiting autophagy via phosphorylation of ULK1 and transcription factor EB (TFEB)[72,73]. mTORC1 promotes *de novo* lipid synthesis through transcription factor sterol-responsive element-binding protein (SREBP)[74–76]. mTORC2 phosphorylates protein kinases (PKA, PKG, and PKC) to influence cytoskeletal remodelling and cell migration[77,78]. Another prominent role of mTORC2 is to promote cell survival and proliferation via activation of the AKT, a key effector of the insulin/PI3K signalling[79]. Activation of AKT leads to inhibition of FOXO1/3a, GSK3β and TSC2[80,81]. Additionally, mTORC2 regulates ion transport and cell survival via phosphorylation of SGK1[82].

Under pro-growth conditions, mTORC1 is activated to promote cell growth and metabolism, while unfavourable conditions trigger mTORC1 inhibition. A major regulator of mTORC1 is the Tuberous Sclerosis Complex (TSC), where various intracellular and environmental signals converge. TSC consists of TSC1, TSC2, and TBC1D7 and functions as a GTPase activating protein (GAP) for the small GTPase Rheb[83]. Since Rheb is a direct activator of mTORC1, TSC is thus a major negative regulator of mTOR[84–87]. mTORC1 is known to be a downstream mediator of several growth factors[62]. Multiple growth factor pathways activate mTORC1 through inhibition of the TSC. For example, the insulin/insulin-like growth factor-1 (IGF-1) pathway and receptor tyrosine kinase-dependent Ras signalling phosphorylate and inhibit TSC2. Other growth factor pathways, such as WNT and TNFα, activate mTORC1 by inhibiting TSC1[88,89].

Intracellular and environmental stress, such as low ATP levels, hypoxia, and DNA damage, trigger various signalling pathways that eventually inhibit mTORC1. During glucose deprivation, a decrease in cellular energy activates AMPK which inhibits mTORC1 by activation of TSC2. AMPK can also directly inhibit mTORC1 by phosphorylating Raptor[90,91]. In addition, mTORC1 can also be inhibited via an AMPK independent Rag GTPases pathway[92,93]. Hypoxia, also an unfavourable condition for cell growth, inhibits mTORC1 partly through AMPK activation and the induction of REDD1, a protein that activates TSC[94]. When DNA damage is detected, the DNA damage-response pathway activates p53 genes, including AMPK, PTEN, and TSC2 and therefore inhibits mTORC1 by enhancing TSC activity[95].

In addition to TSC, mTORC1 activity is affected by amino acid levels in lysosomes and cytosol. mTORC1 is recruited to the lysosomal membrane by the Regulator-Rag complex when the amino acids are abundant[96,97]. In the cytosol, activation of mTORC1 by leucine and arginine is well characterised. Leucine and arginine bind to their cytosolic sensor, Sestrin2 and CASTOR1, respectively[98–100]. The binding triggers the de-inhibition of an mTORC1 activator, GATOR2. Emerging evidence also shows other mechanisms through which amino acids regulate mTORC1 activity[101,102].

Compared to the extensively characterised mTORC1, mTORC2 is mainly known to be activated via the insulin/PI3K pathway and controls proliferation and survival[62]. It is also regulated by mTORC1. Downstream targets of mTORC1, such as GRB10 and S6K1, have been reported to negatively affect AKT and IRS1, upstream of mTORC2 (**Fig 4b**)[103–105].

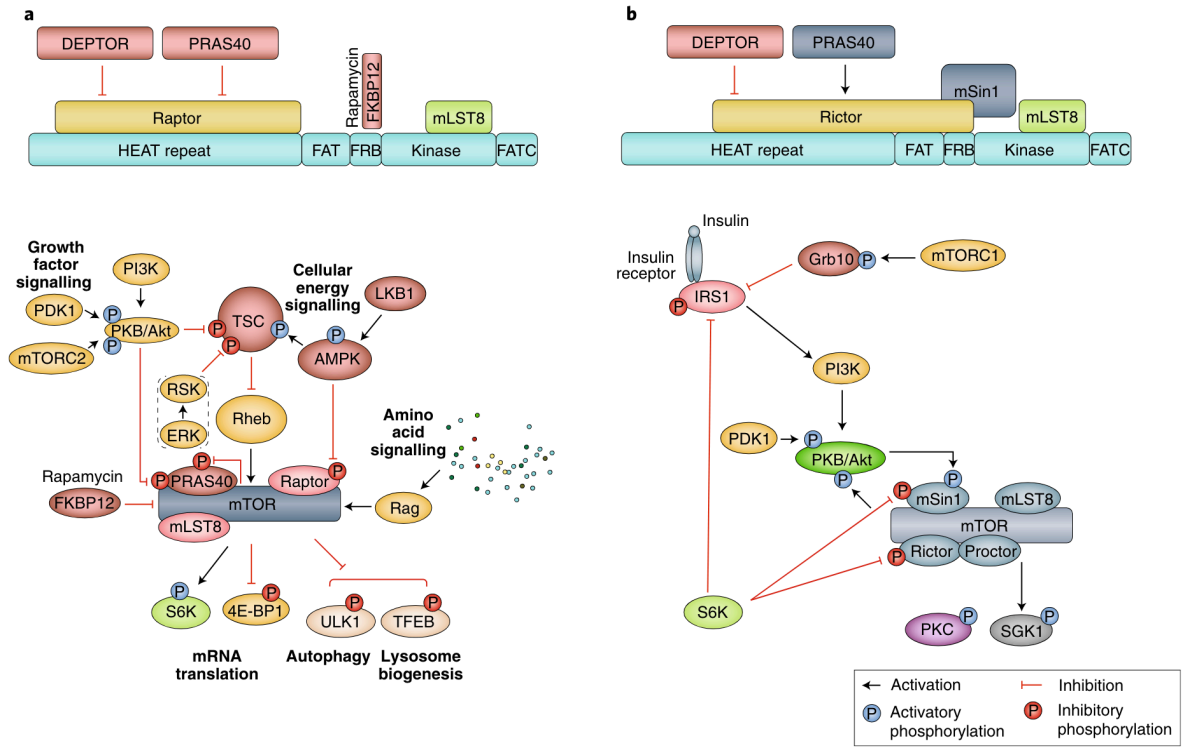

Figure 4 | Protein compositions and canonical signalling pathways of mTORC1 and mTORC2[70]**. a-b.** Major protein compositions and signalling pathways of mTORC1 (**a**) and mTORC2 (**b**). Different domains of mTOR are depicted in green boxes.

1.5.2. Direct involvement of nuclear mTOR in transcription

In addition to modulating the gene expression via phosphorylating downstream targets in the cytoplasm as described above, emerging evidence also shows that mTOR can affect gene expression directly as a transcription cofactor in the nucleus[106]. The presence of mTOR in the nucleus has been documented in several healthy and malignant mammalian cells, such as human primary fibroblasts, thyroid carcinomas, breast cancer, oral squamous cell carcinoma, prostate cancer cell lines, mouse myoblasts, and mouse liver[107–111]. Studies using chromatin immunoprecipitation (ChIP) show that mTOR locates at the promoters of RNA polymerase I- and III-transcribed genes and regulates their gene expression in different cell lines[112–115]. Importantly, mTOR occupancy is not always rapamycin sensitive, suggesting that different mTOR complexes or mechanisms are involved. Nuclear mTOR has been found to regulate mitochondrial gene expression and oxygen consumption in muscle cells[116]. Here, mTOR forms a complex with Raptor, transcription factor YY1, and the coactivator PGC-1α within the nucleus of muscle cells. Rapamycin treatment disrupts the complex and YY1 target gene transcription. Furthermore, mTOR can also directly influence gene expression by affecting the transcription machinery. mTOR can phosphorylate transcription coactivator p300 to prevent p300 self inhibition and results in suppression of cell-starvation-induced autophagy and activation of cell lipogenesis[117]. Overall, these demonstrate that mTOR can directly link metabolism with transcriptional control.

Genome-wide analyses allow researchers to study mTOR at a global scale in a relatively unbiased way. Using ChIP-seq to investigate mTOR chromatin targets in mouse liver and human prostate cancer cell lines, researchers report that mTOR target genes are enriched for genes encoding proteins relevant to mTOR signalling and biological functions[118,119]. In mouse liver, mTOR target genes are enriched for the TCA cycle and lipid metabolism and the mTOR binding at the chromatin is rapamycin sensitive. mTOR shares lots of target genes with the metabolic regulator ERRα, which itself is a downstream target of mTOR[119]. In androgen receptor (AR) positive prostate cancer cell lines, AR reprograms the mTOR chromatin binding profile to induce aerobic glycolysis and mitochondrial respiration. In AR negative prostate cancer cell line, mTOR controls metabolic gene transcription in an AR

independent manner. Clinically, nuclear mTOR activity correlates with prostate cancer progression and poor prognosis[118].

The involvement of nuclear mTOR in gene expression raises intriguing questions regarding its nuclear translocation and regulation. Studies have indicated that the L545A/L547A mutation hampers the nuclear import of mTOR, potentially regulated by a nucleocytoplasmic shuttling signal[120]. Additionally, mTOR has been observed to translocate to the nucleus along with other proteins, such as AR[118]. However, the precise mechanisms and regulatory factors governing mTOR's nuclear localisation remain elusive. Another important aspect to explore is the identification of interaction partners of nuclear mTOR and the potential formation of complexes beyond mTORC1 and mTORC2. Furthermore, it is yet to be determined whether mTOR directly binds to DNA, as current de novo DNA motif analyses have not found a DNA binding motif for mTOR[118,119]. Further investigations are needed to unravel these aspects and deepen the understanding of the complex role of nuclear mTOR in gene regulation.

1.5.3. mTOR in early mouse development

The crucial role of mTOR in mouse embryogenesis is well-documented, as evidenced by the peri-implantation lethality observed in mTOR$^{-/-}$ mouse embryos[121,122]. Further studies utilising knockouts of different subunits of mTORC1 and mTORC2 have shed light on the specific contributions of these complexes during different developmental stages. For instance, embryos lacking Raptor, an essential component of mTORC1, exhibit a similar phenotype to mTOR$^{-/-}$ embryos, characterised by proliferation arrest and peri-implantation lethality[80]. On the other hand, Rictor$^{-/-}$ embryos survive until a later stage, with growth arrest becoming apparent around E9.5 and eventually die at approximately E10.5-E11.5[123]. These findings suggest that mTORC1 plays a critical role in early embryonic development and the regulation of pluripotency.

It is worth noting that studies targeting individual downstream targets of mTORC1 do not consistently report the same detrimental effects on embryos as observed in mTOR$^{-/-}$ embryos. S6K1/2 double knockout mice display a reduction in viability due to perinatal lethality[124]. Mice lacking 4E-BP1 and 4E-BP2 are viable but exhibit increased sensitivity to diet-induced obesity and insulin resistance[125]. These observations underscore the complex nature of mTOR signalling and highlight the

need for a deeper understanding of the interplay and contributions of specific pathways within the mTOR network. Furthermore, it remains unclear whether mTOR can function independently of its association with mTORC1 in early embryogenesis.
In mESCs, differentiation induced by LIF withdrawal activates the mTOR signalling pathway through the MEK/ERK/TSC2 pathway[126]. Consistent with this, the level of DEPTOR, a negative regulator of mTOR signalling, decreases during differentiation[127].

1.6. Aims of the study

In this study, I aimed to investigate the nuclear functions of mTOR in mESC. First, mTOR localisation and whether mESCs can differentiate without mTOR kinase activity were tested. Once the essential role of mTOR in pluripotency had been established, I aimed to generate an mTOR degron mESC line using the dTAG system. Genetic manipulation should overcome the potential off target effects caused by small molecule mTOR inhibitors. Long term mTOR depletion is lethal to mESC and likely to cause many secondary effects. The mTOR degron cell line would provide the system to study cellular responses upon acute mTOR depletion. It also potentially paved the way to further generate a nuclear specific mTOR knockout mESCs.
Secondly, I applied a genome-wide approach, ChIP-seq, to study mTOR chromatin targets in mESCs.
Thirdly, the nuclear localisation of mTOR also led me to search for its nuclear substrates. Radioactive and non-radioactive *in vitro* mTOR kinase assay was used to address this question.
Lastly, CUT&Tag, TT-SLAM-seq and integrative computational analyses were used to study the potential interplays and crosstalks between mTOR, H2AT120ph, the Polycomb repressive complexes and the Polycomb chromatin marks in mESC differentiation. TT-SLAM-seq was a collaboration with Dr. Henri Niskanen, a postdoctoral researcher from the Hniz lab at the Max Planck Institute of Molecular Genetics. The integrative computational analyses were in collaboration with Persia Akbari Omgba, a bioinformatic doctoral candidate in the lab. Detailed contributions are listed in the Materials and Methods section.

2. Results

2.1. The essential role of mTOR kinase activity in mESC pluripotency exit

2.1.1. Generation of FKBP^{F36V}-mTOR degron mESC cell lines

The cells isolated from the ICM of mTOR$^{-/-}$ blastocysts fail to proliferate when cultured in vitro, suggesting the crucial roles of mTOR[121,122]. As mTOR is known to be a master metabolism regulator, prolonged and systematic mTOR depletion is anticipated to cause secondary effects in the cells, which makes it difficult to decipher the functions of mTOR in mESCs. To overcome such difficulty, an mTOR degron mESC cell line, FKBP^{F36V}-mTOR mESC, was established using the dTAG system[128,129]. The degron system is a technique used to achieve a rapid, specific, and conditional degradation of target proteins in cells. It involves the fusion of a specific protein domain, the so-called degron, to the protein of interest. Depending on the property of the degron, the conditional and reversible protein degradation can be induced in several ways, for example, changes in temperature, addition of small molecules, exposure to light or the expression level of other proteins[128,130–133]. Due to its rapid induction and reversibility, the degron system is much more versatile and flexible compared to the methods that perturb protein expression at the DNA or mRNA levels. Among established degron methods, the dTAG system has been successfully demonstrated for use in mammalian cells[128]. The degron in this system is a mutant version of the FKBP12 protein, FKBP^{F36V}. FKBP^{F36V} is featured by its ability to be selectively recognised by a heterobifunctional small molecule, dTAG13. The dimerisation of the FKBP^{F36V}-tagged protein of interest and CRBN E3 ligase complex by dTAG-13 eventually leads to the degradation of the protein through the proteasomal pathway[128].

To establish an FKBP^{F36V}-mTOR mESC cell line, a gene cassette containing degradation-sensitive FKBP^{F36V} was knocked in to the N-terminus of the endogenous mTOR allele using the CRISPR-PITCh system[128,134] (**Fig. 5a**). The knock-in cassette also contained the puromycin resistant gene which enabled selection of positive knock-in cells. The CRISPR-PITCh differs from other CRISPR/Cas9 gene editing approaches in that it is assisted by microhomology-mediated end-joining, which

requires a very short homologous sequence (5-25 bp) for double strand break repair[134].

The genotype of individual mESC clones was verified using allele specific PCR and Sanger sequencing (**Fig. 5b**). Next, the FKBP^{F36V}-mTOR cell line was then subjected to functional characterisation to assess mTOR degradation upon dTAG-13 treatment. The FKBP^{F36V}-mTOR mESCs were treated by dTAG-13 for various lengths of time and the proteins were extracted for western blot analysis. Despite the correct genomic sequences, the homozygous FKBP^{F36V}-mTOR mESC cell line did not exhibit mTOR degradation after up to 6 hours dTAG-13 treatment (**Fig. 5c**). Further investigation using both heterozygous and homozygous FKBP^{F36V}-mTOR mESC cell lines revealed that the FKBP^{F36V}-mTOR was susceptible to degradation under dTAG-13 treatment in the heterozygous cell line, while minimal or no degradation was observed in the homozygous line (**Fig. 5d**). This suggested that when properly expressed, FKBP^{F36V}-mTOR was degradable under dTAG-13 treatment. However, for unknown reasons, the homozygous FKBP^{F36V}-mTOR mESC line was able to express mTOR without the degradation-sensitive FKBP^{F36V} tag, as evidenced by the western blot analysis detecting the HA-tag (**Fig. 5d**). To test the potential impact of insertion position on degradation, efforts were made to knock in a similar degradation-sensitive FKBP^{F36V} cassette at the C-terminus of mTOR. However, no positive cell line was established. This could be due to the detrimental effects of inserting a protein tag at the C-terminus of mTOR, where the catalytic domain is located. Additionally, the efficiency of the gRNA may have also contributed to the lack of positive clones. At this point, it was concluded that establishing an mTOR degron mESC cell line using the dTAG system was not feasible under the current technical and experimental conditions.

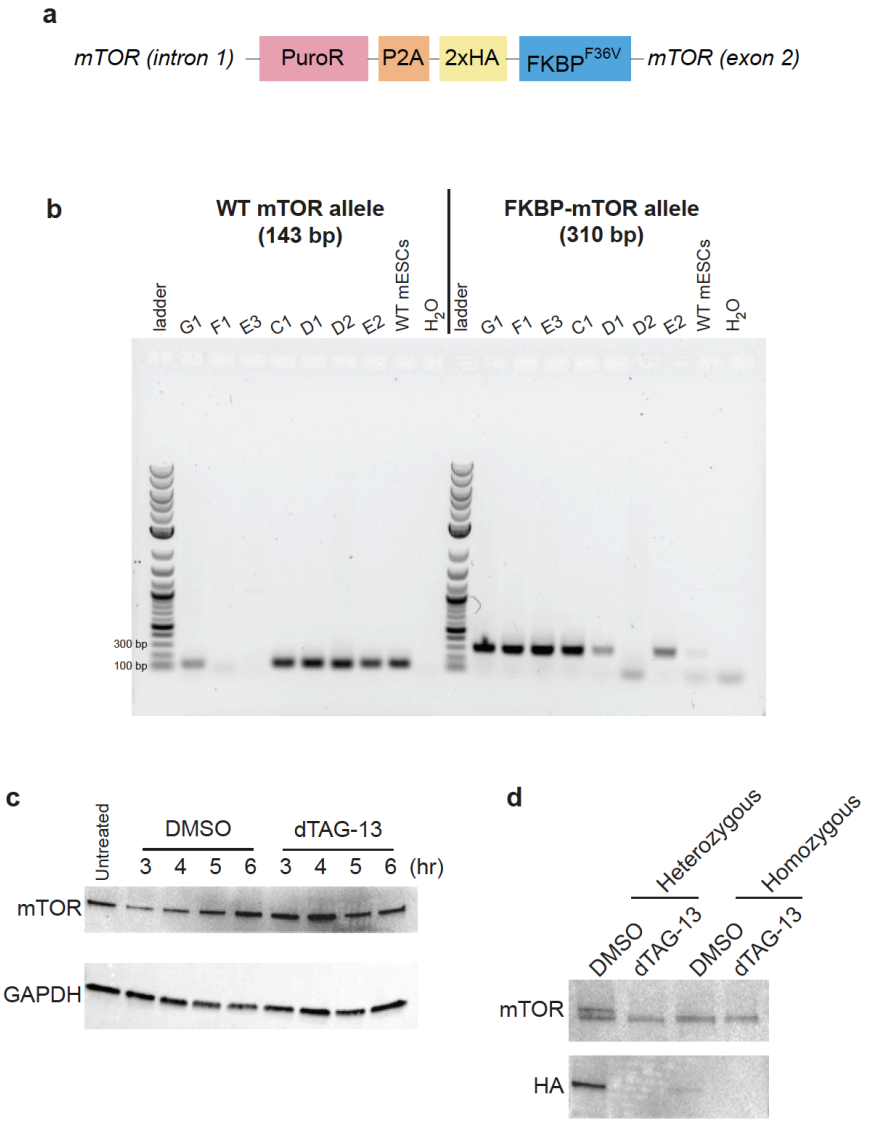

Figure 5 | Characterisation of FKBP^{F36V}-mTOR degron mESC cell lines. a. Schematic overview of the endogenous FKBP^{F36V}-mTOR allele. Gene size not drawn to scale. PuroR: puromycin resistant gene. **b**. Agarose gel showing the results of allele specific PCR. **c**. Western blot of a homozygous FKBP-mTOR mESC line treated with DMSO or dTAG-13 for the indicated times. GAPDH was used as a loading control. **d**. Western blot of heterozygous and homozygous FKBP^{F36V}-mTOR mESC lines treated with DMSO or dTAG-13 for 3 hours.

2.1.2. mTOR nuclear and chromatin localisation in mESCs

The paused state induced by the treatment of mTOR inhibitors in mESCs is reversible. The cells return to the previous active state shortly after the mTORi is removed[59]. However, it remained unclear whether mESCs were able to react to differentiation signals in the absence of mTOR activity. As described above, the attempt to generate an mTOR degron mESC cell line was not successful. An alternative strategy was employed. The activity of mTOR was inhibited by treating mESCs with the catalytic mTOR inhibitor, INK-128, and differentiation was induced by the removal of LIF. The results revealed that the mESCs demonstrated a massive amount of cell death within 48 hours of differentiation under INK-128 treatment. As indicated by the results of alkaline phosphatase staining, the surviving colonies remained pluripotent (**Fig. 6a**). Notably, mESCs treated with allosteric mTORi, rapamycin, or the translation inhibitor, cycloheximide, did not exhibit cell death and showed unhindered differentiation ability compared to control cells treated with DMSO (**Fig. 6b, c**). Overall, these results suggested that mTOR kinase activity is essential for mESCs to respond to differentiation signals and the failure to achieve this is not only attributed to the general metabolic shutdown. This also implies that mTOR likely regulates mESC pluripotency through functions beyond its role in moderating metabolism. To study these potential functions, an investigation into the subcellular localisation of mTOR during mESC differentiation was conducted. Proteins from the cytoplasmic, nuclear and chromatin fractions were extracted from differentiating mESCs at various time points up to 24 hours and subjected to western blot analysis. The signals of mTOR were detected within all three cytoplasmic, nuclear, and chromatin fractions of mESCs within the initial 24 hours of differentiation. The absence of H2A signals in the cytoplasmic and nuclear fractions served as an indicator of the purity of the fractionation preparation (**Fig. 7**).

Previous studies have shown that chromatin-associated mTOR plays a role in the regulation of gene expression[116,118,119]. The identification of mTOR presence within the chromatin of mESCs prompted the hypothesis that mTOR might exert its regulatory influence on pluripotency through interactions with specific genes. In order to study mTOR association at the chromatin of mESCs, an optimal experimental condition for mTOR ChIP-seq was first established. This included applying

ChIP-qPCR to identify positive and negative genomic regions, testing various mTOR antibodies and comparing antibody titrations.

Due to the absence of established positive and negative genomic regions for mTOR association in mESCs, preliminary investigations utilised regions identified as positive for mTOR binding in other mouse tissues, for example, the transcription start site (TSS) of Tsc1. Additionally, potential negative regions were selected, including several TSS of selected bivalent developmental genes readily available in the laboratory, such as *Pax9*, *Hoxb9*, and *Gata6*. Surprisingly, the most pronounced mTOR association was observed at the TSS of bivalent developmental genes (**Fig. 8**). Notably, mTOR association was not observed at the gene bodies of these bivalent developmental genes, indicating the specificity of the signals (**Fig. 8**). The identification of such genomic regions provided a foundation for subsequent mTOR ChIP-qPCR analyses in mESCs. Two frequently cited antibodies were evaluated and only the one from Abcam showed positive signals (**Fig. 8a**). Further, an antibody titration was conducted using the Abcam mTOR antibody to test whether an increased amount of antibody would amplify the signal. The ChIP-qPCR results suggested that an increased amount of antibody did not enhance the signal-to-noise ratio (**Fig. 8b**). Consequently, the optimised mTOR ChIP protocol was established using 1 mg of the Abcam mTOR antibody (Abcam, ab32028) for chromatin corresponding to 25 µg of DNA. Rigorous testing of the optimised mTOR ChIP protocol in 3 biological replicates was conducted. The results showed clear distinctions of mTOR association between the positive and negative genomic regions. Moreover, a clear contrast was observed between ChIP using mTOR antibody and IgG (**Fig. 8c**). These confirmed the robustness and reliability of the optimised protocol.

Following the establishment of the optimised mTOR ChIP-seq protocol in mESCs, it was applied to study mTOR association at the chromatin. Of note, the ChIP-seq data processing pipeline, including data preprocessing, filtering, mapping and up to peak calling, was developed by me, with subsequent refinements in parameter tuning and script adjustments carried out by Persia Akbari Omgba, a doctoral candidate in the lab. The conceptual input provided by me influenced all stages of the process. At the global level, the mTOR ChIP-seq data revealed widespread mTOR signals at TSSs across the genome (**Fig. 9a**). Peak calling was performed to identify significantly enriched mTOR peaks compared to the background. A total of 1390 mTOR peaks

were identified while the peaks were most frequently located at intergenic regions (25.4%), promoters (23%), exons (22.8%) and introns (19.2%) (**Fig. 9b**). In this study, special attention was directed towards mTOR peaks at the promoters. Gene ontology (GO) analysis was carried out on the mTOR promoter peaks to understand the functions of genes potentially regulated by mTOR. These peaks exhibited substantial enrichment for terms related to embryonic development (**Fig. 9c-f**). The enrichment was also in agreement with the above mentioned mTOR ChIP-qPCR results. Overall, these findings strongly hinted towards the regulatory roles of mTOR at key processes crucial for pluripotency regulation in mESCs embryonic development.

To investigate the association of mTOR with developmental gene promoters across distinct developmental stages, mTOR ChIP-seq was conducted on mESCs cultured in 2i media (mESC 2i) and terminally differentiated mouse embryonic fibroblasts (MEF). Similar to mESCs cultured in serum/LIF media, mESCs 2i represent naive pluripotent cells capable of contributing to chimaera animals when injected into the ICM of a blastocyst. However, mESC 2i exhibits a more morphologically and transcriptionally homogenous culture than mESC serum/LIF[25], which displays different populations of cells resembling transcriptomes similar to the ICM or the epiblast, reflecting varying developmental stages[25]. The data revealed minimal mTOR levels across the entire genome in both cell lines (**Fig. 10**). The drastic contrast of mTOR chromatin association observed between these cell lines implied that mTOR might exert cell-type and developmental-stage-specific functions.

In summary, these findings underlined the pivotal role of mTOR kinase activity in the regulation of mESC pluripotency. In addition to the well established cytoplasmic mTOR functions, the optimised mTOR ChIP-seq revealed mTOR association at the TSSs of developmental genes, suggesting potential regulatory functions of mTOR in pluripotency.

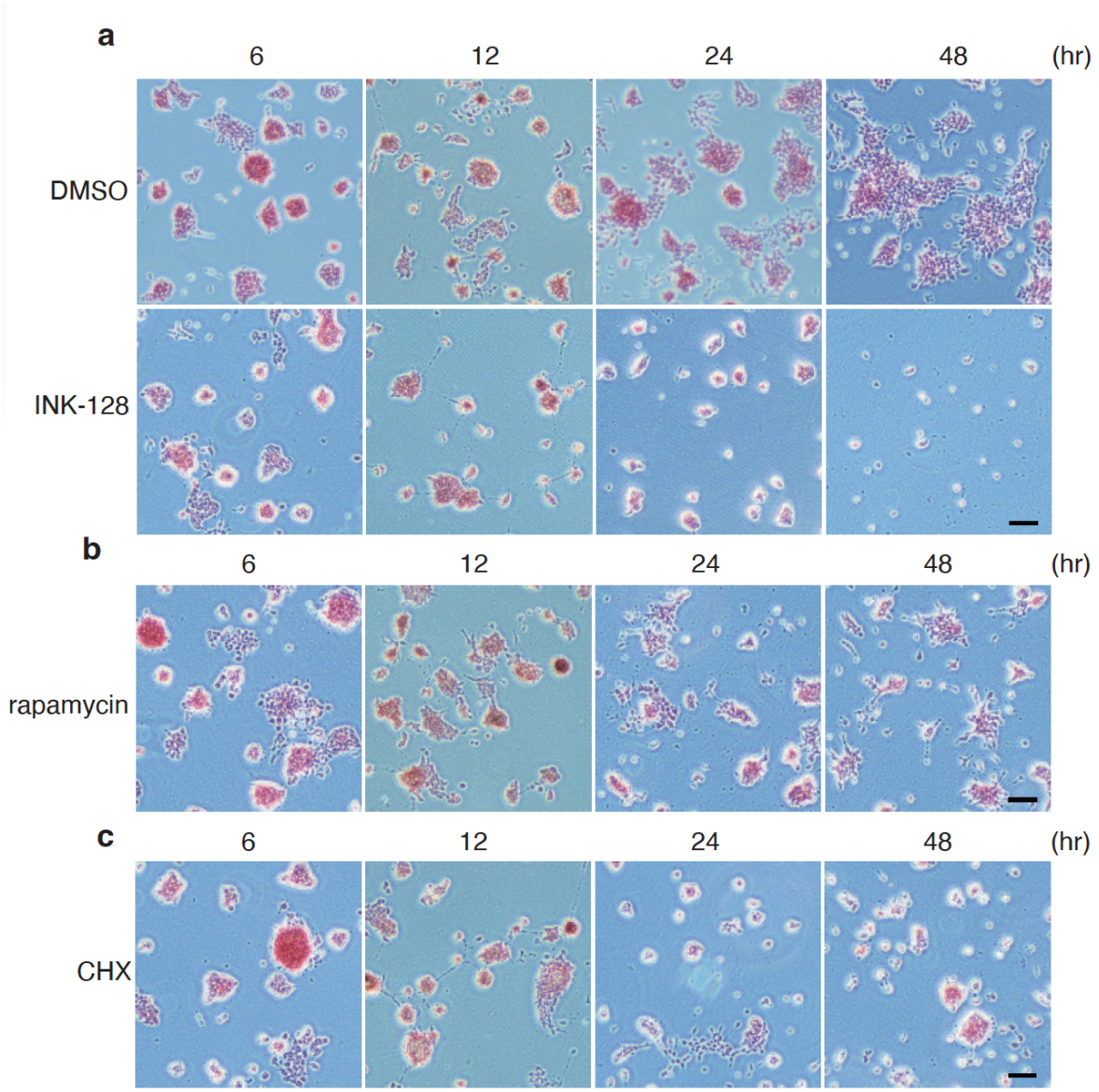

Figure 6 | mTOR kinase activity is essential for mESCs pluripotency exit. Representative images of alkaline phosphatase staining of mESCs differentiated for the indicated times under 200 nM INK-128 (**a**), 200 nM rapamycin (**b**), and 100 nM cycloheximide (CHX, **c**) treatments. Scale bar: 200 μm.

Figure 7 | mTOR nuclear and chromatin localisation in mESCs. Western blot of cytoplasmic (**a**), nuclear (**b**) and chromatin (**c**) fractions from mESCs differentiated for the indicated times. Input for each lane: 20 μg of proteins.

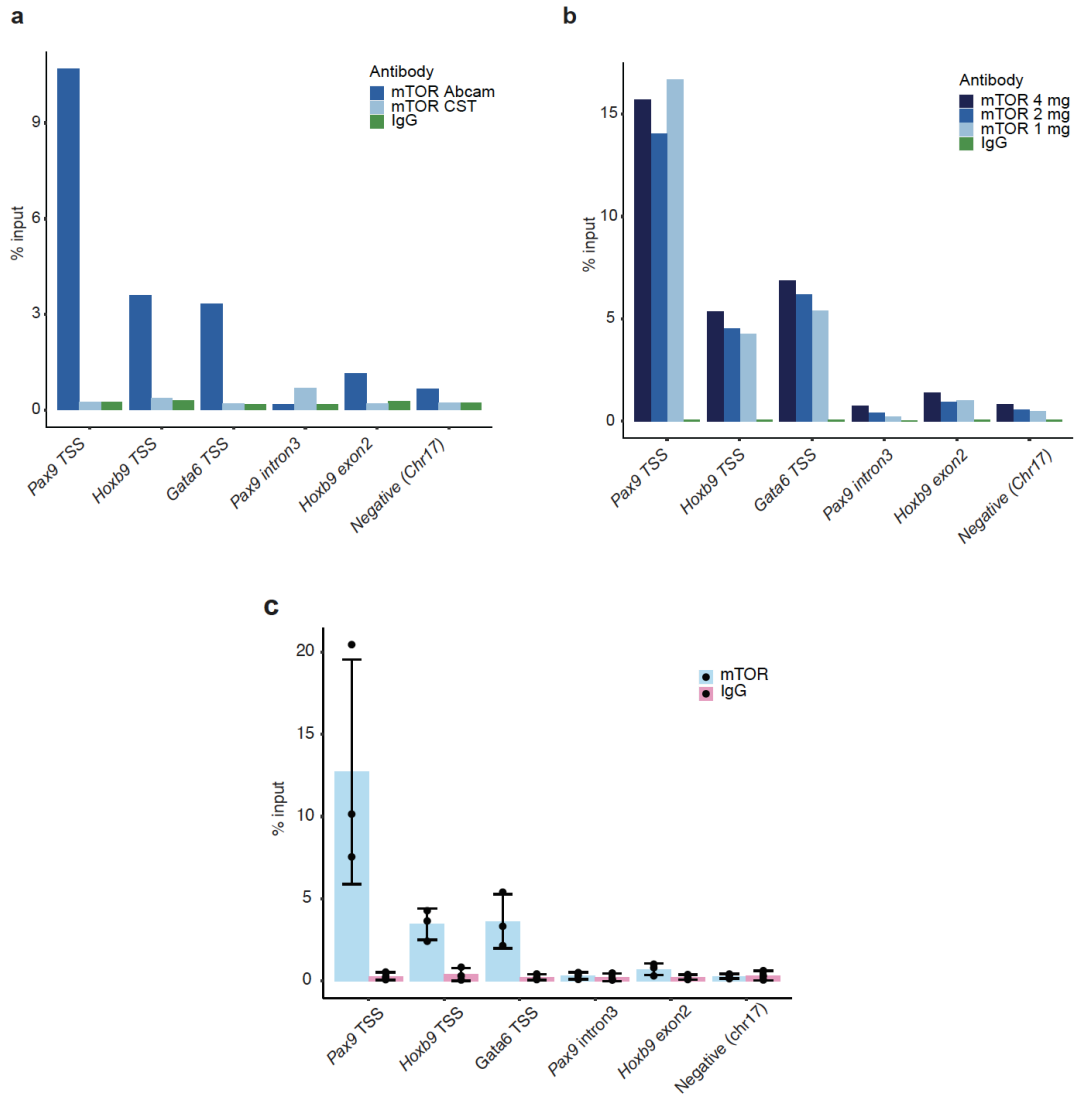

Figure 8 | Optimisation of mTOR ChIP-seq. **a.** Bar plots of mTOR ChIP-qPCR results using different antibodies. No biological replicate. **b.** Bar plots of mTOR ChIP-qPCR results with different antibody titration. No biological replicate. **c.** Bar plot of mTOR ChIP-qPCR results using the optimised protocol. 3 biological replicates. Error bar: standard deviation. Positive regions: *Pax9* TSS, *Hoxb9* TSS and *Gata6* TSS. Negative regions: *Pax9* intron 3, *Hoxb9* exon 2 and a gene desert on chromosome 17.

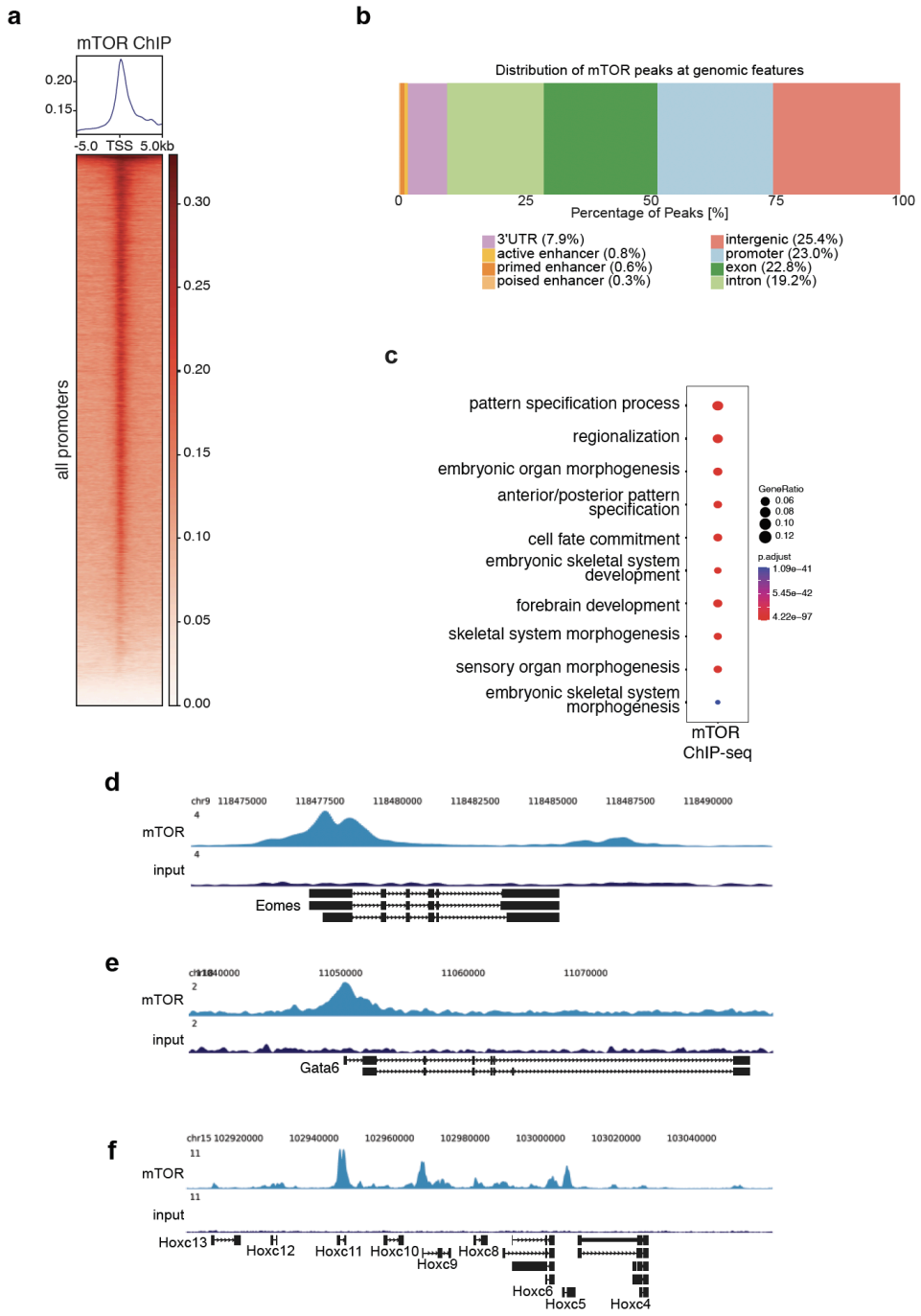

Figure 9 | mTOR ChIP-seq in mESCs. a. Metaplot and heatmap of mTOR ChIP-seq at all gene promoters in mESCs. Promoters were defined as TSS±2kb while regions of TSS±5kb were depicted. **b.** Bar plot showing the distribution of mTOR ChIP-seq peaks in mESC across genomic features. **c.** Gene ontology analysis of mTOR promoter peaks (TSS±2kb) while regions of TSS±5kb were depicted. The top 10 enriched GO terms with the lowest p.adjust were shown. **d-f.** Genome browser tracks of mTOR ChIP-seq of indicated cell lines and input control at *Eomes* (**d**), *Gata6* (**e**), and *Hoxc* locus (**f**).

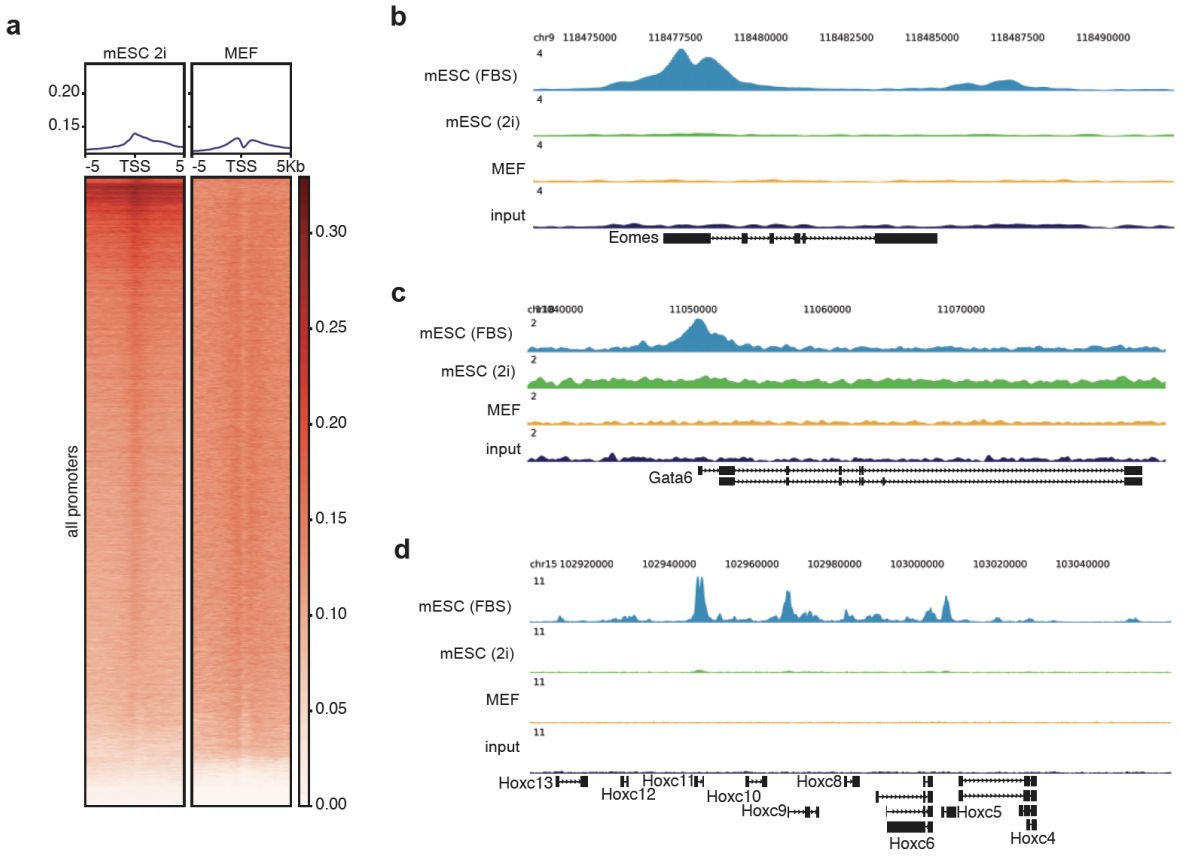

Figure 10 | mTOR ChIP-seq in mESCs 2i and MEF. **a.** Metaplots and heatmaps of mTOR ChIP-seq around all gene promoters in mESCs 2i and MEFs. Promoters were defined as TSS±2kb while regions of TSS±5kb were depicted. **b-d.** Genome browser tracks of mTOR ChIP-seq of indicated cell lines and input control at *Eomes* (**b**), *Gata6* (**c**), and *Hoxc* locus (**d**).

2.2. mTOR phosphorylates histone H2A at T120

As a serine/threonine kinase, mTOR executes its biological functions via phosphorylating various substrates. The identification of mTOR within the chromatin of mESCs and its association with developmental genes prompted the investigation into the nuclear substrates of mTOR. Among the myriad of nuclear proteins, histones emerged as particularly intriguing targets. Previous studies have reported the direct involvement of histone kinases in gene regulation. For example, a recent study showed that IκB kinase (IKK) phosphorylates histone H3.3 at serine 31 in a stimulation dependent manner to induce rapid gene expression in mouse macrophages[135].

An *in vitro* mTOR kinase assay was established to investigate whether mTOR functions as a histone kinase. The mTOR kinase assay was adapted from Sanack et al. and further refined through consultation with other relevant studies[87,112,136]. In this *in vitro* kinase assay, endogenous mTOR was first immunoprecipitated from mESCs and mixed with recombinant histone variants and [γ-32P]-ATP. The reaction mixture was separated on an SDS-PAGE before the development and detection of the radioactivity. To ensure that the radioactivity signals indeed came from incorporation of [γ-32P]-ATP to the histones by mTOR, control reactions were conducted in parallel. These included a reaction without mTOR (no kinase), a reaction without histone (no substrate), a reaction without [γ-32P]-ATP (no ATP) and a reaction with addition of the catalytic mTOR inhibitor INK-128. In total, four common histone variants, H2A, H2B, H3 and H4 were tested. Only histone H2A showed positive incorporation of [γ-32P]-ATP, indicated by the ^{32}P between 15 to 20 kDa (**Fig. 11a**). This demonstrated that mTOR was able to phosphorylate histone H2A *in vitro*.

This immediately prompted the search for the specific amino acid residues of H2A phosphorylated by mTOR. Initial efforts were made to employ mass spectrometry for screening potential serine and threonine residues phosphorylated by mTOR. However, technical difficulties preclude the acquisition of samples that qualified for mass spec analysis. As a result, an alternative method modified based on the radioactive *in vitro* mTOR kinase assay was implemented. This non-radioactive *in vitro* mTOR kinase allowed the identification of one phosphorylated amino acid site at a time. [γ-32P]-ATP was replaced by non-radioactive ATP and the SDS-PAGE was subsequently subjected to western blot analysis. The detection of phosphorylated

amino acid residue of interest was achieved through the use of specific antibodies. During the search, special attention was focused on the threonine 120 (T120) on the tail of H2A. Ubiquitination of its immediate neighbour lysine 119 (H2AK119ub) by Polycomb repressive complex 1 (PRC1) is essential for proper developmental gene regulation in mESCs[31,32]. Therefore, the non-radioactive *in vitro* mTOR kinase assay was applied to examine whether mTOR can phosphorylate H2A at T120 (H2AT120ph). The kinase reaction products were analysed using an antibody specifically targeting H2AT120ph. The results showed that mTOR was able to phosphorylate histone H2A at T120. Importantly, this phosphorylation was fully abolished when the mTOR kinase inhibitor, INK-128, was present in the reaction (**Fig. 11b**). Here, mTOR was shown to be a histone H2A kinase *in vitro* which had not been reported before. Since H2AT120ph can antagonise H2AK119ub, the results here hinted that there might be cross-talk between the two marks or between mTOR and PRC1 which eventually leads to changes in gene expression in mESCs[137].

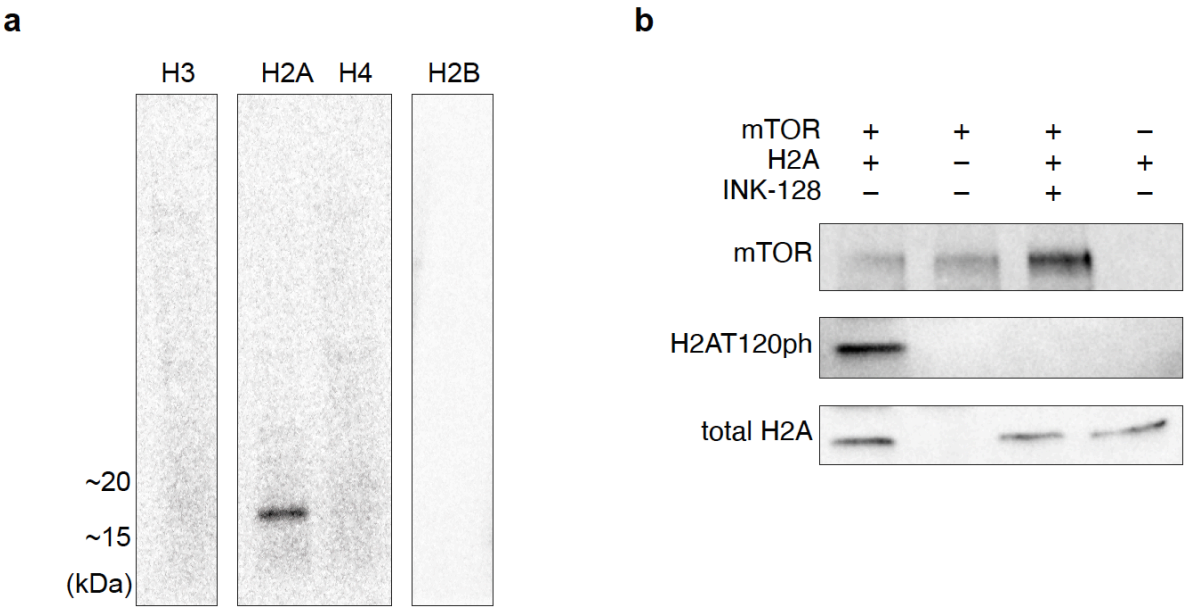

Figure 11 | mTOR phosphorylates histone H2A at T120 *in vitro*. a. Autoradiography (^{32}P) of the results of an *in vitro* mTOR kinase assay using indicated histone variants. **b.** Western blot of non-radioactive *in vitro* mTOR kinase assay using H2A under indicated conditions. Total H2A served as loading control.

2.3. Changes of mTOR, H2AT120ph and transcription in mESC differentiation

So far the data revealed the indispensable role of mTOR kinase activity in mESC differentiation. Notably, its association with chromatin targets exhibits cell-type-specific variations, suggesting a dynamic behaviour. To better understand the behaviour of mTOR during mESC differentiation, a time-course experiment was devised. mTOR ChIP-seq was carried out on mESCs differentiated for 0, 6, 12 and 24 hours. The peak calling analysis revealed that mTOR association with its chromatin targets indeed showed a dynamic turnover. The number of mTOR promoter peaks greatly decreased from 1390 to 108 within the initial 12 hours of differentiation, further dropping to only 10 peaks at 24 hours. Importantly, mTOR did not gain new chromatin targets throughout the differentiation process (**Fig. 12a,b**). In line with this finding, gene ontology analysis showed that mTOR promoter peaks within 12 hours of differentiation were enriched for similar developmental related terms and the enrichment mostly disappeared at 24 hours (**Fig. 12c**). Together these results suggested a potential involvement of mTOR in the regulatory processes governing developmental genes during the initial 24 hours of mESC differentiation.

Considering the close spatial relationship between H2AK119ub and H2AT120ph, it was hypothesised that mTOR might catalyse H2AT120ph, which potentially facilitates gene activation via competing with H2AK119ub, during mESC pluripotency exit. To explore these dynamics, a time-course experiment to profile both chromatin and transcription was devised. mESC differentiation was induced by LIF removal for 0, 6, 12, and 24 hours, with or without INK-128 treatment (**Fig. 12d**)[138,139]. Initial attempts to establish a ChIP-seq protocol of H2AT120ph and PRC related histone modifications (H2AK119ub and H3K27me3) for chromatin level analyses was not successful. Therefore, an alternative approach using the Cleavage Under Targets and Tagmentation (CUT&Tag) protocol was pursued. In CUT&Tag, the targeted chromatin protein or histone modification is recognised by a specific antibody in situ. The primary antibody then serves as an anchor for a protein A-Tn5 transposase fusion protein. The transposase is then activated and generates sequencing library fragments. The whole experimental procedures, starting from cells or nuclei, can be seamlessly executed in PCR tubes or microwell, hence greatly increasing the throughput[138]. CUT&Tag provides several advantages over conventional ChIP-seq.

First, it requires substantially fewer cells than ChIP-seq. For one CUT&Tag reaction 1×10^5 cells are abundant whereas the ChIP-seq protocol in this study requires about 1×10^7 cells. Second, CUT&Tag provides a superior signal-to-noise ratio. The reduced background is due to the direct tagging of DNA at the target site. Third, the experimental procedures are more streamlined and require less time to generate a sequencing ready library. This also makes the results more reproducible. Overall, it is a more efficient, cost-effective and high resolution method for chromatin profiling. As for transcriptional analysis, the preliminary bulk mRNA sequencing experiments revealed minimal to no changes in the expression of the mTOR target genes during the experimental time course. There are many processing steps between nascent transcripts and mature transcription. The changes at the nascent transcription level may not be reflected at the mRNA level. As mTOR is hypothesised to be involved in gene activation directly at the chromatin, TT-SLAM-seq was employed to capture changes in nascent transcription[139]. As the name suggests, TT-SLAM-seq is a combination of transient transcriptome sequencing (TT-seq) and SLAMseq[140,141]. In TT-seq, the newly synthesised RNAs are metabolically labelled using 4-thiouridine (4sU). The labelled RNAs were enriched using sonication followed by affinity purification. However, the 4sU-capturing based methods often suffer from contamination in the RNA libraries by the unlabeled transcripts. To decrease the contamination, SLAMseq introduces a chemical conversion step where the incorporated 4sU is converted to cytosine. SLAMseq does not require isolation of labelled RNA as the distinction between nascent and non-nascent RNA is done at the data processing steps[141]. The modified TT-SLAM-seq further combines both labelled RNA isolation and the chemical conversion to improve the quality of the sequencing library. The unlabeled transcripts are eliminated bioinformatically[139].

Overall, the level of H2AT120ph at mTOR target genes was higher than at non-mTOR target control genes in mESCs. During differentiation, a transient increase of H2AT120ph at mTOR target genes was observed within the initial 12 hours. The elevation was followed by a decrease to slightly above the initial level at 24 hours. In comparison, at non-mTOR target control genes, H2AT120ph exhibited a consistent trend throughout the time course. The transient increase of H2AT120ph at mTOR target genes was entirely abolished under mTORi treatment, suggesting that the increase was dependent on mTOR (**Fig. 13a-c**).

At the nascent transcription level, similar to H2AT120ph, mTOR target genes showed a higher level of nascent transcription compared to non-mTOR target control genes in mESCs. Throughout differentiation, the nascent transcription of mTOR target genes first peaked at 6 hours and then consistently remained higher than the initial level up to 24 hours. On the contrary, the expression level of mTOR target genes continued to decrease under INK-128 treatment over time (**Fig. 13d-f**). There was no general gene upregulation observed in non-mTOR target genes over time, suggesting that the upregulation in mTOR target genes was specific and not a result of overall gene activation during differentiation (**Fig. 13d, f**). The results revealed a correlation between the increased level of H2AT120ph and higher nascent transcription at mTOR target genes during mESC differentiation. The observed patterns suggested a potential association between mTOR-dependent H2AT120ph and enhanced nascent transcription. Further investigation is needed to clarify the mechanisms underlying the correlation and establish whether a causal relationship exists.

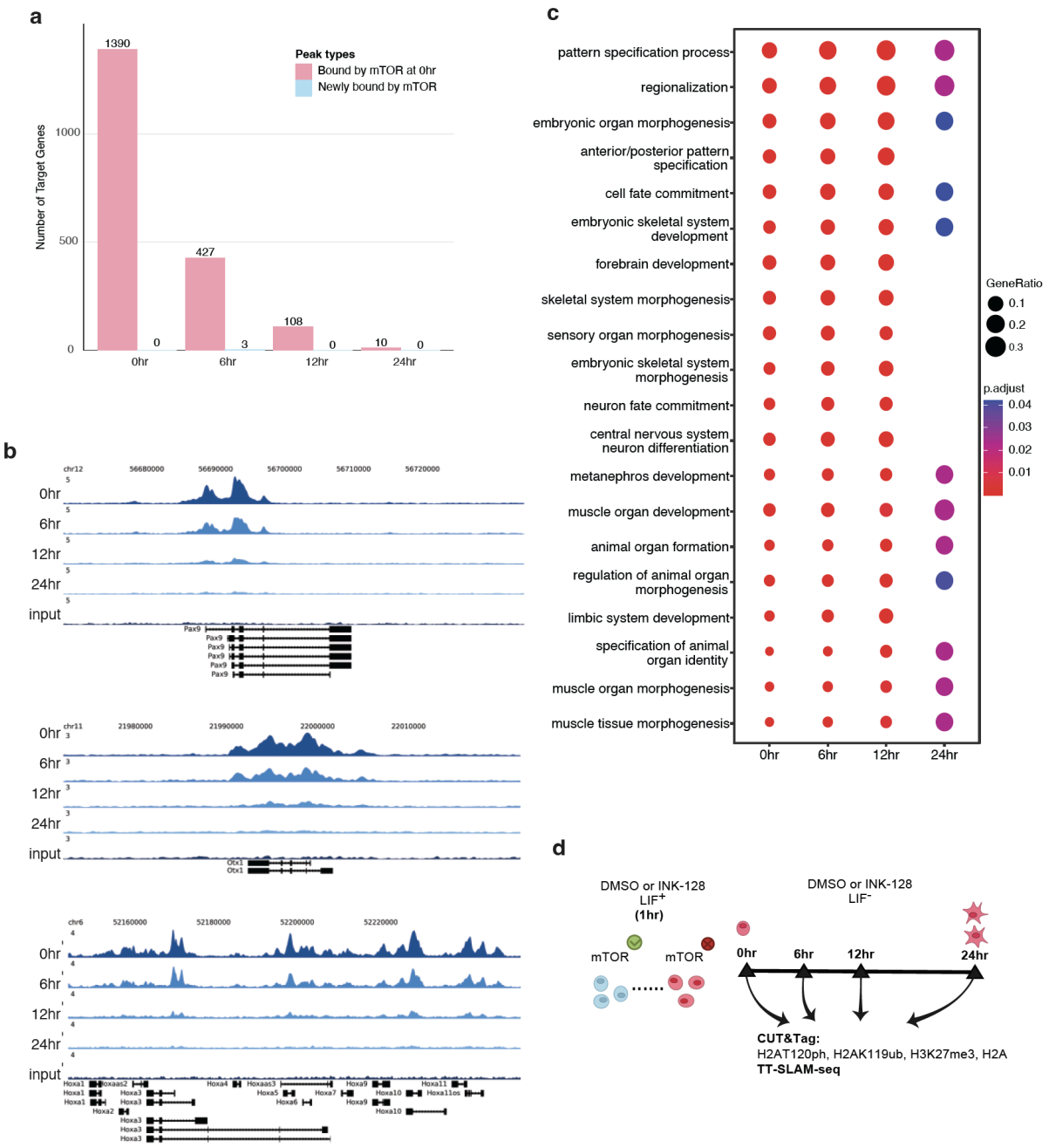

Figure 12 | Loss of mTOR association and increase of H2AT120ph and nascent transcription at mTOR target genes in mESCs differentiation. a. Bar plot of the number of mTOR target promoters (ChIP-seq) during mESCs differentiation for the indicated times. **b.** Genome browser tracks of mTOR ChIP-seq and input control in at *Pax9, Otc1,* and the *Hoxa* locus in mESCs differentiated for the indicated times. **c.** Gene ontology analysis of mTOR ChIP-seq promoter peaks (TSS±2kb) during mESCs differentiation for the indicated times. The top 20 enriched GO terms with the lowest p.adjust were shown. **d.** Schematic overview of the experimental design.

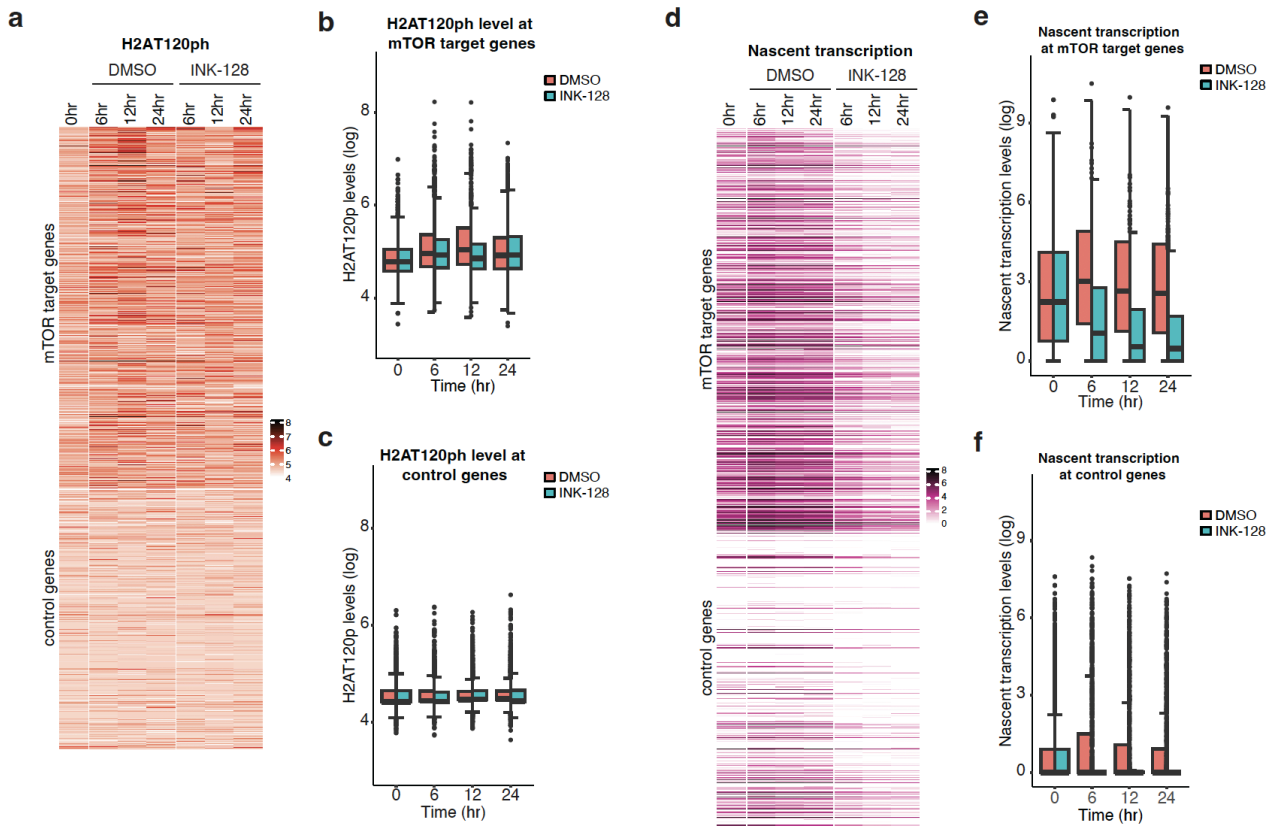

Figure 13 | Increase of H2AT120ph and nascent transcription at mTOR target genes during mESCs differentiation. a. Heatmap of the sum of H2AT120ph level at the promoters (TSS±2kb) of mTOR target and non-mTOR control genes in mESCs differentiated for the indicated times with DMSO or INK-128 treatment. **b-c.** Box plots of the sum of H2AT120ph level at mTOR target (**b**) and control genes (**c**) as shown in **a**. **d.** Heatmap of the nascent transcription level of mTOR target and non-mTOR control genes in mESCs differentiated for the indicated times with DMSO or INK-128 treatment. **e-f**. Box plots of nascent transcription level at mTOR target (**e**) and non-mTOR control genes (**f**) as shown in **d.** For box plots, the top and bottom lines of the box represent the 75th and the 25th percentile with the median represented by the centre line. The whiskers represent ±1.5 IQR. Due to space limitations, in-depth calculations for the construction of the heatmaps and box plots are described in the Material and Method section (see Sections 4.10.9 and 4.10.10 for detailed procedures).

2.4. mTOR and PRC1 may co-regulate gene expression

In the subsequent analyses, the levels of PRC related histone modifications, H2AK119ub and H3K27me3, at mTOR target genes in mESCs were assessed. Generally, mTOR target genes exhibited higher levels of the Polycomb repressive marks than non-mTOR control genes (**Fig. 14a, 16a and 17a**). This was consistent with previous studies indicating that these developmental genes are inhibited in pluripotent mESCs and are only activated during differentiation[31,31,32]. Nevertheless, the variability in abundance of these two marks across mTOR target genes implied that there might be diverse functions and regulatory mechanisms governing these genes. The active turnover of H2AK119ub, but not H3K27me3, is associated with the depression of Polycomb target genes, highlighting potential differences in regulatory dynamics[142]. To further characterise mTOR target genes, they were categorised into three clusters based on their H2AK119ub levels over time. Since H2AK119ub is catalysed by PRC1, the level of PRC1 at mTOR target genes was checked. PRC1 is composed of the catalytic core (RING1A/B) and one of six Polycomb group RING finger proteins (PCGF1-6). Depending on the specific PCGF component present, PRC1 complexes are classified as canonical PRC1 (cPRC1) or variant PRC1 (vPRC1)[37,38]. While cPRC1 complexes are built around PCGF2/4 and include one of the chromobox proteins (CBX2/4/7/8) and one of the Polyhomeotic subunits (PHC1/2/3), vPRC1 can assemble around any of the six PCGF proteins and include YY1-binding protein (RYBP), or its paralogue YAF2[37–39]. Notably, vPRC1 exhibits significantly higher catalytic activity than cPRC1 and contributes to most H2AK119ub *in vivo*[42,43]. Using ChIP-seq data of different PRC1 variants (Cbx7 and Rybp) from a recent publication, distinct enrichment of PRC1 variants within these clusters was observed (**Fig. 14a**)[143]. Overall, the pattern of H2AK119ub, Ring1b and Cbx7 exhibited a correlated trend, with Cluster 1 showing the highest enrichment and Cluster 3 the least. The enrichment of Rybp displayed comparable levels across all three clusters. Cluster 1 demonstrated an association with both Cbx7-containing cPRC1 and Rybp-containing vPRC1. Based on the level of Ring1b, cluster 1 showed to have the highest level of PRC1 enrichment. Cluster 2, with an intermediate level of H2AK119ub, showed an association with both cPRC1 and vPRC1. However, the lower level association with Cbx7 indicated that vPRC1 was the predominant variant in this cluster. In Cluster 3, enrichment for Rybp was observed but a very low level of

Cbx7 suggested that vPRC1 was the predominant variant (**Fig. 13a**). Both cPRC1 and vPRC1 can deposit H2AK119ub but have been shown to have different catalytic activities and targets[32,38,42,43,144]. To investigate the relationship between mTOR, Polycomb repressive marks, and PRC1 variants at mTOR target genes, a correlation analysis using the Spearman coefficient was conducted. mTOR exhibited strong correlations with H2AK119ub (R^2=0.571), H3K27me3 (R^2=0.494), Cbx7 (R^2=0.487), and Ring1b (R^2=0.45). However, a low correlation was found between mTOR and H3K4me3 (R^2=-0.081) (**Fig. 15**). These results further suggested that mTOR regulates target gene expression together with the Polycomb repressive system while showing limited association with other histone marks, such as H3K4me3.

Subsequent investigation was performed to assess whether the variations in H2AK119ub levels and PRC1 composition at mTOR targets could be linked to differences in H2AT120ph levels and nascent transcription.

Subsequent analyses were conducted to assess whether the variations in H2AK119ub levels and PRC1 composition at mTOR targets could be linked to differences in H2AT120ph levels and nascent transcription. The most substantial increase in H2AT120ph was observed in Cluster 1 and 3. In Cluster 1, the mean H2AT120ph level steadily increased to more than double the initial level at 12 hours. In Cluster 3, it reached a plateau of approximately 75% more than the initial level by 6 hours (**Fig. 14b, d**). On the other hand, nascent transcription followed a different pattern. The increase in transcription of mTOR target genes strongly correlated with their initial H2AK119ub levels. Cluster 1, with the highest H2AK119ub levels, exhibited a 200% increase, followed by Cluster and 3, which exhibited approximately 100% increase at 6 hours of differentiation (**Fig. 14c, e**). In contrast to the dynamic changes in H2AT120ph and nascent transcription, both Polycomb repressive marks, H2AK119ub and H3K27me3, remained relatively constant (about ±10%) across all three clusters over time (**Fig. 16, 17**). Functionally, the three clusters of mTOR target genes showed distinct characteristics according to gene ontology analysis. Genes in Cluster 1 were associated with embryonic development, while Cluster 3 was more related to cell activation and cell signalling (**Fig. 14f**). Overall, these results suggested that mTOR regulates gene expression differently by interacting with different PRC1 variants in mESCs.

In the mammalian cytoplasm, mTOR forms 2 different complexes: mTORC1 (with Raptor) and mTORC2 (with Rictor). However, it remains unclear whether mTOR forms the same complexes in the nucleus in mESCs. To address this, CUT&Tag was used to profile Raptor and Rictor in mESCs to evaluate the extent of their signal overlap with mTOR. Firstly, the prominent presence of Raptor and Rictor at the chromatin was observed. But Raptor and Rictor exhibited minimal overlap with mTOR at target promoters, while showing substantial overlap with each other (**Fig. 18a, b**). Functional analysis revealed that the target genes of Raptor and Rictor were primarily enriched for biological processes distinct from those targeted by mTOR (**Fig. 18c**). Together, these findings suggested that nuclear mTOR might not form the same mTORC1 and mTORC2 complexes observed in the cytoplasm.

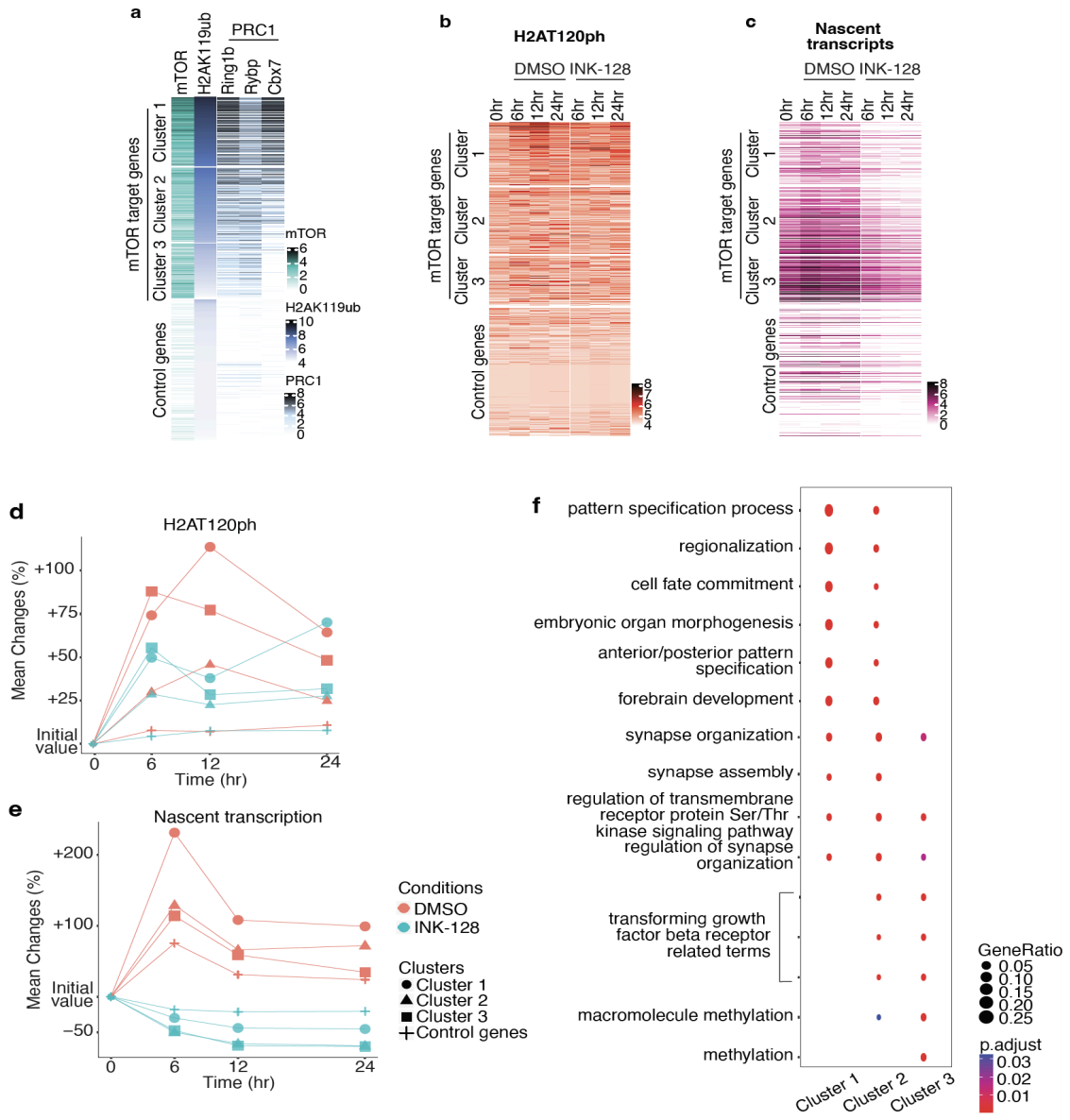

Figure 14 | Different behaviours of three clusters of mTOR target genes based on their H2K119ub levels. a. Heatmap of the sum of mTOR, H2AK119ub and PRC1 components (Ring1b, Rybp and Cbx7) at the promoters (TSS±2kb) of three clusters of mTOR target and non-mTOR control genes in mESCs. The mTOR target genes were clustered based on their H2AK119ub levels during differentiation. **b.** Heatmap of the sum of H2AT120ph at the promoters (TSS±2kb) of the three clusters of mTOR target and non-mTOR control genes in 24 hours of mESCs differentiation with DMSO or INK-128 treatment. **c.** Heatmap of the nascent transcription levels at the promoters (TSS±2kb) of the three clusters of mTOR target and non-mTOR control genes in 24-hour mESCs differentiation with DMSO or INK-128 treatment. **d.** Line plot of the percentage changes in mean H2AT120ph across the three mTOR target

gene clusters in 24 hours of mESCs differentiation with DMSO or INK-128 treatment. **e.** Line plot of the percentage changes in mean nascent transcription across the three mTOR target gene clusters in 24 hours of mESCs differentiation with DMSO or INK-128 treatment. **f.** Gene ontology analysis of the three clusters of mTOR target genes in mESCs, highlighting 15 terms. Due to space limitations, in-depth calculations for the construction of the heatmaps and line plots are described in the Material and Method section (see Sections 4.10.9 and 4.10.10 for detailed procedures).

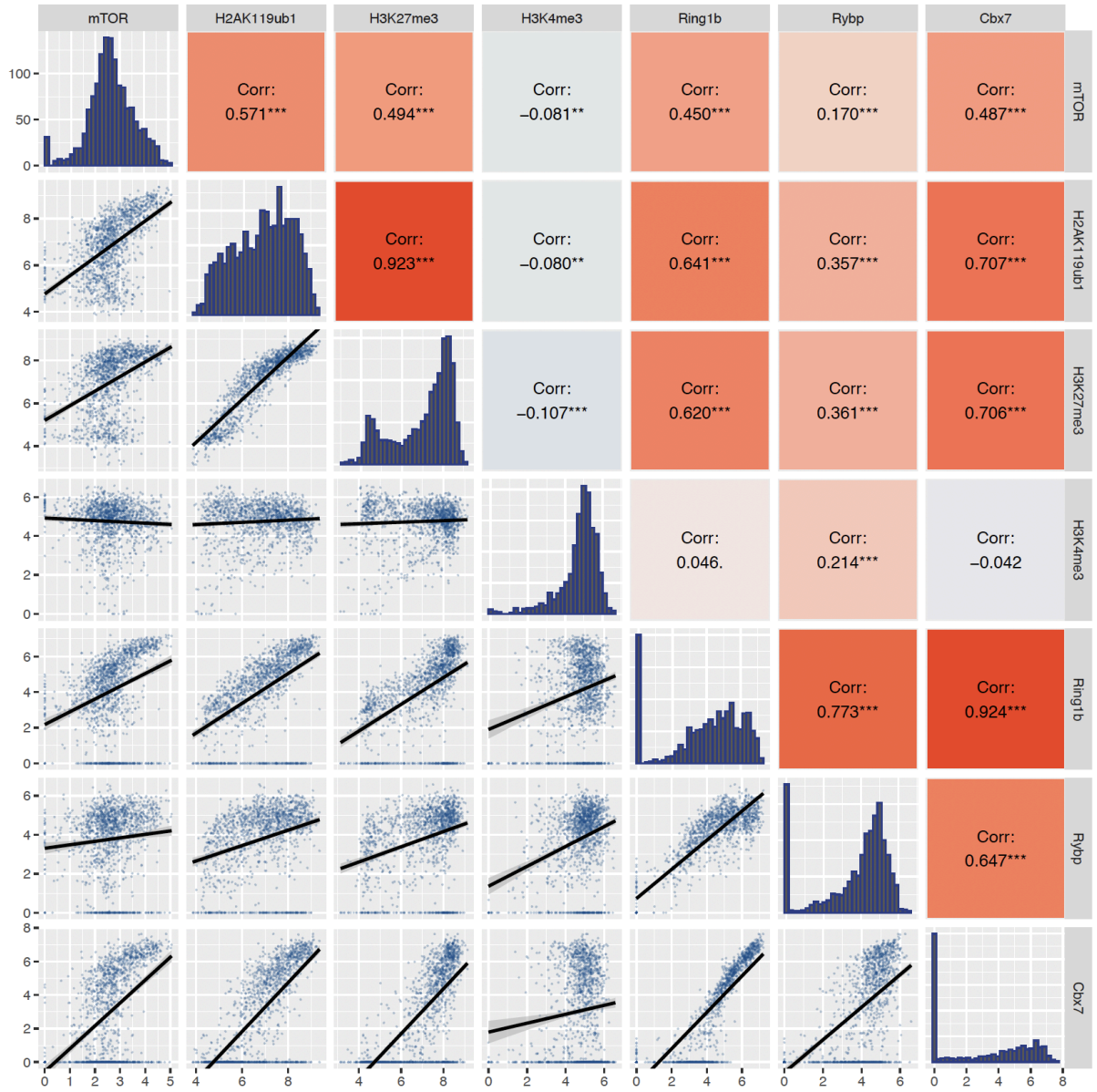

Figure 15 | Spearman correlation between mTOR, Polycomb repressive marks, PRC1 subunits and H3K4me.

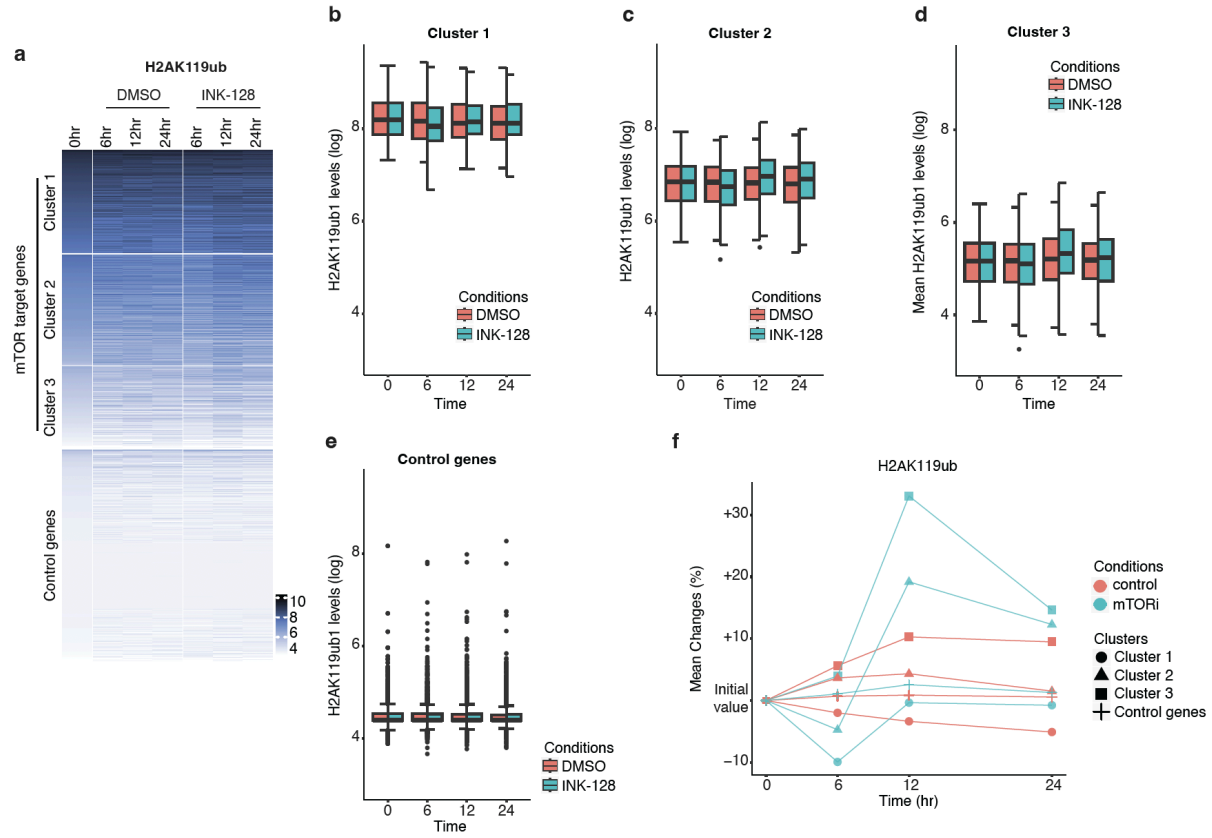

Figure 16 | Changes in H2AK119ub levels among the three mTOR target gene clusters during mESCs differentiation. a. Heatmap of the sum of H2AK119ub at the promoters (TSS±2kb) of the three mTOR target gene clusters and non-mTOR control genes within 24 hours of mESCs differentiation with DMSO or INK-128 treatment. **b-e.** Box plots of H2AK119ub levels in the three mTOR target gene clusters (**b-d**) and non-mTOR control genes (**e**) within 24 hours of mESCs differentiation with DMSO or INK-128 treatment, as shown in **a. f.** Line plot of the percentage changes in mean H3K27me3 across the three mTOR target gene clusters in 24 hours of mESCs differentiation with DMSO or INK-128 treatment. For box plots, the top and bottom lines of the box represent the 75th and the 25th percentile with the median represented by the centre line. The whiskers represent ±1.5 IQR. Due to space limitations, in-depth calculations for the construction of the heatmaps, box plots and line plots are described in the Material and Method section (see Sections 4.10.9 and 4.10.10 for detailed procedures).

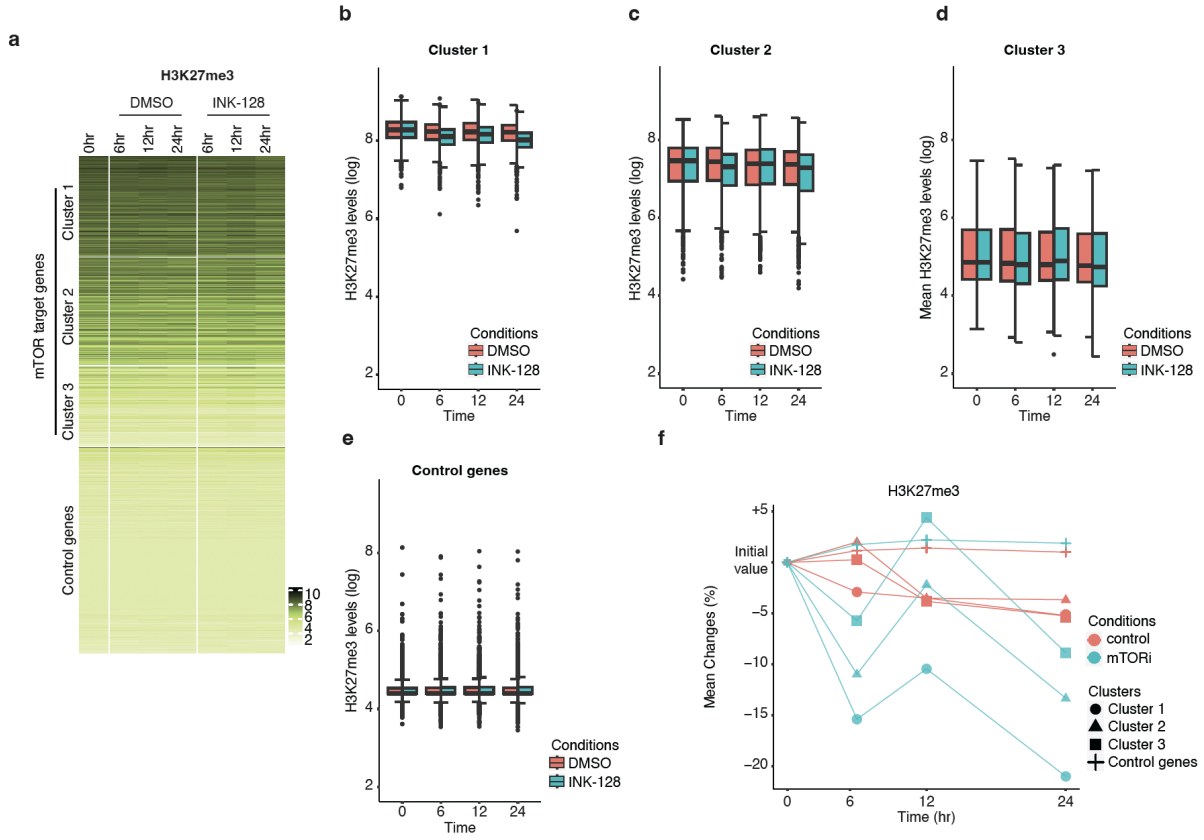

Figure 17 | Changes in H3K27me3 levels among the three mTOR target gene clusters during mESCs differentiation. a. Heatmap of the sum of H3K27me3 at the promoters (TSS±2kb) of the three mTOR target gene clusters and non-mTOR control genes within 24 hours of mESCs differentiation with DMSO or INK-128 treatment. **b-e.** Box plots of H3K27me3 levels in the three mTOR target gene clusters (**b-d**) and non-mTOR control genes (**e**) within 24 hours of mESCs differentiation with DMSO or INK-128 treatment, as shown in **a. f.** Line plot of the percentage changes in mean H3K27me3 across the three mTOR target gene clusters in 24 hours of mESCs differentiation with DMSO or INK-128 treatment. For box plots, the top and bottom lines of the box represent the 75th and the 25th percentile with the median represented by the centre line. The whiskers represent ±1.5 IQR. Due to space limitations, in-depth calculations for the construction of the heatmaps, box plots and line plots are described in the Material and Method section (see Sections 4.10.9 and 4.10.10 for detailed procedures).

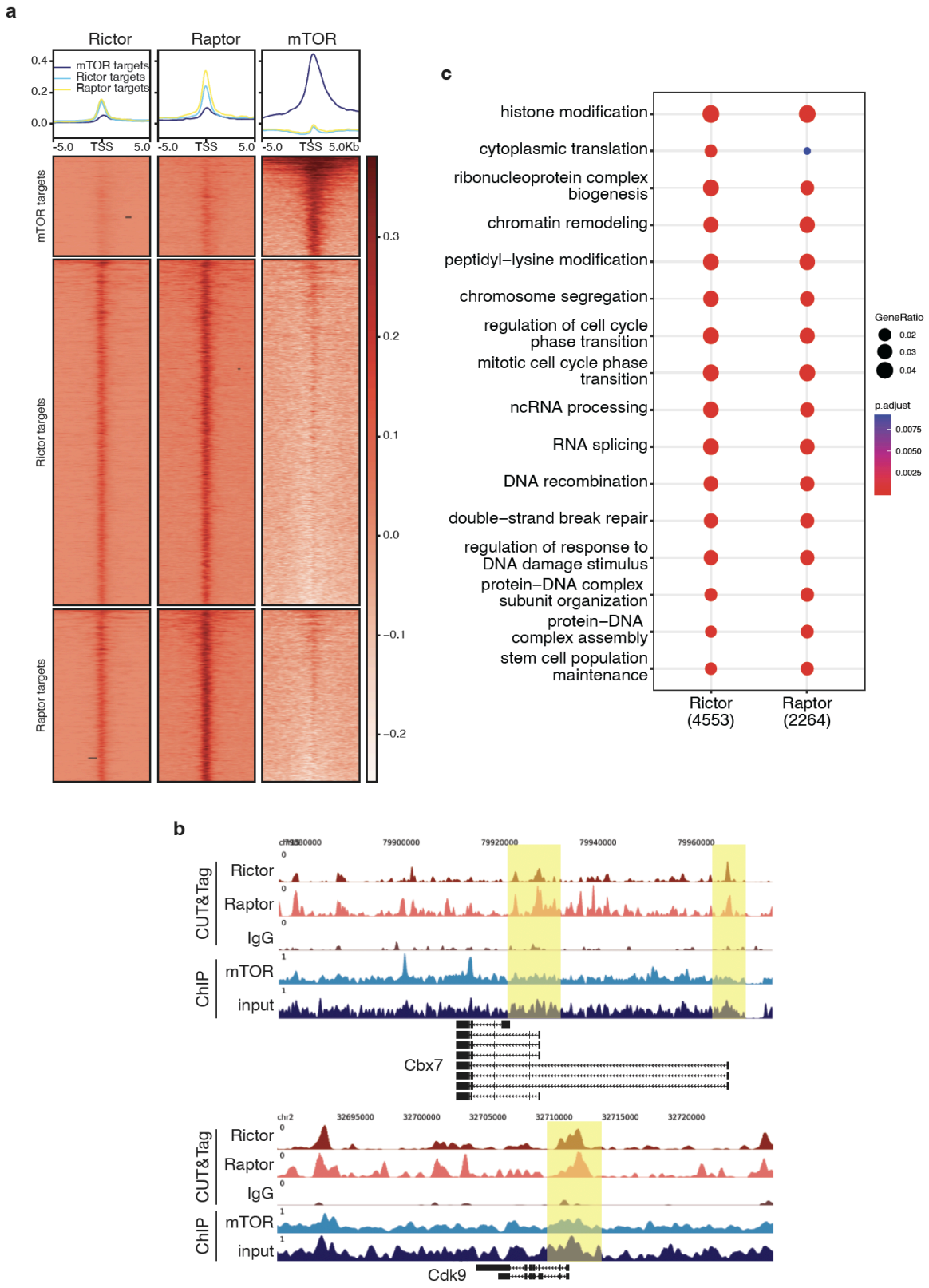

Figure 18 | Rictor and Raptor associate with different gene promoters than mTOR in mESCs. a. deepTool heatmap illustrating Rictor, Raptor and mTOR signals at their respective target promoters. Promoters were defined as TSS±2kb with

signals at TSS±5kb were shown. **b.** Genome browser tracks of CUT&Tag (Raptor, Raptor and IgG control), mTOR ChIP-seq, and input control at *Cbx7* and *Cdk9*. Yellow shading indicates promoter peaks with Rictor and Raptor but without mTOR signals. **c.** Gene ontology analysis of Rictor and Raptor CUT&Tag promoter peaks in mESCs. The top 16 enriched GO terms with the lowest p.adjust were shown. Due to space limitations, in-depth calculation for the construction of the heatmap is described in the Material and Method section (see Section 4.10.9 and 4.10.10 for detailed procedures).

2.5. mESCs with higher mTOR activity were prone to pluripotency exit

So far the results have demonstrated that pluripotency exit is impaired in mESCs lacking mTOR kinase activity. To test whether increased mTOR activity would promote pluripotency exit in mESCs, cells overexpressing wild type- (WT), hyperactive- (hyper) or kinase dead- (KD) mTOR were generated using the PiggyBac system[145,146]. The PiggyBac overexpression system is composed of two plasmids: the PiggyBac transposon plasmids, containing the cargos, and the PiggyBac transposase plasmid. The sequence between the 3'- and 5'-ITR of the PiggyBac transposon plasmid, was replaced with gene cassettes containing the respective mTOR variants, along with mCherry serving as a selection marker (**Fig. 19a**). Plasmids harbouring $mTOR^{WT}$ and $mTOR^{hyper}$ were generous gifts from Prof. Tatsuya Maeda. The $mTOR^{hyper}$ was generated through four mutations (V2198A, L2216H, L2260P in the kinase domain and I2017T in the FKBP-rapamycin-binding (FRB) domain)[145]. Plasmids containing $mTOR^{KD}$ carrying the mutations D2357E and V2364I were obtained from Addgene.

Two to three days following nucleofection with the two PiggyBac plasmids, mESCs were sorted based on their mCherry intensity using FACS. The mCherry positive cells were further cultured and subjected to a second round of sorting after three to four days to enhance enrichment for cells with high and stable mCherry expression (**Fig. 19b, 20**). The overexpression of exogenous mTOR variants was assessed using western blot. All three mESC cell lines exhibited increased levels of mTOR compared to untransfected mESCs (**Fig. 19c**). mESCs transfected with $mTOR^{WT}$ and $mTOR^{hyper}$, but not $mTOR^{KD}$, showed higher levels of pS6, a downstream target of mTOR, indicating increased mTOR activity compared to untransfected mESCs (**Fig. 19c**). Additionally, alkaline phosphatase staining revealed that under standard culture conditions mESCs expressing $mTOR^{hyper}$ and $mTOR^{WT}$ exhibited increased levels of spontaneous differentiation, with $mTOR^{hyper}$ exhibiting a higher tendency than $mTOR^{WT}$. In contrast, mESCs expressing $mTOR^{KD}$ closely resembled the low level of spontaneous differentiation tendency observed in untransfected mESCs (**Fig. 19d**). These results further supported the findings described above that mTOR kinase activity plays a critical role in mESC pluripotency exit.

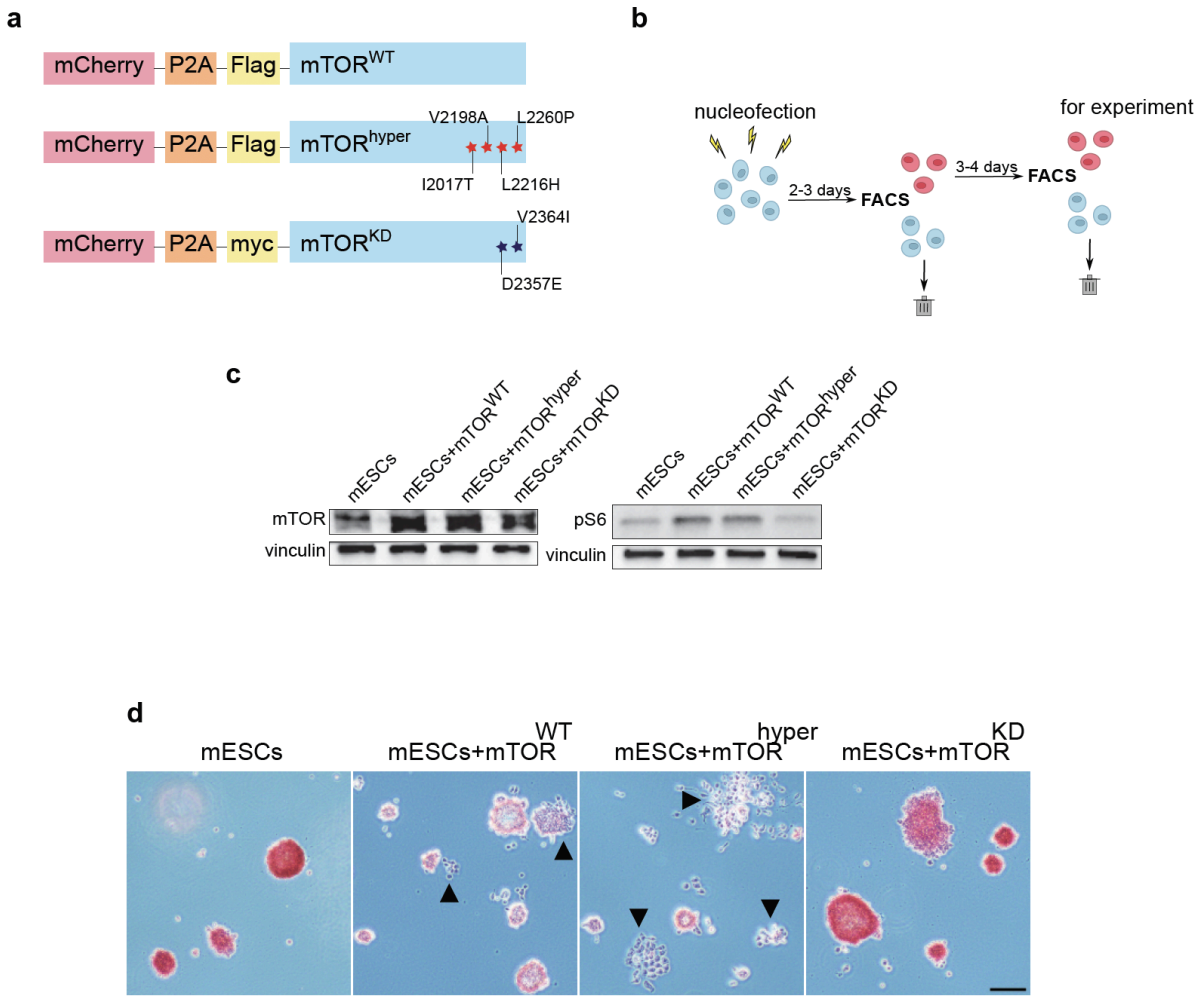

Figure 19 | mESCs having higher mTOR activity are more prone to pluripotency exit. a. Schematic representation of the gene cassettes inserted between the 3'- and 5'-ITR of the PiggyBac transposon plasmid. WT: wild type; hyper: hyperactive; KD: kinase dead. **b.** Experimental overview of the generation of mTOR overexpression mESCs. **c.** Western blot of mESCs overexpressing different versions of mTOR. **d.** Alkaline phosphatase staining of mESCs overexpressing different variants of mTOR. Arrowheads indicate differentiated colonies with decreased redness. Scale bar: 200 μm.

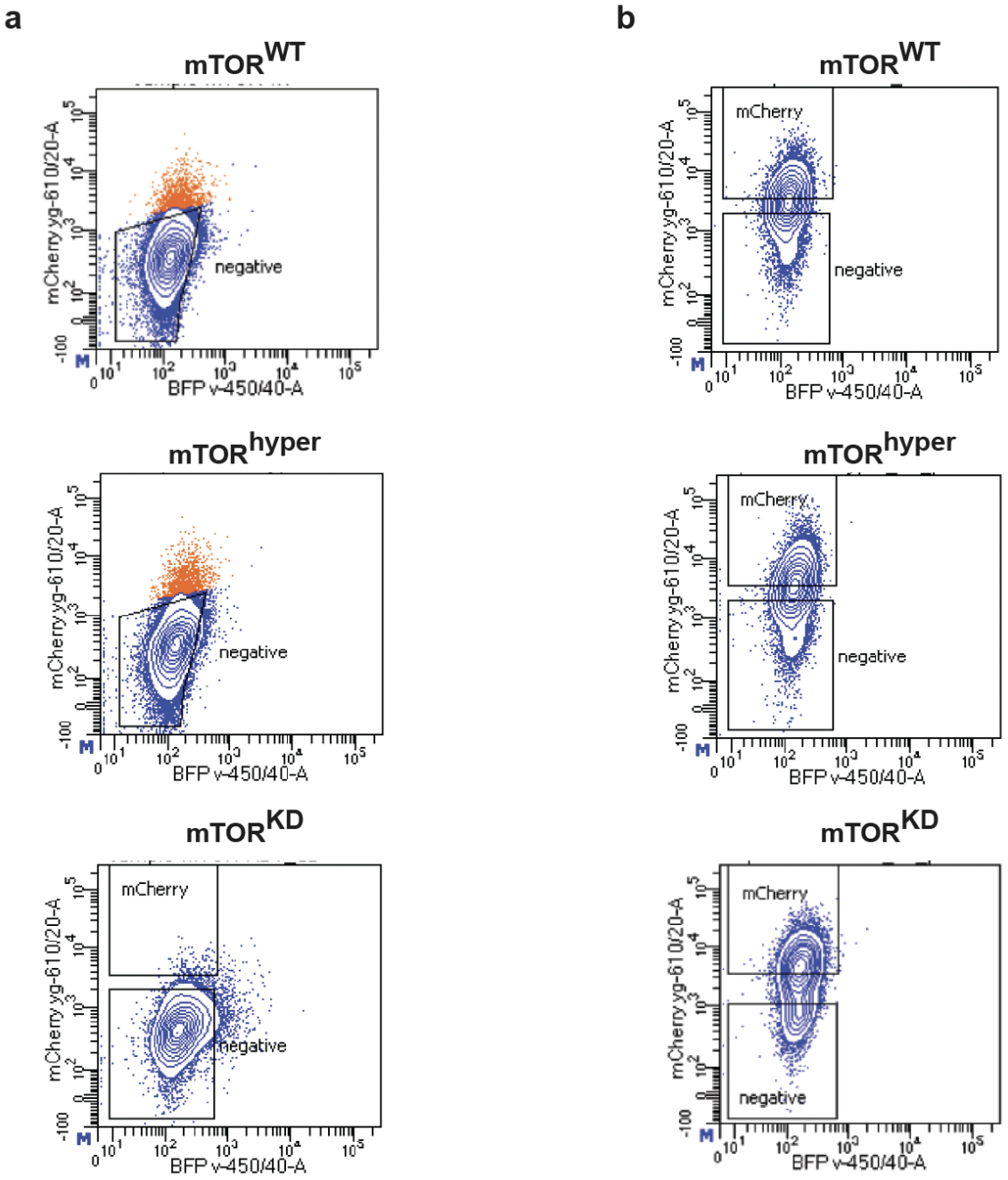

Figure 20 | FACS profiles of mESCs after nucleofection. a-b. FACS profiles of mESCs nucleofected with indicated transgenes after first (**a**) and second (**b**) sorting. Cells with positive mCherry expression (depicted as red dots or within the mCherry gate) were sorted for subsequent culture.

3. Discussion

3.1. Identification of novel mTOR functions in mESCs

The cells isolated from the ICM of $mTOR^{-/-}$ blastocysts fail to proliferate when cultured *in vitro*, emphasising the pivotal role of mTOR[121,122]. As mTOR is known to be a master regulator of metabolism, prolonged and systematic mTOR depletion is anticipated to induce secondary effects in the cells. Recognising the challenge, an $FKBP^{F36V}$-mTOR degron mESC line was established using the dTAG and CRISPR-PITCh systems. Despite the successful establishment of the cell line, unexpected results were observed during functional characterisation. Although mTOR degradation was observed in heterozygous $FKBP^{F36V}$-mTOR mESCs following the dTAG-13 treatment, the mTOR in the homozygous $FKBP^{F36V}$-mTOR mESCs remained undegraded. It is noteworthy that the reproducibility of the results was confirmed through the testing of various homozygous $FKBP^{F36V}$-mTOR mESC lines. This included cell lines independently generated by Iván Fernández Muñoz, a master's student supervised by me.

Since the dTAG-13 degron system has been successfully employed in mESCs for other proteins, it is reasonable to assume that proteasome protein degradation efficiency in mESCs is sufficient enough[147,148]. Various scenarios at the DNA, transcription and protein level were explored to explain the discrepancy. Firstly, at the DNA level, given that mammals are reported to possess only one copy of the *MTOR* gene, the production of undegraded from alternative genomic loci seems unlikely[62]. Secondly, in the examination of transcription initiation sites using CAGE data in both serum/LIF and 2i mESCs, no alternative TSSs were identified[149,150]. Lastly, at the protein level, a potential scenario where mTOR lacking the complete $FKBP^{F36V}$ tag might be generated through an alternative translation start site was considered. Western blot analysis of heterozygous $FKBP^{F36V}$-mTOR mESCs revealed the presence of two distinct mTOR bands. The band with a higher molecular weight representing the $FKBP^{F36V}$-tagged mTOR was fully degraded after dTAG-13 treatment. The same results were observed in the western blot detecting the HA-tag, which was fused to mTOR together with the $FKBP^{F36V}$ tag (**Fig. 5d**). In contrast, the homozygous line exhibited a single band whose size was closer to that of endogenous mTOR. Faint signals of the HA-tag in the homozygous line suggested that the cells were able to produce $FKBP^{F36V}$-tagged mTOR (**Fig. 5d**). Together these

findings hinted that the homozygous FKBP^{F36V}-mTOR mESCs were able to produce wild-type without the FKBP^{F36V} tag and therefore maintained a certain level of mTOR. This mechanism has not been reported previously and additional experiments are needed to confirm the hypothesis. Nevertheless, given the critical role of mTOR in cellular processes, it is plausible that cells are equipped with multiple layers of regulatory mechanisms to ensure their stable expression. It would be interesting to investigate how cells sense the level of mTOR as it might provide valuable insights for future designs aimed at achieving rapid degradation.

Embryonic diapause, utilised by over 130 mammalian species to fine-tune the timing of offspring birth, is characterised by embryos exhibiting minimal cell proliferation, reduced metabolism, and delayed development[51,52]. Diapause embryos retain the full potential to develop into healthy animals upon reactivation. mTOR inhibition has been shown to induce a paused pluripotent state in serum/LIF mESCs, mirroring the characteristics of diapause embryos. This induced paused state is reversible, as mESCs swiftly return to an active state upon removal of the mTOR inhibitor, and can contribute to chimaera formation[59]. However, it remained unclear whether mESCs were able to react to differentiation signals in the absence of mTOR activity. In this study, I demonstrated that the absence of mTOR kinase activity resulted in the failure of mESC exit pluripotency and caused a massive cell death within 48 hours (**Fig. 6a**). It is noteworthy that selective inhibition of mTORC1 using rapamycin alone only slowed down the differentiation progress but did not lead to massive cell death (**Fig. 6b**). Conversely, the introduction of hyperactive mTOR in mESCs greatly increased the spontaneous differentiation (**Fig. 19d**). Previous studies have shown growth arrest and peri-implantation lethality in mTOR$^{-/-}$ mouse embryos[121,122]. The results reported in this study further suggested that mTOR may be involved in cellular processes beyond growth regulation and the failure to progress toward differentiation might be a contributing factor to the observed cell death. From the mTOR ChIP-seq results, mTOR target genes were not enriched for cell death related genes. Therefore, whether there is a direct involvement of mTOR in cell death activation and which type of cell death was triggered remain to be elucidated.

In this study, the mTOR ChIP-seq data revealed that mTOR is associated with developmental genes at chromatin in mESCs (**Fig. 9**). Prior investigations using genome-wide approaches have demonstrated the involvement of mTOR in the regulation of gene promoters associated with mTOR signalling pathways[118,119]. Here,

the finding of mTOR's association with the promoters of developmental genes represents an unprecedented observation. The primary focus of this study was on investigating the promoter peaks associated with mTOR in mESCs. However, it is important to note that these promoter peaks constituted only 23% of the total mTOR called peaks. A significant proportion of mTOR peaks (25%) were observed in the intergenic regions, which are known to harbour regulatory elements such as enhancers (**Fig. 9b**). Preliminary analysis by overlapping mTOR peaks and known enhancer regions did not show a substantial intersection[151]. Further investigations, such as using chromosome conformation capture based methods to study interactions between genomic regions, are needed to understand the role of these mTOR peaks.

In this study, the mTOR *in vitro* kinase assay revealed an unprecedented role of mTOR as a histone H2A kinase (**Fig. 11**). Recombinant histones, in their unassembled form, were used for this assay. To better resemble the *in vivo* situation, attempts were made to use assembled nucleosomes in the assay. Regrettably, conclusive results were not attained within the scope of this thesis. One of the primary challenges encountered when using nucleosomes in the kinase assay was the presence of EDTA in the nucleosome buffer. EDTA, functioning as a chelating agent, forms stable complexes with Mg^{2+}, an essential cofactor required for the activity of mTOR kinase assay, preventing the reliable assessment[87]. More optimisations are needed to develop a suitable buffer system. The idea of threonine 120 of histone H2A in the context of assembled nucleosomes being phosphorylated by mTOR remains plausible. H2AT120 is situated at the tail region of histone H2A and lysine 119 in close proximity is known to be susceptible to ubiquitination by PRC1.

In the mTOR *in vitro* kinase assay, mTOR was immunoprecipitated from whole cell lysate of mESCs. No extra steps were taken to obtain nuclear or chromatin mTOR. The buffers used are designed to maintain the integrity of mTORC1[87]. Therefore, mTORC1 is likely to be the predominant variant in the kinase reaction. It is unclear whether mTORC1 is present in the nucleus and whether nuclear mTOR may form distinct complexes compared to the conventional mTORC1 and mTORC2. The ChIP-seq results of Rictor and Raptor did not support that mTOR forms mTORC1 or mTORC2 in the chromatin in mESCs as minimal overlap in signals were observed (**Fig. 18**). Intriguingly, Rictor and Raptor shared many target promoters which were

involved in histone modification and chromatin remodelling, suggesting that they may play different crucial roles than mTOR in mESCs (**Fig. 18c**). Further investigations are needed to understand the protein composition surrounding mTOR in the chromatin, shedding light on the interaction partners and regulatory mechanisms governing mTOR. In other cell lines, mTOR has been reported to interact with various nuclear partners, such as YY1, AR and PGC-1α[116,118]. Unexpectedly, the Raptor and Rictor CUT&Tag data showed low overlapping with mTOR ChIP-seq, suggesting that mTOR might not form the conventional mTORC1 and mTORC2 in this context. Additionally, the presence of mTOR, Rictor and Raptor in chromatin prompted questions: Are other core subunits of mTORC1 and mTORC2 also present in the nucleus? Do mTOR complexes enter the nucleus as a unified entity, only to disassemble and execute distinct functions individually? More experiments, such as nuclear mTOR co-immunoprecipitation with other proteins of interest, or mass-spec-based analysis, are needed to obtain a better understanding of nuclear mTOR.

3.2. Nuclear mTOR localisation and its regulation

mTOR nuclear localisation has been reported in several healthy and malignant cells[107–111]. In the case of mESCs, mTOR was primarily observed in the cytoplasm, with a minor fraction observed in the nucleus and chromatin, further expanding the repertoire of cells where nuclear mTOR can be found (**Fig. 7**). While the presence of mTOR in chromatin was consistently detected through western blot analysis during a 24-hour differentiation period, the ChIP-seq results showed a rapid decline in the number of mTOR-associated promoter peaks in the first 12 hours of differentiation. This discrepancy may be attributed to mTOR potentially translocating away from DNA, while still residing within the chromatin fraction during differentiation, thereby surpassing the detection limits of the ChIP-seq technique. Another possibility could be the experimental setup. Western blot profiles the bulk proteins extracted from the mESC culture which included both pluripotent and differentiated cells. It was not possible to know the contribution of mTOR from cells at different pluripotent states. Applying single-cell *in situ* methods, such as immunofluorescence staining, could provide a better distinction.

Among the cell lines examined in this study, only mESCs cultured in serum/LIF media exhibited an association between mTOR and developmental genes. In comparison mESCs cultured in 2i media showed almost no enrichment of mTOR at these genes (**Fig. 10**). Although both mESCs cultured in serum/LIF and 2i represent naive pluripotent cells capable of contributing to chimeric animals, they exhibit distinct characteristics. mESCs cultured in 2i display a more morphologically and transcriptionally homogeneous culture compared to the heterogeneous population of mESCs cultured in serum/LIF, which encompasses cells resembling transcriptomes similar to the ICM or the epiblast, reflecting varying developmental stages[25,28,29]. The ChIP-seq protocol in this study profiled mTOR association in the chromatin at a population level. It was not possible to know the origin and contribution of mTOR signals from subpopulations. The differences in the mTOR ChIP-seq results suggested that the recruitment of mTOR to its chromatin targets is conditional and tightly regulated. The underlying mechanisms governing mTOR recruitment to chromatin targets and its translocation from the cytoplasm to the nucleus in mESCs require further investigation.

Conditional recruitment of mTOR to its chromatin targets has been observed in prostate cancer, where the activation of androgen receptor induces mTOR nuclear translocation[118]. The mechanisms governing mTOR nuclear transportation have been investigated. With a molecular weight of 289 kDa, mTOR most likely relies on active import and export processes for nuclear transport through the nuclear pore. The absence of a classical nuclear localisation signal (NLS) in the primary sequence of mTOR implies a more intricate nuclear translocation mechanism. Notably, it has been reported that mTOR with double mutation L545A and L547A showed impairment in nuclear import[120]. However, a comprehensive understanding of mTOR nuclear import remains elusive. Potential scenarios include, for example, that mTOR might rely on other proteins which utilise the standard importin dependent nuclear import to enter the nucleus. Or a direct interaction with the nuclear pore complex as identified in other proteins, like β-catenin and Smad proteins, could be an alternative model[152]. In contrast, the nuclear export of mTOR is better understood. Nuclear mTOR accumulation in cells treated with leptomycin B, an inhibitor of the export receptor Crm1, suggests a Crm1-dependent export mechanism[153].

3.3. Potential mechanisms underlying gene regulation by mTOR

The CUT&Tag results in this study showed that the level of H2AT120ph at mTOR target genes was higher than at non-mTOR target control genes in mESCs and the dynamic changes of H2AT120ph during differentiation, where a transient increase of H2AT120ph at mTOR target genes was observed within the initial 12 hours (**Fig. 13**) hinted that mTOR may regulate gene expression via phosphorylating H2AT120. Here, it was proposed that mTOR may catalyse H2AT120ph which facilitates gene activation, potentially via antagonising the repressive H2AK119ub. Two histone kinases that catalyse the phosphorylation of H2AT120 have been reported, Bub1 and VRK1[154,155]. Bub1 is a crucial protein required for proper chromosome segregation in eukaryotes. Bub1 deposits H2AT120ph and phosphorylation of histone H3 threonine 3 mediated by Haspin create a binding site for Shugoshin proteins, which helps the chromosomal passenger complex to localise properly at the centre of paired kinetochores[154,156,157]. VRK1 has been reported to phosphorylate H2A T120 at the promoter region of *CCND1* and regulate its transcription in human cancer cell lines[158,159]. It is shown that the activation of *CCND1* is facilitated by the mutually exclusive nature of H2AT120ph and the repressive H2AK119ub[158]. No direct correlation was observed between the phosphorylation of H2AT120 catalysed by Bub1 and mTOR. However, the gene activation mechanism facilitated by VRK1 is more similar to the proposed model in this study. Comparing VRK1 and mTOR targets in mESCs would provide insights into the potential cross-talk between these two histone H2A kinases. Intriguingly, a recent study reported that inhibition of VRK1 suppresses the proliferation and migration of vascular smooth muscle cells via mTORC1/β-catenin pathway[160]. As demonstrated in this study, mTOR activity level is crucial for mESC, it would be worthy to examine whether VRK1 expression affects mTOR activity and mESC pluripotency.

Integrative analysis of CUT&Tag and TT-SLAM-seq techniques revealed an mTOR-dependent elevation of H2AT120ph levels and nascent transcription at mTOR target genes during mESC differentiation. However, the level of H2AK119ub and H3K27me3 remained relatively stable. H2AT120ph has been reported to antagonise H2AK119ub and promote oncogene expression in cancer cell lines[137]. The kinetics of H2AK119ub1 deposition and removal are rapid, whereas PRC2-dependent H3K27me3 addition and removal are far slower[41,142,161,162]. The absence of dynamic

changes in H2AK119ub observed in our data might be attributed to technical considerations. At the 24-hour differentiation time point, the mESC population consisted of both pluripotent and differentiated cells. Changes occurring specifically in differentiating cells could be attenuated when analysing bulk populations, particularly for histone marks that are more abundant in mESCs than in differentiated cells. The significance of utilising single-cell, single-molecule resolution techniques, coupled with genetic manipulation, becomes evident in recent studies that have yielded valuable insights into the Polycomb repressive system[41,142]. Additionally, the data processing methods, such as CPM normalisation, may have influenced the outcome by smoothing out subtle changes. Besides technical concerns, the stability of H2AK119ub could be attributed to the presence of an unknown phosphatase that removes H2AT120ph. Nonetheless, the strong correlation observed between mTOR and Polycomb repressive marks implies a probable intricate interplay between them. Nevertheless, the high correlation between mTOR and the Polycomb repressive marks suggests that there is likely a close crosstalk between them.

mTOR targets could be clustered into 3 different clusters based on the H2AK119ub level. The three clusters had different underlying PRC1 variants and were functionally distinct. This is consistent with previous studies reporting distinct gene targets of vPRC1 and cPRC1 in mESCs[144]. However, the relationship between mTOR and the Polycomb repressive system required more experiments to clarify.

3.4. Future perspectives

While this study unveiled unprecedented functions of mTOR in mESCs, it also raised intriguing questions worth further investigation. A key question is to identify nuclear mTOR interaction partners. Applying mass spectrometry or co-immunoprecipitation specifically targeting nuclear mTOR could yield insights into how mTOR regulates gene expression and how mTOR itself may be regulated within the mESC chromatin. This information potentially would also shed light on the mechanisms underlying mTOR's recruitment to the nucleus and chromatin. Single-molecule resolution live cell imaging could be used to track mTOR localisation in differentiation.

Three clusters of mTOR target promoters featuring distinct levels of H2AK119ub and PRC1 subunits were reported in this study. However, the relationship between mTOR and the Polycomb repressive system required more experiments to clarify.

PRC1 degron mESCs may help to address whether mTOR recruitment to chromatin is PRC1 dependent. As the level of H2AK119ub decreases rapidly after PRC1 degradation, it would be interesting to see the behaviour of H2AT120ph under such a situation[142]. It is worthy to apply degron cell lines targeting different subunits of the PRC1 to decipher mTOR regulation on its target genes.

In summary, this study uncovers a previously unknown function of mTOR in mESCs. mTOR associates with the promoters of developmental genes and potentially regulates their expression via catalysing H2AT120ph. Aberrant mTOR activity has been reported in various diseases, especially metabolic disorders and cancers[62]. It is hereby proposed that screening and investigation into similar roles of nuclear mTOR in other cells may lead to useful therapeutic insights.

4. Materials and Methods

4.1. Cell culture conditions and chemical treatments

4.1.1. serum/LIF mESCs culture

Wild-type and genetically modified E14 mESCs were cultured without feeders on 0.1% gelatin-coated dishes (Sigma-Aldrich, G1393) with daily media change and were passaged every other day. At each passage, cells were dissociated using TrypLE (Thermo Fisher, 12604-021) and replated at an appropriate density or a density specified by experiments. The DMEM/High glucose with Glutamax media (Thermo, 31966047) was supplemented with 15% FBS (Thermo, 2206648RP), 1x NEAA (Gibco, 11140-035), 1x Penicillin/streptomycin (Life Technologies, 15140148), 0.2% β-mercaptoethanol (Thermo, 21985023) and 1000 U/mL LIF (homemade). Cells were cultured at 37 °C in 20% O_2 and 5% CO_2 incubator.

4.1.2. 2i mESCs culture

For mESC cultured in 2i media, the N2B27 media (1:1 neurobasal media (Thermo, 21103-049) and DMEM/High glucose with Glutamax media, 1x NEAA, 1x Penicillin/streptomycin, 1x Glutamax (Thermo, 61870044), 15% BSA fraction V (Gibco, 15260-037), 0.2% β-mercaptoethanol (Thermo, 21985023)) was supplemented with 1 μM PD0325901 (Tebubio, 25704-0006), 3 μM CHIR-99021 (Sigma, SML1046) and 1000U/mL LIF. Other cultural conditions were the same as mentioned above.

4.1.3. Mouse embryonic fibroblasts

Mouse embryonic fibroblasts were cultured in MEF media (DMEM/High glucose with Glutamax media (Thermo, 31966047), 10% (v/v) FBS (Thermo, 2206648RP) and 1x Penicillin/streptomycin (Life Technologies, 15140148)).

4.1.4. Chemical treatments and differentiation

The chemicals used to treat mESCs were 200 nM INK-128 (MedChemExpress/Biozol, MCE-HY-13328), 100 nM cycloheximide (Biomol, 54646.1) and 200 nM rapamycin (MedChemExpress, HY-10219) dissolved in DMSO (Sigma-Aldrich, D2650). The mESCs were first washed once in PBS and

supplemented with fresh LIF+ media containing respective chemicals for 1 hour. Next, the cells were then washed once in PBS before being supplemented with fresh LIF- media containing respective chemicals for the indicated period of time.

4.2. Generation of the mTOR degron mESC cell line

The design and cloning strategy of endogenous tagged FKBP^{F36V}-mTOR mESCs using the CRISPR-PITCh system were based on Nabet et al and Sakuma et al (**Fig. 20**)[128,134]. Two plasmids were necessary for the transfection of mESCs. The first plasmid, pX330A-Mtor/PITCh, contained a mouse mTOR specific gRNA and a PITCh-gRNA (**Fig. 20a**). The second plasmid, pCRIS-PITChv2-Puro-dTAG(MTOR), harbored the FKBP^{F36V} cassette with mouse mTOR specific homology ends flanked by PITCh-gRNA target sites (**Fig. 20b**). During co-transfection into mESCs, the PITCh-gRNA would free the FKBP^{F36V} cassette from its plasmid backbone. While the mTOR specific gRNA initiated cleavage of the targeted genomic loci. The insertion of the FKBP^{F36V} cassette was facilitated by the presence of corresponding 5'- and 3'-homology ends. The sequences of the oligos and primers used for the cloning are listed in **Table. 1**.

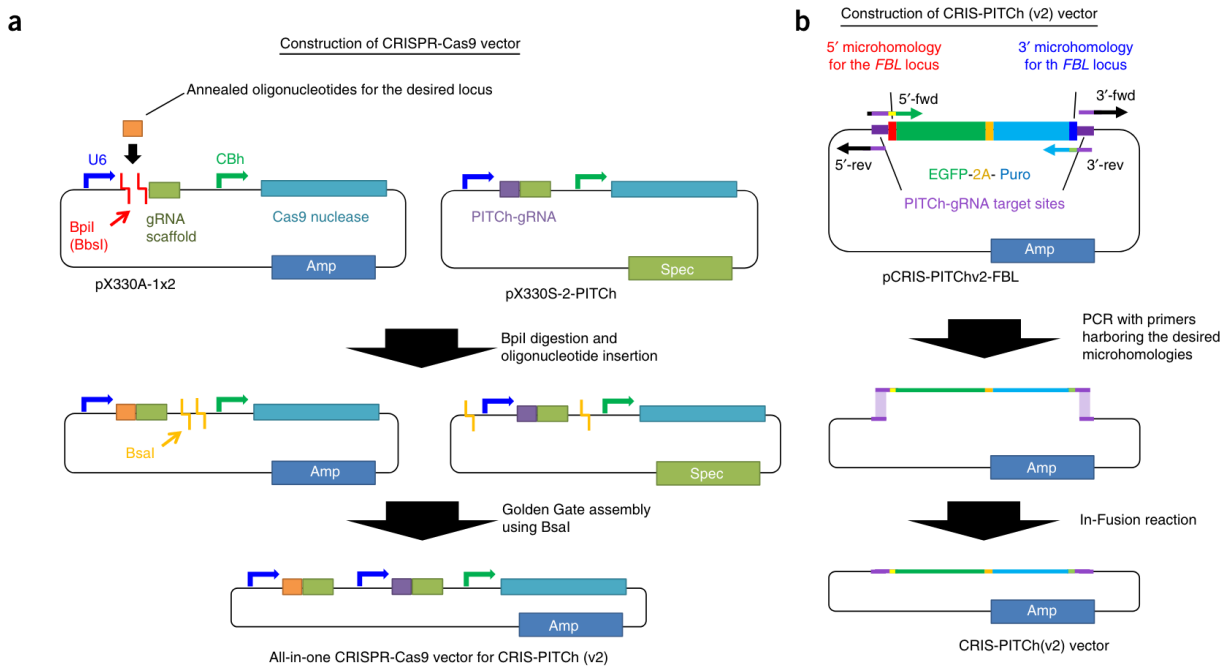

Figure 21 | A schematic illustration of vector construction for CRISPR-PITCh gene knock-in[134]. a. Construction of pX330A-Mtor/PITCh. The all-in-one plasmid contains sequences of a Cas9 nuclease (tranquil box) and two gRNAs, an mTOR

specific gRNA (orange box) and a generic PITCh-gRNA (purple box). Amp, ampicillin resistance gene; Spec, spectinomycin resistance gene; U6, human U6 promoter; CBh, chicken β-actin short promoter. **b.** Construction of the CRIS-PITCh donor vector, pCRIS-PITChv2-Puro-dTAG(MTOR), harbouring microhomologies for the mouse *MTOR* locus.

4.2.1. Construction of pX330A-Mtor/PITCh

A gRNA targeting the first mTOR coding exon (exon 2) was designed using Benchling. Oligos containing the mTOR gRNA sequences and the sticky ends corresponding to pX330A-1x2 (Addgene #58766) were purchased as standard PCR primers.

To prepare the oligos carrying the mTOR sgRNA sequences for further use, the oligonucleotides Mtor_dTAG_sgRNA_FWD and Mtor_dTAG_sgRNA_REV were annealed and phosphorylated. Specifically, 1 µl of each oligo (at a concentration of 100 µM) was mixed with the T4 Polynucleotide kinase (NEB, M0201L) in the T4 DNA ligase reaction buffer (NEB, B0202S). The reaction was performed at 37 °C for 30 minutes and terminated by incubation at 95 °C for 5 minutes. Immediately afterwards, the sample was left standing at room temperature for 30 minutes to cool down. The annealed mTOR sgRNA oligos were subsequently diluted 1:200 in water. One µl of the diluted mTOR sgRNA was then ligated with the pX330A-1x2 (50 ng) using the T4 DNA ligase (NEB, M0202S) in the T4 DNA ligase reaction buffer at room temperature for 10 minutes. The ligation products were used to transform *E. coli* (*DH5α*) on an ampicillin selection plate. Single colonies were picked and the proper insertion of the mTOR sgRNA sequence to pX330A-1x2-Mtor was verified through Sanger sequencing (with the primer U6_seq_F). This intermediate plasmid was named as pX330A-1x2-Mtor.

To create the all-in-one plasmid pX330A-Mtor/PITCh (**Fig. 20a**), the golden gate assembly was employed. The process assembles the two plasmids, pX330A-1x2-Mtor from previous steps and pX330S-2-PITCh (Addgene #63670), to the desired all-in-one plasmid pX330A-Mtor/PITCh. Specifically, the golden gate assembly was performed by mixing 75 ng of pX330A-1x2-Mtor, 150 ng of pX330S-2-PITCh, BsaI-HFv2 (NEB, R3733S), Quick ligase (NEB, M2200L) and T4 DNA ligase reaction buffer in a 20 µl reaction. The sample was incubated in a thermal cycler with the program: (37 °C, 5 min → 16 °C, 10 min) × 25 → 4 °C on

hold. Afterwards, an additional digestion step to eliminate the intact pX330A-1x2-Mtor was performed to decrease the number of blue colonies in later steps. This was achieved by adding NEBuffer 4 (NEB, B7004S), BSA (NEB, B9000S) and BsaI-HF to the reaction, resulting in a final reaction volume of 25 µl. The sample was incubated at 37 °C for 30 minutes followed by 80 °C for 5 minutes. The digested assembled products were then used to transform *E. coli* (*DH5α*). Single colonies were picked and the correct sequence of pX330A-Mtor/PITCh was confirmed using Sanger sequencing (with the primers PITCh-colony-FWD and PITCh-colony-REV).

4.2.2. Construction of pCRIS-PITChv2-Puro-dTAG(MTOR)

The construction of pCRIS-PITChv2-Puro-dTAG(MTOR) involved the replacement of microhomologies originally corresponding to the *BRD4* gene in pCRIS-PITChv2-Puro-dTAG(BRD4) (Addgene #91793) with those specific to the mouse *MTOR* gene.

To amplify the knock-in $FKBP^{F36V}$ cassette from pCRIS-PITChv2-Puro-dTAG(BRD4), specific primers (Mtor dTAG cassette-FWD and -REV) were designed to incorporate microhomologies for mouse MTOR (exon 2). Notably, the cut site introduced by the mTOR sgRNA is 4 base pairs downstream of the transcription start site. Therefore, special consideration was taken to correct the frameshift during the primer design.

With this pair of primers, the cassette PCR was performed using the Q5 Hot Start High-Fidelity 2X Master Mix (NEB, M0494L) with the following thermal cycles: 98 °C, 30 sec → (98 °C, 10 sec → 72 °C, 45 sec) × 27 → 72 °C, 2 min → 12 °C on hold. The resulting PCR products were separated and visualised on an agarose gel, and the band with the size of 1215 bp was isolated and purified using the QIAquick Gel Extraction Kit (Qiagen, 28706).

Subsequently, the knock-in $FKBP^{F36V}$ cassette was assembled with pCRIS-PITChv2-Puro-dTAG(BRD4), which had been previously digested with MluI-HF (NEB, R3198S). This assembly was achieved using the NEBuilder HiFi DNA Assembly Master Mix, maintaining a vector-to-insert ratio of 1:2.

The assembly products were used for the transformation of *E. coli (DH5α)*. Single colonies were picked and the sequence of pCRIS-PITChv2-Puro-dTAG(MTOR) was verified using Sanger sequencing (with the primers dTAG-seq-FWD, and -REV).

4.2.3. mESCs transfection and characterisation of monoclonal cell lines

The co-transfection of pX330A-Mtor/PITCh and pCRIS-PITChv2-Puro-dTAG(MTOR) into mESCs was carried out using the Amaxa 4D Nucleofector X Unit (Lonza), following the manufacturer's instructions. Subsequently, two days after nucleofection, the mESCs were subjected to selection using puromycin (Sigma, A1113803) for a minimum of 5 days. Individual mESC clones that survived the process were isolated and expanded to establish monoclonal cell lines.

To screen for the presence of positive insertion and accurate sequences, the clones underwent genotyping via PCR, using the following primer combinations: [geno-Mtor-ex2-F1 and geno-Mtor-ex2-R] and [geno-Mtor-ex2-F2, and geno-Mtor-ex2-R]. The first primer combination was designed to amplify the wild-type mTOR allele, without insertion. The second primer combination was aimed to amplify the mTOR allele with knocked-in $FKBP^{F36V}$ cassette.

In cases where clones exhibited a positive insertion, the exact insertion sequence was further verified. The transgene sequences were first amplified via PCR using the primers geno-seq-Mtor-dTAG-F and geno-seq-Mtor-ex2-R. However, the amount of purified DNA after gel purification would not be sufficient for Sanger sequencing. To obtain an adequate amount of material, the purified PCR products were subsequently cloned into a pJET plasmid using the CloneJET PCR Cloning Kit (Thermo, K1231) following the manufacturer's instructions.

The monoclonal mESC cell lines were then subjected to the degradation test after dTAG-13 treatment. The mESCs were exposed to 500 nM dTAG-13 (Torcis, 6605) for the specified durations. After treatment, the cells were subjected to protein extraction and subsequent western blot analysis to examine the effects of dTAG-13 on the amount of mTOR in the cell lines.

4.3. Alkaline phosphatase staining and imaging

The alkaline phosphatase staining was done using the Vector Red Substrate Kit (Vector Laboratories, VEC-SK-5100) following the manufacturer's guidelines. The mESCs were washed once in PBS and incubated with the freshly made substrate working solution (For 5 ml of 100 mM Tris-HCl, pH 8.2, added 2 drops of Vector Red Reagent 1, 2 drops of Vector Red Reagent 2 and 2 drops of Vector Red Reagent 3)

at 37 °C for 20 minutes. The substrate working solution was removed and the cells were washed in PBS for 10 minutes at 37 °C before imaging. The bright field images were taken by an Olympus CKX53 microscope.

4.4. mTOR ChIP-seq and ChIP-qPCR

4.4.1. ChIP sample preparation

One day before sample preparation, mESCs were seeded on a 10-cm dish at the density of 1.5 $\times 10^6$ cells per dish. To obtain one final ChIP-seq sample, two plates were needed.

On the day of preparation, mESCs were first washed once in PBS and then incubated with 1% formaldehyde at room temperature for 10 minutes in the dark with gentle shaking. The formaldehyde was freshly diluted in PBS from a newly opened ampule (Thermo Fisher Scientific, 28906) on the day of preparation and kept in the dark whenever possible to minimise the spontaneous polymerisation of formaldehyde. After the 10-minute fixation, glycine was immediately added to the cells to quench the reaction. The cells were incubated at room temperature for 5 minutes in the dark with gentle shaking. The quantity of glycine added depended on the original volume of 1% formaldehyde. The final concentration of glycine was 125 mM.

After fixation, the cells were then washed 2 times in ice-cold PBS. They were subsequently incubated at 4 °C in 5 ml of swelling buffer (25 mM HEPES, pH 7.9, 1.5 mM $MgCl_2$, 10 mM KCl, 0.1% Igepal 630, 1x protease and phosphatase inhibitor cocktail (Thermo Fisher, 78443), 1 mM PMSF, 1 mM NaVO3, 5 mM NaF) for 10 minutes with gentle shaking to prepare the cells for nuclei isolation. From this step on, the samples were handled and kept at low temperatures whenever possible. To collect the nuclei, the cells were scraped on ice using a cell scraper, passed through an 18G needle 5 times, and spun at 3000 x g for 5 minutes at 4 °C. The nuclei pellets were then resuspended in 1 ml of sonication buffer (50 mM HEPES, pH 7.9, 140 mM NaCl, 1 mM EDTA, 1% Triton X-100, 0.1% sodium deoxycholate (Thermo Fisher Scientific, 89904), 0.1% SDS, 1 mM PMSF, 1 mM NaVO3, 5 mM NaF) and were incubated on ice for 10 minutes.

Subsequently, the 1 ml nuclei suspension was transferred to a milliTUBE 1 ml AFA Fiber (Covaris, 520130) and underwent sonication using an E220 Evolution Covaris

sonicator. To shear the chromatin to an average size of 500-1000 bp, 6 cycles of sonication were conducted, each lasting 1 minute. The manufacturer's instructions were followed for settings other than the number and duration of the sonication cycle. The choice of a broader range of chromatin sizes was made due to the uncertainty of whether mTOR directly binds to DNA. This approach allowed for flexibility in subsequent analyses.

Chromatin immunoprecipitation (ChIP) was performed by mixing chromatin, corresponding to 25 µg of DNA, 1µg of mTOR antibody (Abcam, ab32028) and 20 µl of Protein A dynabeads (Thermo Fisher Scientific, 10002D), which had been priorly subjected to washing and resuspension in sonication buffer. The ChIP reaction was conducted at 4 °C with rotation overnight. In parallel, an input control was established. 0.25 µg of the chromatin (representing 1% of the total) was preserved in sonication buffer, with a final volume of 100 µl. The input control was set aside at 4 °C while the ChIP was in progress.

After the ChIP procedure, the beads were subjected to sequences of washing to reduce unspecific binding. The washing steps included twice in a sonication buffer, once in a high salt wash buffer (same composition as sonication buffer but with 500 mM NaCl) and once in a TE buffer (10 mM Tris-HCl, pH 8.5, 1 mM EDTA, 1% SDS). Subsequently, the beads were resuspended in 100 µl of freshly made elution buffer (50 mM Tris-HCl, pH 7.5, 1 mM EDTA, 1% SDS).

The subsequent steps were to release the DNA from chromatin following the ChIP procedure, the samples were treated with RNase and proteinase. Note that both the ChIP samples and the input control were processed the same way. First, 1 µl of RNaseA (Thermo Fisher Scientific, EN0531) was added to the samples and incubated at 37 °C for 30 minutes with vigorous shaking. Afterwards, a Proteinase K treatment was carried out. Five µl of Proteinase K (NEB, P8107S) was added to the samples and the samples were incubated at 65 °C for 2 hours or up to overnight with vigorous shaking. The DNA was purified using the ChIP DNA Clean & Concentrator (D5205, Zymo Research) and the DNA concentration was determined using Qubit dsDNA HS Assay (Invitrogen, Q32851) following the manufacturer's instructions. The ChIPped DNAs were then used for qPCR analysis or further processing before sequencing.

4.4.2. ChIP-qPCR

The quality of the ChIP DNAs was controlled using ChIP-qPCR. ChIP-qPCR primers were designed to target mTOR positive and negative binding regions (Table 2). For each ChIP-qPCR reaction, 3 technical replicates were included. The ChIP DNAs were first diluted 1:100 in PCR water and mixed with corresponding primers and the KAPA SYBR FAST qPCR Master Mix (2X) ABI Prism (Thermo Fisher Scientific, KK4617). The amplification and detection were performed on a QuantStudio 7 Flex Real-Time PCR System (Applied Biosystems) thermal cycler.

The percentage of input method was used to assess the enrichment of mTOR binding. First, the Ct value of the 1% input was subtracted by 6.644, resulting in the adjusted input value, which corresponds to 100% input. The mTOR enrichment of a target was then calculated by 100 × 2^(adjusted input - the Ct value of the target).

4.4.3. Sequencing

For all ChIP-seq, 2 biological replicates were conducted. Before library preparation, the ChIPped DNAs were sonicated for 15 seconds on an E220 Evolution Covaris sonicator. This is necessary to bring the DNA fragment size to below 700 bp, which is the upper limit specified by the library preparation kit. The ChIP libraries were prepared using the KAPA Hyper Prep Kit (Roche, 7962363001). The library preparation was carried out by the Sequencing Core facility at the Max Planck Institute for Molecular Genetics. Samples were sequenced on a NovaSeq 6000 with 100-bp paired end mode and approximately 50 million fragments per library.

4.5. CUT&Tag

Cleavage Under Targets and Tagmentation (CUT&Tag) on cryopreserved nuclei was based on Kaya-Okur et al with minor modifications[138]. For all CUT&Tag experiments, 2 biological replicates were conducted.

4.5.1. Preparation of cryopreserved nuclei

Cells from one plate of 10-cm dish were dissociated using accutase (Sigma-Aldrich A6964) and washed in PBS. Importantly, trypsin should not be used as it interferes with the subsequent binding of nuclei to Concanavalin A beads. Nuclei were extracted by resuspending the cells in an ice-cold NE1 buffer (20 mM HEPES,

pH7.5, 10 mM KCl, 0.5 mM Spermidine, 0.1% Triton X-100, 20% glycerol, 1 mM PMSF, 5 mM NaF, 1 mM Na_3VO_4, 1x protease phosphatase inhibitor cocktail (Thermo Fisher, 78443)) and incubating on ice for 10 min. The nuclei were pelleted by being centrifuged for 4 min at 1300 x g at 4 °C. After the removal of supernatant, the nuclei were briefly fixed in 0.1% formaldehyde at room temperature for 2 min followed by adding glycine (final concentration = 1.25 M) to stop the cross-linking. The formaldehyde was freshly diluted in PBS from a newly opened ampule (Thermo Fisher Scientific, 28906) on the day of preparation and kept in the dark whenever possible to minimise the spontaneous polymerisation of formaldehyde. The fixed nuclei were centrifuged for 4 minutes at 1300 x g at 4 °C and the pellet was resuspended in a Wash buffer (20 mM HEPES-KOH, pH 7.5, 150 mM NaCl, 0.5 mM Spermidine, 1 mM PMSF, 5 mM NaF, 1 mM Na_3VO_4, 1x protease phosphatase inhibitor cocktail) with the addition of 10% DMSO. The nuclei suspensions were cryopreserved at -80 °C until further processing.

4.5.2. CUT&Tag library preparation

The cryopreserved nuclei were quickly thawed by immersing the tubes in room temperature water. The morphology and the number of nuclei were assessed using trypan blue staining and a cell counter. Nuclei of high quality were characterised by their positive trypan blue staining and well-defined, round edges. Additionally, the overall purity of the nuclei preparation was assessed by the absence of cellular debris in the background. This quality control step ensured the suitability of the nuclei for subsequent experimental procedures. For each CUT&Tag reaction, 1×10^4 nuclei were aliquoted and set aside. For one CUT&Tag reaction, 3.5 µl of the Concanavalin A beads (Polysciences, 86057) was used. Throughout the procedure, extra precautions were taken to prevent the beads from drying out. The beads were initially equilibrated by subjecting them to two washes in 100 µl of Binding buffer (20 mM HEPES-KOH, pH 7.5, 10 mM KCl, 1 mM CaCl2, and 1 mM MnCl2). Following this equilibration, the beads were carefully concentrated back to their original volume in the Binding buffer. To bind the nuclei to the beads, 3.5 µl of Concanavalin A beads were added to 1×10^4 thawed cryopreserved nuclei. This mixture was incubated for 10 minutes with rotation at room temperature.

Subsequently, the nuclei-bound beads progressed through a sequence of in situ hybridization steps, including primary antibody, secondary antibody, and 3xFLAG-pA-Tn5 preloaded with Mosaic-end adapters (homemade). After the nuclei-bound beads were separated using a magnet, they were resuspended in 25 µl of cold Antibody buffer (Wash buffer with 0.1% BSA). Within this buffer, the appropriate primary antibody or IgG (Table 3) was diluted and added. The hybridisation of the primary antibody took place at 4 °C with gentle nutation overnight. Special care was taken to prevent the beads from drying out on the tube wall during this long incubation. Following the overnight primary antibody incubation, the beads were separated from the primary antibody using a magnet. To amplify the signals, the separated beads were then resuspended in 25 µl of Wash buffer containing the matching secondary antibody (guinea pig α-rabbit antibody, 1:100, (Antibodies online, ABIN101961)). The binding of the secondary antibody took place at room temperature for 30 minutes with gentle nutation. Following the secondary antibody incubation, the beads were once again separated from the secondary antibody using a magnet. The beads were washed one time in 200 µl of Wash buffer while being maintained on a magnet to remove any unbound antibodies before proceeding with the hybridization of 3xFLAG-pA-Tn5. The 3xFLAG-pA-Tn5 was diluted 1:250 in 300-wash buffer (20 mM HEPES-KOH, pH 7.5, 300 mM NaCl, 0.5 mM Spermidine, 1 mM PMSF, 5 mM NaF, 1 mM Na_3VO_4, 1x protease phosphatase inhibitor cocktail) and 25 µl of it were used to resuspend the beads. The elevated NaCl concentration in the 300-wash buffer, in contrast to the standard Wash-buffer, was essential to inhibit the activity of 3xFLAG-pA-Tn5. The beads were incubated for 1 hour at room temperature with gentle nutation. After binding of 3xFLAG-pA-Tn5, the beads were washed once in 200 µl of 300-wash buffer while being held on a magnet to remove excess 3xFLAG-pA-Tn5. The beads were then ready for the tagmentation process.

The tagmentation process involved resuspending the beads in 50 µl of Tagmentation buffer (10 mM $MgCl_2$ in 300-wash buffer). This incubation was carried out for 1 hour at 37 °C. The presence of Mg^{2+} in the Tagmentation buffer was a crucial component in activating 3xFLAG-pA-Tn5. Tagmentation was stopped by adding 2.25 µl of 500 mM EDTA and 2.75 µl of 10% SDS to the beads. Additionally, 0.5 µl of Proteinase K (20 mg/ml, Invitrogen, AM2546) was added. The beads were subjected to vortex for 10 seconds before being incubated at 55 °C for 1 hour, or an extended period

overnight, to release the DNA fragments. The Proteinase K treatment was partially halted by increasing the incubation temperature to 70 °C for 30 minutes. The beads were separated from the liquid containing solubilised DNA on a magnet. The DNAs were purified from the liquid using the ChIP DNA Clean & Concentrator (D5205, Zymo Research) following the manufacturer's instructions. The CUT&Tag DNA was eluted in a final volume of 25 µl of elution buffer.

To amplify the NGS libraries, a total of 21 µl of the CUT&Tag DNA was mixed with 25 µl of NEBNext HiFi 2x PCR Master Mix (New England BioLabs, M0541L), along with 2 µl of 10 µM i5- and 2 µl of 10 µM i7- unique barcoded primers[163]. The PCR amplification was carried out using the following program on a thermocycler with the program: 72 °C, 5 min → 98 °C, 30 sec → (98 °C for 10 sec → 63 °C, 10 sec) × 16 → 72 °C, 1 min → 8 °C on hold. Note that as suggested by the original paper, the cycling parameters are optimised for a conventional Peltier cycler. The ramping times were designed to allow adequate annealing during the gradual cooling from 98 °C to 60 °C. For post-PCR cleanup, 55 µl (1.1x volume) of the Ampure XP beads were added to the PCR mix and incubated for 10 minutes at room temperature. The beads were then separated and washed two times using 80% ethanol on a magnet. Finally, the CUT&Tag libraries were eluted in 25 µl of Tris-HCl (pH 8.0).

4.5.3. Sequencing

The quality of the CUT&Tag libraries was assessed using Agilent High Sensitivity D5000 ScreenTape System (Agilent, 5067-5592) and Qubit dsDNA HS Assay (Invitrogen, Q32851). Sequencing libraries were pooled in an equimolar ratio and further concentrated using 1.1x volume of Ampure XP beads to reach a final volume ideal for sequencing (~ 20 µl). The libraries were sequenced on a NovaSeq 6000 with 100-bp paired end mode, generating approximately 5 million fragments per library.

4.6. Protein extraction and western blotting

4.6.1. Whole cell protein extraction

Cells were lysed using RIPA buffer (Thermo Fisher, 89901) following the manufacturer's instructions. The RIPA buffer was supplemented with a protease and

phosphatase inhibitor cocktail (Thermo Fisher, 78443). The lysates were first incubated at 4 °C with occasional vortex for 30 min and then sonicated for 5 cycles (30 sec ON, 30 sec OFF) using a Bioruptor (Diagenode). The lysates were spun at 14000 x g for 30 minutes at 4 °C and the supernatants were collected. The protein concentration was quantified using BCA assay (Thermo Fisher, 23225) and an equal amount of protein (5 to 20 µg) was used for each experiment. Lastly, the protein extracts were mixed with 1x Laemmli Sample Buffer and 5% β-mercaptoethanol and boiled for 5 min at 99 °C.

4.6.2. Subcellular fractionation of cytoplasm, nucleus and chromatin

For each preparation, 5×10^6 mESCs were harvested and washed once in cold PBS before being spun down at 1000 x g for 5 minutes. To permeabilise the cytoplasm and the nuclei, the cell pellets were resuspended in 500 µl of Buffer A (10 mM HEPES pH 7.9, 10 mM KCl, 340 mM sucrose, 10% glycerol, 1 mM DTT, 0.1% Triton X-100, 1x protease and phosphatase inhibitor cocktail, 1 mM PMSF, 5 mM NaF, 1 mM Na_3VO_4) and incubated on ice for 10 minutes. The cell lysates were centrifuged at 1300 x g for 5 minutes at 4 °C to separate the cytoplasmic fraction and the nuclei. The cytoplasmic supernatants were collected in new tubes and stored on ice until the extraction of nuclear and chromatin fractions was completed. The nuclei pellets were washed once in Buffer A and spun at 1300 x g for 5 minutes at 4 °C to minimise the risk of cytoplasmic contamination. To permeabilise the nuclei, the pellets were then resuspended in 500 µl of Buffer B (3 mM EDTA, 0.2 mM EGTA, 1 mM DTT, 1x protease and phosphatase inhibitor cocktail, 1 mM PMSF, 5 mM NaF, 1 mM Na_3VO_4) and incubated on ice for 5 minutes. The lysates were spun at 1700 x g for 5 minutes at 4 °C and the supernatants containing the nucleoplasmic fraction were transferred to new tubes on ice. The pellets containing insoluble chromatin were resuspended in 100 µl of 1x Laemmli Sample Buffer (Bio-Rad, 161-0747) and 5% β-mercaptoethanol and sonicated using the Bioruptor for 5 cycles (30 sec ON, 30 sec OFF). Finally, the cytoplasmic and nucleoplasmic fractions were mixed with 1x Laemmli Sample Buffer and 5% β-mercaptoethanol. Together with the chromatin fraction, all samples were boiled at 99 °C for 5 minutes.

4.6.3. SDS-PAGE and western blotting

The denatured samples were loaded on a 4-15% Mini-PROTEAN TGS precast protein gel (Bio-Rad, 4561083) and separated by electrophoresis at 200 V for 30 min using 1x Tris/Glycine/SDS running buffer (Bio-Rad, 1610772). The proteins were transferred to a PVDF membrane (Thermo Fisher IB24001) using the pre-programmed method P0 on an iBlot2 gel transfer device (Thermo Fisher IB21001). The PVDF membranes were incubated in a blocking buffer (5% non-fat milk in 1x TBST (Thermo Fisher, 28360)) at room temperature for 30 min. The membranes were then incubated with primary antibodies diluted in the blocking buffer at 4 °C overnight (**Table 3**). The membranes were washed 3 times in 1x TBST for 30 min before being subjected to 1-hour secondary antibody incubation at room temperature (**Table 3**). The membranes were washed 3 times in 1x TBST for 30 min before detection using SuperSignal WestDura duration substrate (Thermo Fisher, 34075). The blots were imaged on a ChemiDoc imaging system (Bio-Rad).

4.7. Generation of PiggyBac mTOR overexpression mESCs

The PiggyBac overexpression system is composed of 2 plasmids, the PiggyBac transposon plasmids, containing the cargos and the PiggyBac transposase plasmid. The PiggyBac transposase plasmid was shared by the Meissner department at the Max Planck Institute of Molecular Genetics.

In total, 3 variants of transposon plasmids were generated, including a wild-type mTOR, a hyperactive mTOR, and a kinase dead mTOR (Fig. 18a). The sequences between the 3'- and 5'-ITR of the PiggyBac transposon plasmids, pSLQ2818 pPB plasmid (Addgene, #84241), were replaced by gene cassettes containing the wild-type mTOR, the hyperactive mTOR, or the kinase dead mTOR. Specifically, the gene cassette of the wild-type mTOR transposon plasmid is composed of mCherry, P2A, FLAG-tag, and the wild-type mTOR amplified from pcDNA3.1-FLAG-mTOR. The gene cassette of the kinase dead mTOR transposon plasmid is composed of mCherry, P2A, FLAG-tag, and the kinase dead mTOR amplified from pcDNA3.1-FLAG-mTOR^{SL1+IT}. Both pcDNA3.1-FLAG-mTOR and pcDNA3.1-FLAG-mTOR^{SL1+IT} were generous gifts from Prof. Tatsuya Maeda, Hamamatsu University School of Medicine[145]. The gene cassette of the kinase dead mTOR transposon plasmid is composed of mCherry, P2A, myc-tag, and the kinase

dead mTOR, amplified from a myc-mTOR kinase dead plasmid (Addgene, #8482). The sequences were confirmed using Sanger sequencing.

The PiggyBac transposon plasmids and the PiggyBac transposase plasmids were co-transfected in a 6:1 ratio into mESCs using an Amaxa 4D Nucleofector X Unit (Lonza) according to the manufacturer's instructions. To screen for positive integrations, 3-4 days after transfection, the cells were sorted based on the mCherry fluorescent level using a FACS Aria II flow cytometry (Becton Dickinson), followed by a second sorting another 3-4 days afterwards. The second sorting was needed to filter out cells with only transient overexpression. FACS sorting was conducted by the FACS core facility at the Max Planck Institute of Molecular Genetics.

4.8. *In vitro* mTOR kinase assay

The mTOR kinase assay was adapted from Sanack et al. and further refined through consultation with other relevant studies[87,112,136]. The radioactive experiments were conducted in a certified radioactive laboratory supervised by Dr. Heinrich Schrewe at the Max Planck Institute of Molecular Genetics. Dr. Heinrich Schrewe provided necessary radioactive safety training and technical expertise.

For each reaction, a full 10-cm plate of mESCs was used. The cells were scraped and harvested in 500 µl of lysis buffer (40 mM HEPES pH 7.4, 2 mM EDTA, 10 mM pyrophosphate, 10 mM glycerophosphate, 0.3% (w/v) CHAPS, 1x protease and phosphatase inhibitor cocktail), followed by centrifugation for 10 minutes at 13000 x g at 4 °C. To immunoprecipitate mTOR from mESC, the supernatants were combined with 20 µl of Protein A dynabeads (pre-washed 3 times in lysis buffer) and 1 µg of mTOR antibody (Abcam, ab32028). The mixture was incubated at 4 °C with rotation for 3 hours. Subsequently, the beads underwent a sequence of washing steps to reduce nonspecific IP binding. The washing steps contained three times washes in a low salt buffer (40 mM HEPES pH 7.4, 2 mM EDTA, 10 mM pyrophosphate, 10 mM glycerophosphate, 0.3% (w/v) CHAPS, 150 mM NaCl) and two additional washes in a washing buffer (25 mM HEPES pH 7.4, 20 mM KCl). To perform the kinase assay, the beads were suspended in 20 µl of kinase buffer (25 mM HEPES pH 7.4, 50 mM KCl, 20 mM MgCl2, 250 µM [γ-32P]-ATP (0.5 µCi/µl, Perkin Elmer, BLU502H250UC) and 1 µg of recombinant histones. For negative control or nonradioactive kinase assay, the radioactive [γ-32P]-ATP was replaced by

nonradioactive ATP (NEB, P0756S). The reactions were conducted at 30 °C for 45 minutes with vigorous shaking. The reactions were stopped by adding 1x Laemmli buffer followed by boiling for 5 minutes. The samples were analysed by SDS-PAGE. In the case of the radioactive kinase assay, the imaging film was developed overnight. For the non-radioactive kinase assay, the SDS-PAGE was continued to be analysed by western blot using an antibody against H2AT120ph (1:1000, Active Motif, 39391). The procedures of the SDS-PAGE and the western blot analysis were the same as described above in 4.6.3.

4.9. TT-SLAM-seq

TT-SLAM-seq was performed in 2 biological replicates and the procedures were described previously[139]. TT-SLAM-seq was a collaborative effort with Dr. Henri Niskanen, a postdoctoral researcher from the Hniz lab at the Max Planck Institute of Molecular Genetics. Cell culture and the 4-thiouridine labelling were conducted by me while the Qiazol samples were processed by Dr. Henri Niskanen to generate sequencing libraries.

To label the nascent transcription, mESCs were washed once in PBS and supplemented with fresh medium containing 500 µM of 4-thiouridine (4sU, Sigma, T4509). The labelling was performed in the dark at 37 °C for precisely 15 minutes. After labelling, the cells were immediately lysed using Qiazol (Qiagen, 79306) and frozen at -80 °C. Once all conditions and replicates were collected, all samples were processed under the same conditions.

Qiazol and 24:1 chloroform:isoamylalcohol (Sigma) was used to extract total RNA. 0.1 mM dithiothreitol (DTT) was used in isopropanol precipitation and ethanol washes. For each sample, 50 µg of total RNA was fragmented with a Magnesium RNA Fragmentation Module (NEB, E6150S), and the fragmentation buffer was removed from samples with ethanol precipitation in the presence of 0.1 mM DTT. RNA was then resuspended in 350 µl RNase-free water, diluted in biotinylation buffer (200 mM HEPES pH 7.5, and 10 mM EDTA) and topped up with 5 µg MTS-Biotin (previously diluted to 50 µg ml–1 in dimethylformamide, Hölzel, B-90066-1) to reach a final volume of 500 µl. The biotinylation reaction was incubated for 30 min at room temperature while keeping samples in rotation and protected from light. Unbound biotin was removed with acid-phenol:chloroform extraction (125:24:1, Ambion) and

isopropanol precipitation. Biotinylated RNA was resuspended in 100 µl RNase-free water, denatured at 65 °C for 10 min and then cooled on ice for 5 min. The biotinylated RNA was captured with 100 µl µMACS streptavidin beads (Miltenyi, 130-074-101) by incubating for 15 min in rotation while keeping samples protected from light. µMACS columns were equilibrated on a magnetic stand with a nucleic acid equilibration buffer and two times with biotinylation buffer (20 mM HEPES, 1 mM EDTA pH 8). Beads were transferred to columns and washed three times with wash buffer (100 mM Tris-HCl pH 7.5, 10 mM EDTA, 1 M NaCl and 0.1 % Tween 20), and labelled RNA was eluted twice with a total of 200 µl of 100 mM DTT. RNA was cleaned up with RNeasy MinElute columns (Qiagen, 74204) and eluted to RNase-free water with 1 mM DTT. 4sU residues of RNA were alkylated with iodoacetamide treatment (10 mM iodoacetamide in 50 mM NaPO4, pH 8 and 50 % DMSO) by incubating samples in 50 °C for 15 min, followed by quenching with 20 mM DTT. RNA samples were purified with ethanol precipitation and treated with Turbo DNase (Invitrogen, AM1907).

Sequencing libraries were prepared with NEBNext Ultra II Directional RNA Library Prep Kit and NEBNext Multiplex Oligos (NEB, 47760S), according to the manufacturer's instructions, except that an 8 minutes incubation time in the fragmentation step was used. The libraries were sequenced on a NovaSeq 6000 with 100-bp single end mode and approximately 75 million fragments per library.

4.10. Computational analyses

The computational analyses were in collaboration with Persia Akbari Omgba, a bioinformatic doctoral candidate in the lab. The data processing pipelines, including data preprocessing, filtering, mapping and up to peak calling for ChIP-seq and CUT&Tag were developed by me. For TT-SLAM-seq, the data processing pipeline was provided by Dr. Henri Niskanen, a postdoctoral researcher from the Hniz lab at the Max Planck Institute of Molecular Genetics. Persia Akbari Omgba, a doctoral candidate in the lab, fine tuned the parameters and adjusted the scripts to accommodate the large dataset. The comparative and integrative analyses were developed by Persia Akbari Omgba. The conceptual input provided by me influenced all stages of the study.

The computational analyses were done either by the indicated tools or in R (4.2.2)[164]. The TSS of the mouse genes were extracted using either

TxDb.Mmusculus.UCSC.mm10.knownGene (3.10.0) or TxDb.Mmusculus.UCSC.mm9.knownGene (3.2.2) from Bioconductor (1.30.20)[165–167]. Gene ontology analysis was carried out using clusterProfiler (4.6.0) with a cut-off of 0.05 for p-values and 0.1 for q-values[168]. The p-values were corrected using the Benjamini-Hochberg procedure.

The following tools were used for visualisations, deepTools (3.5.1) plotHeatmap and R packages: ComplexHeatmap (2.15.1), ggplot2 (3.4.1), and gghalves (0.1.4)[169–172]. Genome browser tracks were generated using fluff (2.1.3)[173].

4.10.1. mTOR ChIP-seq

The fastq files were first trimmed with Trim Galore! using cutadapt (2.4) and then mapped to the mm10 genome using bowtie2 (2.5.0)[174,175]. The SAM files were converted to BAM files using Samtools[176]. The BAM files were filtered for uniquely mapped reads (no unmapped or duplicate reads) using Sambamba and then sorted and indexed using Samtools[177].

mTOR peaks were called using the peakcall (--broad) function of MACS2 (2.2.7.1) with the input experiments as the control and default parameter settings[178].

To generate the BigWig files, firstly, individual smoothed (300 bp windows) and CPM normalised BigWig files were generated using the bamCoverage function of deepTools, followed by background correction using the log2 ratio of the mTOR coverage and the input coverage[169]. In the case of merging, the replicates were merged by taking the means.

4.10.2. CUT&Tag data preprocessing

The fastq files were trimmed using Trim Galore! (with cutadapt 2.4) and then mapped to the mm10 genome using bowtie2 (2.5.0) with parameters --end-to-end --very-sensitive --no-mixed --no-discordant --phred33 -I 10 -X 700[174,175]. The SAM files were filtered (mapping quality >= 2) and converted to BAM files using the view function of Samtools[176]. The BAM files were sorted and indexed using the sort function of sambamba (0.8.2)[177].

4.10.3. CUT&Tag - H2AK119ub, H2AT120ph and H3K27me3

For the spike-in calibration, the trimmed reads were mapped to the *E. coli* genome using bowtie2 with parameter settings --local --very-sensitive --no-overlap

--no-dovetail --no-mixed --no-discordant --phred33 -I 10 -X 700[175]. The reads of the sample x aligned to the *E. coli* genome were used to infer a scaling factor S_x for the respective sample:

$$1. \quad S_x = \frac{C}{N_x}$$

where $C = 10,000$ is a constant and N_x is the number of fragments from sample x that mapped to the *E. coli* genome.

The coverage levels of H2A, H3K27me3, H2AK119ub, and H2AT120ph were smoothed (300 bp windows), CPM normalised and spike-in calibrated by multiplying the original coverage of the sample x with S_x using the bamCoverage function of deepTools[169]. To facilitate the comparison of the coverage levels between H2AK119ub, H2AT120ph, and H3K27me3 samples, the coverage levels were quantile normalised using the function normalize.quantiles of the R package preprocessCore 1.60.2[179]. The quantile normalised data were further corrected for background using the H2A samples. For sample H^a_{ijk} containing the coverage levels in genomic bin a of histone mark H ($H \in \{H2AT120p, H2AK119ub, H3K27me3\}$) at time point i ($i \in \{0, 6, 12, 24\}$) in condition j ($j \in \{DMSO, INK\}$) for replicate k ($k \in \{1, 2\}$), the adjusted coverage levels were computed in R as follows:

$$(2) \quad \widehat{H^a_{ijk}} = log_2\left(\frac{H^a_{ijk} + PC}{H2A^a_{ijk} + PC}\right)$$

with $PC = 0.1$ as pseudo count.

In case of merging, the mean of each replicate was taken using the bigwigCompare function of deepTools with pseudocount 0 and operation “mean”[169].

4.10.4. CUT&Tag - Rictor and Raptor

The Rictor and Raptor samples were CPM normalised, smoothed and spike-in calibrated similarly to 3.9.3. Neither quantile normalisation nor H2A background correction were performed.

4.10.5. CUT&Tag - H3K4me3

The H3K4me3 CUT&Tag data was downloaded from Galle et al[180]. The samples were CPM normalised and smoothed similarly to 3.9.3. These samples were not spike-in calibrated, quantile normalised or H2A corrected.

4.10.6. CUT&Tag - peak calling

SEACR (1.3) was used to call peaks for the CUT&Tag data (H2AT120ph, Rictor and Raptor) with parameter settings 0.01 non stringent[181].

For H2AT120ph, the H2A-corrected coverage levels were first filtered to have all values less than 0.1 set to 0 before peak calling. For the Rictor and Raptor samples, the normalised and spike-in calibrated BigWig files were converted to the bedGraph format using the R package rtracklayer (1.58.0) before peak calling[182].

As SEACR has the tendency to call many narrow peaks clustered together rather than one broad peak for the target sites, the resulting peak regions were further processed. Peak clusters, defined as groups of peaks where all adjacent peaks have a distance of less than 6 kb, were summarised into broad peaks. The start of the resulting broad peak was defined as the start of the most upstream peak in the cluster and the end was defined as the end of the most downstream peak in the cluster. The summarised peaks were used for downstream analyses, i.e. detection of target genes.

4.10.7. ChIP-seq, CUT&Tag target genes detection

To find the target genes of mTOR, H2AT120ph, Rictor, and Raptor, all TSSs extracted from the mm10 genome were used. If a peak fell within the ±2 kb area of a TSS, the gene was considered as a target gene. The final lists of target genes were composed of genes that were identified as target genes in all replicates.

4.10.8. TT-SLAM-seq

The TT-SLAM-seq reads were first trimmed 2 times using cutadapt[174]. In the first round, the Illumina adapters were trimmed and quality clipping was performed with a minimum quality of 20, a minimum read length of 25 bp and a minimum overlap between read and adaptor sequence of 5 bp. In the second round, the Poly-A tails were trimmed by setting the adapters to "A{100}" and "T{100}", the minimum read length to 25 bp and the minimum overlap to 20 bp. Next, the trimmed reads were

filtered for rRNA. STAR (2.7.9a) was used to align the reads to an rRNA database with the maximum number of multimaps for a read set to 50. The unmapped reads (rRNA free) were stored in separate FASTQ files[183].

The rRNA-free reads were reversed using seqtk (1.3.-r106)[184]. SLAM-DUNK (0.4.1) was used to map the reversed reads, filter the alignments according to their quality and call SNPs[185]. The maximum read length was set to 100 bp and the number of base pairs to trim from the 5' end was set to 0. The read-separator function of alleyoop (0.4.1) was used to separate the mapped and filtered reads according to TC converted reads and background reads[185]. A modified version of the R package rCube (1.1.1) was used to quantify the number of T to C converted reads mapping over gene bodies (the raw gene expression counts) and to infer size factors for the spike-in normalisation[186].

The raw gene expression counts C_i^x were normalised with reference to the spike-in size factors, gene size and number of fragments in the sample. The normalised gene expression counts $\widehat{C_{ij}^x}$ of a gene x for replicate j of sample i were computed as:

$$(3)\ \widehat{C_i^x} = \frac{C_{ij}^x * K}{L_x * \sigma_{ij} * N_{ij}}$$

with constant $K = 10^{12}$, gene length L_x of gene x, size factor σ_{ij} for replicate j of sample i as computed by rCube and number of total fragments originally sequences (not only the TC converted reads) N_{ij} in replicate j of sample i. The replicates were merged in R by taking the mean of their respective counts.

4.10.9. Generation of count matrices for the heatmaps and line plots

The heatmaps and line plots were generated based on one count matrix $M_{ij} \in \Re^{n \times m}$ with n = number of genes and m = number of samples (with the merged replicates). All 24,528 genes of the mm10 genome build were used for the rows and the CUT&Tag data (H2AT120ph, H2AK119ub, H3K27me3, Rybp, Cbx7, Ring1b, H3K4me3, Rictor, Raptor), mTOR ChIP-seq data, and TT-SLAM-seq data were used for the columns.

4.10.9.1. CUT&Tag - H2AK119ub, H2AT120ph, and H3K27me3

The promoter region was defined as TSS±2kb. The H2A-corrected, spike-in calibrated coverage levels of the histone marks were exponentiated and the replicates were merged (see eq. 4). For

$j \in \{H2AK119ub\ 0hr,..., H2AK119ub\ DMSO\ 24hr,..., H2AK119ub\ INK\ 24h,\ H2AT120ph\ 0hr,...,$

$H2AT120ph\ DMSO\ 24hr,..., H2AT120ph\ INK\ 24hr,..., H3K27me3\ 0hr,..,\ H3K27me3\ DMSO\ 24hr,\ H3K27me3\ INK\ 24hr\}$

the count matrix entry for gene i was computed as:

$$(4)\ M_{ij} = \sum_{a = TSS_i - 2kb}^{TSS_i + 2kb} 0.5 * \left(exp\left(\widehat{H_{j1}^{a}}\right) + exp\left(\widehat{H_{j2}^{a}}\right) \right)$$

the sum of the exponentiated H2A-corrected, spike-in calibrated coverage levels in the genomic bins located ±2kb of gene i.

4.10.9.2. CUT&Tag - H3K4me3, Rictor, and Raptor

The entries in the count matrix were computed as described above in 3.9.9.1. The signals in the TSS±2kb regions were summed up. The coverage levels used for the entries were CPM normalised and spike-in calibrated, but not further corrected like the coverage levels used for H2AK119ub, H2AT120ph, and H3K27me3.

4.10.9.3. mTOR ChIP-seq

The CPM normalised and background corrected mTOR signals in the TSS±2kb regions of every time point were summed up.

4.10.9.4. CUT&Tag -Rybp, Cbx7, and Ring1b

The background-corrected BigWig files were downloaded from Asenjo et al. Each target contains 3 BigWig files from different cell cycle stages (G1, S, and G2). Following the paper, the mm9 genome was used to define the TSS regions. The signals in the TSS±2kb regions were summed up as described in previous sections. The count values of each cell cycle stage were then summed up to generate the final count matrices.

4.10.9.5. CUT&Tag -Rybp, Cbx7, and Ring1b

The TT-SLAM-seq counts that were gained as described in 3.9.8 were used as entries in the count matrices.

4.10.10. Visualisation

4.10.10.1. Complex heatmaps

The values of the count M that was created as described in the last section were used. The values were log-scaled with a pseudo-count of 1. Negative values were set to 0 prior to log-scaling. For the set of control genes, the 1000 genes with the lowest mTOR coverage levels (CPM normalised, but not corrected for the background) were chosen.

4.10.10.2. deepTools heatmaps

For the mTOR metaplots and heatmaps, the CPM normalised coverage levels were used. For the H2AT120ph profiles, the CPM normalised, H2A-corrected coverage levels were used. The same control genes as for the complex heatmaps were used.

5. References

1. Nichols, J. & Smith, A. Naive and Primed Pluripotent States. *Cell Stem Cell* **4**, 487–492 (2009).
2. Saiz, N. & Plusa, B. Early cell fate decisions in the mouse embryo. *REPRODUCTION* **145**, R65–R80 (2013).
3. Varzideh, F., Gambardella, J., Kansakar, U., Jankauskas, S. S. & Santulli, G. Molecular Mechanisms Underlying Pluripotency and Self-Renewal of Embryonic Stem Cells. *Int. J. Mol. Sci.* **24**, 8386 (2023).
4. Takahashi, K. & Yamanaka, S. Induction of Pluripotent Stem Cells from Mouse Embryonic and Adult Fibroblast Cultures by Defined Factors. *Cell* **126**, 663–676 (2006).
5. González, F., Boué, S. & Belmonte, J. C. I. Methods for making induced pluripotent stem cells: reprogramming à la carte. *Nat. Rev. Genet.* **12**, 231–242 (2011).
6. Evans, M. J. & Kaufman, M. H. Establishment in culture of pluripotential cells from mouse embryos. *Nature* **292**, 154–156 (1981).
7. Martin, G. R. Isolation of a pluripotent cell line from early mouse embryos cultured in medium conditioned by teratocarcinoma stem cells. *Proc. Natl. Acad. Sci.* **78**, 7634–7638 (1981).
8. Nagy, A., Rossant, J., Nagy, R., Abramow-Newerly, W. & Roder, J. C. Derivation of completely cell culture-derived mice from early-passage embryonic stem cells. *Proc. Natl. Acad. Sci.* **90**, 8424–8428 (1993).
9. Li, M. & Belmonte, J. C. I. Ground rules of the pluripotency gene regulatory network. *Nat. Rev. Genet.* **18**, 180–191 (2017).
10. Bradley, A., Evans, M., Kaufman, M. H. & Robertson, E. Formation of germ-line

chimaeras from embryo-derived teratocarcinoma cell lines. *Nature* **309**, 255–256 (1984).

11. Brons, I. G. M. *et al.* Derivation of pluripotent epiblast stem cells from mammalian embryos. *Nature* **448**, 191–195 (2007).
12. Tesar, P. J. *et al.* New cell lines from mouse epiblast share defining features with human embryonic stem cells. *Nature* **448**, 196–199 (2007).
13. Huang, Y., Osorno, R., Tsakiridis, A. & Wilson, V. In Vivo Differentiation Potential of Epiblast Stem Cells Revealed by Chimeric Embryo Formation. *Cell Rep.* **2**, 1571–1578 (2012).
14. Wu, J. *et al.* An alternative pluripotent state confers interspecies chimaeric competency. *Nature* **521**, 316–321 (2015).
15. Boyer, L. A. *et al.* Core Transcriptional Regulatory Circuitry in Human Embryonic Stem Cells. *Cell* **122**, 947–956 (2005).
16. Chen, X. *et al.* Integration of External Signaling Pathways with the Core Transcriptional Network in Embryonic Stem Cells. *Cell* **133**, 1106–1117 (2008).
17. Yuan, H., Corbi, N., Basilico, C. & Dailey, L. Developmental-specific activity of the FGF-4 enhancer requires the synergistic action of Sox2 and Oct-3. *Genes Dev.* **9**, 2635–2645 (1995).
18. Kunath, T. *et al.* FGF stimulation of the Erk1/2 signalling cascade triggers transition of pluripotent embryonic stem cells from self-renewal to lineage commitment. *Development* **134**, 2895–2902 (2007).
19. Yoshida, K. & Yasukawa, K. Maintenance of the pluripotential phenotype of embryonic stem cells through direct activation of gpl30 signalling pathways.
20. Martello, G., Bertone, P. & Smith, A. Identification of the missing pluripotency mediator downstream of leukaemia inhibitory factor. *EMBO J.* **32**, 2561–2574

(2013).

21. Ye, S., Li, P., Tong, C. & Ying, Q.-L. Embryonic stem cell self-renewal pathways converge on the transcription factor Tfcp2l1. *EMBO J.* **32**, 2548–2560 (2013).
22. Ying, Q.-L., Nichols, J., Chambers, I. & Smith, A. BMP Induction of Id Proteins Suppresses Differentiation and Sustains Embryonic Stem Cell Self-Renewal in Collaboration with STAT3. *Cell* **115**, 281–292 (2003).
23. Ying, Q.-L. *et al.* The ground state of embryonic stem cell self-renewal. *Nature* **453**, 519–523 (2008).
24. Hackett, J. A. & Surani, M. A. Regulatory Principles of Pluripotency: From the Ground State Up. *Cell Stem Cell* **15**, 416–430 (2014).
25. Papatsenko, D. *et al.* Single-Cell Analyses of ESCs Reveal Alternative Pluripotent Cell States and Molecular Mechanisms that Control Self-Renewal. *Stem Cell Rep.* **5**, 207–220 (2015).
26. Chambers, I. *et al.* Nanog safeguards pluripotency and mediates germline development. *Nature* **450**, 1230–1234 (2007).
27. Toyooka, Y., Shimosato, D., Murakami, K., Takahashi, K. & Niwa, H. Identification and characterization of subpopulations in undifferentiated ES cell culture. *Development* **135**, 909–918 (2008).
28. Kolodziejczyk, A. A. *et al.* Single Cell RNA-Sequencing of Pluripotent States Unlocks Modular Transcriptional Variation. *Cell Stem Cell* **17**, 471–485 (2015).
29. Marks, H. *et al.* The Transcriptional and Epigenomic Foundations of Ground State Pluripotency. *Cell* **149**, 590–604 (2012).
30. Schlesinger, S. & Meshorer, E. Open Chromatin, Epigenetic Plasticity, and Nuclear Organization in Pluripotency. *Dev. Cell* **48**, 135–150 (2019).
31. Blackledge, N. P. & Klose, R. J. The molecular principles of gene regulation by

Polycomb repressive complexes. *Nat. Rev. Mol. Cell Biol.* (2021) doi:10.1038/s41580-021-00398-y.

32. Piunti, A. & Shilatifard, A. The roles of Polycomb repressive complexes in mammalian development and cancer. *Nat. Rev. Mol. Cell Biol.* **22**, 326–345 (2021).
33. Wang, H. *et al.* Role of histone H2A ubiquitination in Polycomb silencing. *Nature* **431**, 873–878 (2004).
34. de Napoles, M. *et al.* Polycomb group proteins Ring1A/B link ubiquitylation of histone H2A to heritable gene silencing and X inactivation. *Dev. Cell* **7**, 663–676 (2004).
35. Buchwald, G. *et al.* Structure and E3-ligase activity of the Ring-Ring complex of polycomb proteins Bmi1 and Ring1b. *EMBO J.* **25**, 2465–2474 (2006).
36. Li, Z. *et al.* Structure of a Bmi-1-Ring1B polycomb group ubiquitin ligase complex. *J. Biol. Chem.* **281**, 20643–20649 (2006).
37. Hauri, S. *et al.* A High-Density Map for Navigating the Human Polycomb Complexome. *Cell Rep.* **17**, 583–595 (2016).
38. Gao, Z. *et al.* PCGF Homologs, CBX Proteins, and RYBP Define Functionally Distinct PRC1 Family Complexes. *Mol. Cell* **45**, 344–356 (2012).
39. Shao, Z. *et al.* Stabilization of chromatin structure by PRC1, a Polycomb complex. *Cell* **98**, 37–46 (1999).
40. Tavares, L. *et al.* RYBP-PRC1 complexes mediate H2A ubiquitylation at polycomb target sites independently of PRC2 and H3K27me3. *Cell* **148**, 664–678 (2012).
41. Huseyin, M. K. & Klose, R. J. Live-cell single particle tracking of PRC1 reveals a highly dynamic system with low target site occupancy. *Nat. Commun.* **12**, 887

(2021).

42. Fursova, N. A. *et al.* Synergy between Variant PRC1 Complexes Defines Polycomb-Mediated Gene Repression. *Mol. Cell* **74**, 1020-1036.e8 (2019).
43. Scelfo, A. *et al.* Functional Landscape of PCGF Proteins Reveals Both RING1A/B-Dependent-and RING1A/B-Independent-Specific Activities. *Mol. Cell* **74**, 1037-1052.e7 (2019).
44. Cao, R. *et al.* Role of histone H3 lysine 27 methylation in Polycomb-group silencing. *Science* **298**, 1039–1043 (2002).
45. Kuzmichev, A., Nishioka, K., Erdjument-Bromage, H., Tempst, P. & Reinberg, D. Histone methyltransferase activity associated with a human multiprotein complex containing the Enhancer of Zeste protein. *Genes Dev.* **16**, 2893–2905 (2002).
46. Cao, R. & Zhang, Y. SUZ12 is required for both the histone methyltransferase activity and the silencing function of the EED-EZH2 complex. *Mol. Cell* **15**, 57–67 (2004).
47. Jiao, L. & Liu, X. Structural basis of histone H3K27 trimethylation by an active polycomb repressive complex 2. *Science* **350**, aac4383 (2015).
48. Beringer, M. *et al.* EPOP Functionally Links Elongin and Polycomb in Pluripotent Stem Cells. *Mol. Cell* **64**, 645–658 (2016).
49. Liefke, R., Karwacki-Neisius, V. & Shi, Y. EPOP Interacts with Elongin BC and USP7 to Modulate the Chromatin Landscape. *Mol. Cell* **64**, 659–672 (2016).
50. Zhang, Z. *et al.* PRC2 complexes with JARID2, MTF2, and esPRC2p48 in ES cells to modulate ES cell pluripotency and somatic cell reprogramming. *Stem Cells Dayt. Ohio* **29**, 229–240 (2011).
51. Fenelon, J. C., Banerjee, A. & Murphy, B. D. Embryonic diapause: development

on hold. *Int. J. Dev. Biol.* **58**, 163–174 (2014).

52. Renfree, M. B. & Fenelon, J. C. The enigma of embryonic diapause. *Development* **144**, 3199–3210 (2017).
53. Van Leeuwen, J., Berg, D. K. & Pfeffer, P. L. Morphological and Gene Expression Changes in Cattle Embryos from Hatched Blastocyst to Early Gastrulation Stages after Transfer of In Vitro Produced Embryos. *PLOS ONE* **10**, e0129787 (2015).
54. Pfeffer, P. L., Smith, C. S., Maclean, P. & Berg, D. K. Gene expression analysis of bovine embryonic disc, trophoblast and parietal hypoblast at the start of gastrulation. *Zygote* **25**, 265–278 (2017).
55. Van Der Weijden, V. A. & Bulut-Karslioglu, A. Molecular Regulation of Paused Pluripotency in Early Mammalian Embryos and Stem Cells. *Front. Cell Dev. Biol.* **9**, 708318 (2021).
56. Lopes, F. L., Desmarais, J. A. & Murphy, B. D. Embryonic diapause and its regulation. *Reproduction* **128**, 669–678 (2004).
57. Murphy, B. Embryonic Diapause: Advances in Understanding the Enigma of Seasonal Delayed Implantation. *Reprod. Domest. Anim.* **47**, 121–124 (2012).
58. Weitlauf, H. M. & Greenwald, G. S. SURVIVAL OF BLASTOCYSTS IN THE UTERI OF OVARIECTOMIZED MICE. *Reproduction* **17**, 515–520 (1968).
59. Bulut-Karslioglu, A. *et al.* Inhibition of mTOR induces a paused pluripotent state. *Nature* **540**, 119–123 (2016).
60. Scognamiglio, R. *et al.* Myc Depletion Induces a Pluripotent Dormant State Mimicking Diapause. *Cell* **164**, 668–680 (2016).
61. Liu, W. M. *et al.* Let-7 derived from endometrial extracellular vesicles is an important inducer of embryonic diapause in mice. *Sci. Adv.* **6**, eaaz7070 (2020).

62. Saxton, R. A. & Sabatini, D. M. mTOR Signaling in Growth, Metabolism, and Disease. *Cell* **168**, 960–976 (2017).

63. Kim, D.-H. *et al.* mTOR Interacts with Raptor to Form a Nutrient-Sensitive Complex that Signals to the Cell Growth Machinery. *Cell* **110**, 163–175 (2002).

64. Hara, K. *et al.* Raptor, a Binding Partner of Target of Rapamycin (TOR), Mediates TOR Action. *Cell* **110**, 177–189 (2002).

65. Jacinto, E. *et al.* Mammalian TOR complex 2 controls the actin cytoskeleton and is rapamycin insensitive. *Nat. Cell Biol.* **6**, 1122–1128 (2004).

66. Dos D. Sarbassov *et al.* Rictor, a Novel Binding Partner of mTOR, Defines a Rapamycin-Insensitive and Raptor-Independent Pathway that Regulates the Cytoskeleton. *Curr. Biol.* **14**, 1296–1302 (2004).

67. Yang, H. *et al.* mTOR kinase structure, mechanism and regulation. *Nature* **497**, 217–223 (2013).

68. Lamming, D. W. *et al.* Rapamycin-Induced Insulin Resistance Is Mediated by mTORC2 Loss and Uncoupled from Longevity. *Science* **335**, 1638–1643 (2012).

69. Sarbassov, D. D. *et al.* Prolonged Rapamycin Treatment Inhibits mTORC2 Assembly and Akt/PKB. *Mol. Cell* **22**, 159–168 (2006).

70. Kim, J. & Guan, K.-L. mTOR as a central hub of nutrient signalling and cell growth. *Nat. Cell Biol.* **21**, 63–71 (2019).

71. Holz, M. K., Ballif, B. A., Gygi, S. P. & Blenis, J. mTOR and S6K1 Mediate Assembly of the Translation Preinitiation Complex through Dynamic Protein Interchange and Ordered Phosphorylation Events. *Cell* **123**, 569–580 (2005).

72. Kim, J., Kundu, M., Viollet, B. & Guan, K.-L. AMPK and mTOR regulate autophagy through direct phosphorylation of Ulk1. *Nat. Cell Biol.* **13**, 132–141 (2011).

73. Roczniak-Ferguson, A. *et al.* The Transcription Factor TFEB Links mTORC1 Signaling to Transcriptional Control of Lysosome Homeostasis. *Sci. Signal.* **5**, ra42–ra42 (2012).
74. Porstmann, T. *et al.* SREBP Activity Is Regulated by mTORC1 and Contributes to Akt-Dependent Cell Growth. *Cell Metab.* **8**, 224–236 (2008).
75. Düvel, K. *et al.* Activation of a Metabolic Gene Regulatory Network Downstream of mTOR Complex 1. *Mol. Cell* **39**, 171–183 (2010).
76. Peterson, T. R. *et al.* mTOR Complex 1 Regulates Lipin 1 Localization to Control the SREBP Pathway. *Cell* **146**, 408–420 (2011).
77. Gan, X. *et al.* PRR5L degradation promotes mTORC2-mediated PKC-δ phosphorylation and cell migration downstream of Gα12. *Nat. Cell Biol.* **14**, 686–696 (2012).
78. Li, X. & Gao, T. mTORC2 phosphorylates protein kinase Cζ to regulate its stability and activity. *EMBO Rep.* **15**, 191–198 (2014).
79. Sarbassov, D. D., Guertin, D. A., Ali, S. M. & Sabatini, D. M. Phosphorylation and Regulation of Akt/PKB by the Rictor-mTOR Complex. *Science* **307**, 1098–1101 (2005).
80. Guertin, D. A. *et al.* Ablation in Mice of the mTORC Components raptor, rictor, or mLST8 Reveals that mTORC2 Is Required for Signaling to Akt-FOXO and PKCα, but Not S6K1. *Dev. Cell* **11**, 859–871 (2006).
81. Jacinto, E. *et al.* SIN1/MIP1 Maintains rictor-mTOR Complex Integrity and Regulates Akt Phosphorylation and Substrate Specificity. *Cell* **127**, 125–137 (2006).
82. García-Martínez, J. M. & Alessi, D. R. mTOR complex 2 (mTORC2) controls hydrophobic motif phosphorylation and activation of serum- and

glucocorticoid-induced protein kinase 1 (SGK1). *Biochem. J.* **416**, 375–385 (2008).

83. Dibble, C. C. *et al.* TBC1D7 Is a Third Subunit of the TSC1-TSC2 Complex Upstream of mTORC1. *Mol. Cell* **47**, 535–546 (2012).
84. Inoki, K., Li, Y., Xu, T. & Guan, K.-L. Rheb GTPase is a direct target of TSC2 GAP activity and regulates mTOR signaling. *Genes Dev.* **17**, 1829–1834 (2003).
85. Tee, A. R., Manning, B. D., Roux, P. P., Cantley, L. C. & Blenis, J. Tuberous Sclerosis Complex Gene Products, Tuberin and Hamartin, Control mTOR Signaling by Acting as a GTPase-Activating Protein Complex toward Rheb. *Curr. Biol.* **13**, 1259–1268 (2003).
86. Long, X., Lin, Y., Ortiz-Vega, S., Yonezawa, K. & Avruch, J. Rheb Binds and Regulates the mTOR Kinase. *Curr. Biol.* **15**, 702–713 (2005).
87. Sancak, Y. *et al.* PRAS40 Is an Insulin-Regulated Inhibitor of the mTORC1 Protein Kinase. *Mol. Cell* **25**, 903–915 (2007).
88. Inoki, K. *et al.* TSC2 Integrates Wnt and Energy Signals via a Coordinated Phosphorylation by AMPK and GSK3 to Regulate Cell Growth. *Cell* **126**, 955–968 (2006).
89. Lee, D.-F. *et al.* IKKβ Suppression of TSC1 Links Inflammation and Tumor Angiogenesis via the mTOR Pathway. *Cell* **130**, 440–455 (2007).
90. Gwinn, D. M. *et al.* AMPK Phosphorylation of Raptor Mediates a Metabolic Checkpoint. *Mol. Cell* **30**, 214–226 (2008).
91. Inoki, K., Zhu, T. & Guan, K.-L. TSC2 Mediates Cellular Energy Response to Control Cell Growth and Survival. *Cell* **115**, 577–590 (2003).
92. Efeyan, A. *et al.* Regulation of mTORC1 by the Rag GTPases is necessary for neonatal autophagy and survival. *Nature* **493**, 679–683 (2013).

93. Kalender, A. *et al.* Metformin, Independent of AMPK, Inhibits mTORC1 in a Rag GTPase-Dependent Manner. *Cell Metab.* **11**, 390–401 (2010).
94. Brugarolas, J. *et al.* Regulation of mTOR function in response to hypoxia by REDD1 and the TSC1/TSC2 tumor suppressor complex. *Genes Dev.* **18**, 2893–2904 (2004).
95. Feng, Z. *et al.* The regulation of AMPK beta1, TSC2, and PTEN expression by p53: stress, cell and tissue specificity, and the role of these gene products in modulating the IGF-1-AKT-mTOR pathways. *Cancer Res.* **67**, 3043–3053 (2007).
96. Zoncu, R. *et al.* mTORC1 Senses Lysosomal Amino Acids Through an Inside-Out Mechanism That Requires the Vacuolar H+-ATPase. *Science* **334**, 678–683 (2011).
97. Bar-Peled, L., Schweitzer, L. D., Zoncu, R. & Sabatini, D. M. Ragulator Is a GEF for the Rag GTPases that Signal Amino Acid Levels to mTORC1. *Cell* **150**, 1196–1208 (2012).
98. Chantranupong, L. *et al.* The CASTOR Proteins Are Arginine Sensors for the mTORC1 Pathway. *Cell* **165**, 153–164 (2016).
99. Chantranupong, L. *et al.* The Sestrins Interact with GATOR2 to Negatively Regulate the Amino-Acid-Sensing Pathway Upstream of mTORC1. *Cell Rep.* **9**, 1–8 (2014).
100. Saxton, R. A., Chantranupong, L., Knockenhauer, K. E., Schwartz, T. U. & Sabatini, D. M. Mechanism of arginine sensing by CASTOR1 upstream of mTORC1. *Nature* **536**, 229–233 (2016).
101. Jewell, J. L. *et al.* Differential regulation of mTORC1 by leucine and glutamine. *Science* **347**, 194–198 (2015).

102. Matsumoto, A. *et al.* mTORC1 and muscle regeneration are regulated by the LINC00961-encoded SPAR polypeptide. *Nature* **541**, 228–232 (2017).
103. Hsu, P. P. *et al.* The mTOR-Regulated Phosphoproteome Reveals a Mechanism of mTORC1-Mediated Inhibition of Growth Factor Signaling. *Science* **332**, 1317–1322 (2011).
104. Yu, Y. *et al.* Phosphoproteomic Analysis Identifies Grb10 as an mTORC1 Substrate That Negatively Regulates Insulin Signaling. *Science* **332**, 1322–1326 (2011).
105. Harrington, L. S. *et al.* The TSC1-2 tumor suppressor controls insulin-PI3K signaling via regulation of IRS proteins. *J. Cell Biol.* **166**, 213–223 (2004).
106. Giguère, V. Canonical signaling and nuclear activity of mTOR —a teamwork effort to regulate metabolism and cell growth. *FEBS J.* **285**, 1572–1588 (2018).
107. Zhang, X., Shu, L., Hosoi, H., Murti, K. G. & Houghton, P. J. Predominant nuclear localization of mammalian target of rapamycin in normal and malignant cells in culture. *J. Biol. Chem.* **277**, 28127–28134 (2002).
108. Rosner, M. & Hengstschläger, M. Cytoplasmic and nuclear distribution of the protein complexes mTORC1 and mTORC2: rapamycin triggers dephosphorylation and delocalization of the mTORC2 components rictor and sin1. *Hum. Mol. Genet.* **17**, 2934–2948 (2008).
109. Liu, J. & Brown, R. E. Morphoproteomics demonstrates activation of mammalian target of rapamycin pathway in papillary thyroid carcinomas with nuclear translocation of MTOR in aggressive histological variants. *Mod. Pathol. Off. J. U. S. Can. Acad. Pathol. Inc* **24**, 1553–1559 (2011).
110. Walsh, S. *et al.* mTOR in breast cancer: Differential expression in triple-negative and non-triple-negative tumors. *The Breast* **21**, 178–182 (2012).

111. Chen, T.-C. *et al.* Significance of nuclear p-mTOR expression in advanced oral squamous cell carcinoma with extracapsular extension of lymph node metastases. *Oral Oncol.* **51**, 493–499 (2015).

112. Kantidakis, T., Ramsbottom, B. A., Birch, J. L., Dowding, S. N. & White, R. J. mTOR associates with TFIIIC, is found at tRNA and 5S rRNA genes, and targets their repressor Maf1. *Proc. Natl. Acad. Sci. U. S. A.* **107**, 11823–11828 (2010).

113. Shor, B., Cavender, D. & Harris, C. A kinase-dead knock-in mutation in mTOR leads to early embryonic lethality and is dispensable for the immune system in heterozygous mice. *BMC Immunol.* **10**, 28 (2009).

114. Tsang, C. K., Liu, H. & Zheng, X. F. S. mTOR binds to the promoters of RNA polymerase I- and III-transcribed genes. *Cell Cycle Georget. Tex* **9**, 953–957 (2010).

115. von Walden, F., Liu, C., Aurigemma, N. & Nader, G. A. mTOR signaling regulates myotube hypertrophy by modulating protein synthesis, rDNA transcription, and chromatin remodeling. *Am. J. Physiol. Cell Physiol.* **311**, C663–C672 (2016).

116. Cunningham, J. T. *et al.* mTOR controls mitochondrial oxidative function through a YY1–PGC-1α transcriptional complex. *Nature* **450**, 736–740 (2007).

117. Wan, W. *et al.* mTORC1 Phosphorylates Acetyltransferase p300 to Regulate Autophagy and Lipogenesis. *Mol. Cell* **68**, 323-335.e6 (2017).

118. Audet-Walsh, É. *et al.* Nuclear mTOR acts as a transcriptional integrator of the androgen signaling pathway in prostate cancer. *Genes Dev.* **31**, 1228–1242 (2017).

119. Chaveroux, C. *et al.* Molecular and Genetic Crosstalks between mTOR and

ERRα Are Key Determinants of Rapamycin-Induced Nonalcoholic Fatty Liver. *Cell Metab.* **17**, 586–598 (2013).

120. Bachmann, R. A., Kim, J.-H., Wu, A.-L., Park, I.-H. & Chen, J. A Nuclear Transport Signal in Mammalian Target of Rapamycin Is Critical for Its Cytoplasmic Signaling to S6 Kinase 1. *J. Biol. Chem.* **281**, 7357–7363 (2006).
121. Gangloff, Y.-G. *et al.* Disruption of the Mouse mTOR Gene Leads to Early Postimplantation Lethality and Prohibits Embryonic Stem Cell Development. *Mol. Cell. Biol.* **24**, 9508–9516 (2004).
122. Murakami, M. *et al.* mTOR Is Essential for Growth and Proliferation in Early Mouse Embryos and Embryonic Stem Cells. *Mol. Cell. Biol.* **24**, 6710–6718 (2004).
123. Shiota, C., Woo, J.-T., Lindner, J., Shelton, K. D. & Magnuson, M. A. Multiallelic Disruption of the rictor Gene in Mice Reveals that mTOR Complex 2 Is Essential for Fetal Growth and Viability. *Dev. Cell* **11**, 583–589 (2006).
124. Pende, M. *et al.* S6K1(-/-)/S6K2(-/-) mice exhibit perinatal lethality and rapamycin-sensitive 5'-terminal oligopyrimidine mRNA translation and reveal a mitogen-activated protein kinase-dependent S6 kinase pathway. *Mol. Cell. Biol.* **24**, 3112–3124 (2004).
125. Le Bacquer, O. *et al.* Elevated sensitivity to diet-induced obesity and insulin resistance in mice lacking 4E-BP1 and 4E-BP2. *J. Clin. Invest.* **117**, 387–396 (2007).
126. Cherepkova, M. Y., Sineva, G. S. & Pospelov, V. A. Leukemia inhibitory factor (LIF) withdrawal activates mTOR signaling pathway in mouse embryonic stem cells through the MEK/ERK/TSC2 pathway. *Cell Death Dis.* **7**, e2050–e2050 (2016).

127. Agrawal, P., Reynolds, J., Chew, S., Lamba, D. A. & Hughes, R. E. DEPTOR Is a Stemness Factor That Regulates Pluripotency of Embryonic Stem Cells *. *J. Biol. Chem.* **289**, 31818–31826 (2014).

128. Nabet, B. *et al.* The dTAG system for immediate and target-specific protein degradation. *Nat. Chem. Biol.* **14**, 431–441 (2018).

129. Natsume, T. & Kanemaki, M. T. Conditional Degrons for Controlling Protein Expression at the Protein Level. *Annu. Rev. Genet.* **51**, 83–102 (2017).

130. Dohmen, R. J., Wu, P. & Varshavsky, A. Heat-Inducible Degron: a Method for Constructing Temperature-Sensitive Mutants. *Science* **263**, 1273–1276 (1994).

131. Nishimura, K. & Kanemaki, M. T. Rapid Depletion of Budding Yeast Proteins via the Fusion of an Auxin-Inducible Degron (AID). *Curr. Protoc. Cell Biol.* **64**, 20.9.1-20.9.16 (2014).

132. Taxis, C., Stier, G., Spadaccini, R. & Knop, M. Efficient protein depletion by genetically controlled deprotection of a dormant N-degron. *Mol. Syst. Biol.* **5**, 267 (2009).

133. Hermann, A., Liewald, J. F. & Gottschalk, A. A photosensitive degron enables acute light-induced protein degradation in the nervous system. *Curr. Biol.* **25**, R749–R750 (2015).

134. Sakuma, T., Nakade, S., Sakane, Y., Suzuki, K.-I. T. & Yamamoto, T. MMEJ-assisted gene knock-in using TALENs and CRISPR-Cas9 with the PITCh systems. *Nat. Protoc.* **11**, 118–133 (2016).

135. Armache, A. *et al.* Histone H3.3 phosphorylation amplifies stimulation-induced transcription. *Nature* (2020) doi:10.1038/s41586-020-2533-0.

136. Hastie, C. J., McLauchlan, H. J. & Cohen, P. Assay of protein kinases using radiolabeled ATP: a protocol. *Nat. Protoc.* **1**, 968–971 (2006).

137. Aihara, H. Histone H2A T120 Phosphorylation Promotes Oncogenic Transformation via Upregulation of Cyclin D1. 14.
138. Kaya-Okur, H. S. *et al.* CUT&Tag for efficient epigenomic profiling of small samples and single cells. *Nat. Commun.* **10**, 1930 (2019).
139. Reichholf, B. *et al.* Time-Resolved Small RNA Sequencing Unravels the Molecular Principles of MicroRNA Homeostasis. *Mol. Cell* **75**, 756-768.e7 (2019).
140. Schwalb, B. *et al.* TT-seq maps the human transient transcriptome. *Science* **352**, 1225–1228 (2016).
141. Herzog, V. A. *et al.* Thiol-linked alkylation of RNA to assess expression dynamics. *Nat. Methods* **14**, 1198–1204 (2017).
142. Dobrinić, P., Szczurek, A. T. & Klose, R. J. PRC1 drives Polycomb-mediated gene repression by controlling transcription initiation and burst frequency. *Nat. Struct. Mol. Biol.* **28**, 811–824 (2021).
143. Asenjo, H. G. *et al.* Changes in PRC1 activity during interphase modulate lineage transition in pluripotent cells. *Nat. Commun.* **14**, 180 (2023).
144. Morey, L., Aloia, L., Cozzuto, L., Benitah, S. A. & Di Croce, L. RYBP and Cbx7 Define Specific Biological Functions of Polycomb Complexes in Mouse Embryonic Stem Cells. *Cell Rep.* **3**, 60–69 (2013).
145. Ohne, Y. *et al.* Isolation of Hyperactive Mutants of Mammalian Target of Rapamycin. *J. Biol. Chem.* **283**, 31861–31870 (2008).
146. Woodard, L. E. & Wilson, M. H. piggyBac-ing models and new therapeutic strategies. *Trends Biotechnol.* **33**, 525–533 (2015).
147. Asimi, V. *et al.* Hijacking of transcriptional condensates by endogenous retroviruses. *Nat. Genet.* **54**, 1238–1247 (2022).

148. Hernández-Romero, I. A. & Valdes, V. J. De Novo Polycomb Recruitment and Repressive Domain Formation. *Epigenomes* **6**, 25 (2022).
149. Lloret-Llinares, M. *et al.* The RNA exosome contributes to gene expression regulation during stem cell differentiation. *Nucleic Acids Res.* **46**, 11502–11513 (2018).
150. Bonetti, A. *et al.* RADICL-seq identifies general and cell type-specific principles of genome-wide RNA-chromatin interactions. *Nat. Commun.* **11**, 1018 (2020).
151. Cruz-Molina, S. *et al.* PRC2 Facilitates the Regulatory Topology Required for Poised Enhancer Function during Pluripotent Stem Cell Differentiation. *Cell Stem Cell* **20**, 689-705.e9 (2017).
152. Xu, L. & Massagué, J. Nucleocytoplasmic shuttling of signal transducers. *Nat. Rev. Mol. Cell Biol.* **5**, 209–219 (2004).
153. Kim, J. E. & Chen, J. Cytoplasmic–nuclear shuttling of FKBP12-rapamycin-associated protein is involved in rapamycin-sensitive signaling and translation initiation. *Proc. Natl. Acad. Sci.* **97**, 14340–14345 (2000).
154. Kawashima, S. A., Yamagishi, Y., Honda, T., Ishiguro, K. & Watanabe, Y. Phosphorylation of H2A by Bub1 Prevents Chromosomal Instability Through Localizing Shugoshin. *Science* **327**, 172–177 (2010).
155. Aihara, H. *et al.* Nucleosomal histone kinase-1 phosphorylates H2A Thr 119 during mitosis in the early Drosophila embryo. *Genes Dev.* **18**, 877–888 (2004).
156. Yamagishi, Y., Honda, T., Tanno, Y. & Watanabe, Y. Two Histone Marks Establish the Inner Centromere and Chromosome Bi-Orientation. *Science* **330**, 239–243 (2010).
157. Ricke, R. M., Jeganathan, K. B., Malureanu, L., Harrison, A. M. & van Deursen,

J. M. Bub1 kinase activity drives error correction and mitotic checkpoint control but not tumor suppression. *J. Cell Biol.* **199**, 931–949 (2012).

158. Aihara, H. *et al.* Histone H2A T120 Phosphorylation Promotes Oncogenic Transformation via Upregulation of Cyclin D1. *Mol. Cell* **64**, 176–188 (2016).
159. Xu, X. & Yu, H. Ras-PI3K pathway promotes osteosarcoma progression via regulating VRK1-mediated H2A phosphorylation at threonine 120. *Artif. Cells Nanomedicine Biotechnol.* **47**, 4274–4283 (2019).
160. Sun, X., Zhao, W., Wang, Q., Zhao, J. & Yang, D. Y. & Y. Inhibition of VRK1 suppresses proliferation and migration of vascular smooth muscle cells and intima hyperplasia after injury via mTORC1/β-catenin axis. *BMB Rep.* **55**, 244–249 (2022).
161. Højfeldt, J. W. *et al.* Accurate H3K27 methylation can be established de novo by SUZ12-directed PRC2. *Nat. Struct. Mol. Biol.* **25**, 225–232 (2018).
162. Alabert, C. *et al.* Domain Model Explains Propagation Dynamics and Stability of Histone H3K27 and H3K36 Methylation Landscapes. *Cell Rep.* **30**, 1223-1234.e8 (2020).
163. Buenrostro, J. D. *et al.* Single-cell chromatin accessibility reveals principles of regulatory variation. *Nature* **523**, 486–490 (2015).
164. R Core Team. R: A language and environment for statistical computing. R Foundation for Statistical Computing. (2022).
165. Maintainer BP, T. B. TxDb.Mmusculus.UCSC.mm10.knownGene: Annotation package for TxDb object(s). (2019).
166. Carlson, M. & Bioconductor Package Maintainer. TxDb.Mmusculus.UCSC.mm9.knownGene: Annotation package for TxDb object(s). (2015).

167. Morgan, M. BiocManager: Access the Bioconductor Project Package Repository. (2023).
168. Wu, T. *et al.* clusterProfiler 4.0: A universal enrichment tool for interpreting omics data. *The Innovation* **2**, (2021).
169. Ramírez, F. *et al.* deepTools2: a next generation web server for deep-sequencing data analysis. *Nucleic Acids Res.* **44**, W160–W165 (2016).
170. Gu, Z., Eils, R. & Schlesner, M. Complex heatmaps reveal patterns and correlations in multidimensional genomic data. *Bioinformatics* **32**, 2847–2849 (2016).
171. Wickham, H. *ggplot2: Elegant Graphics for Data Analysis*. (Springer New York, NY, 2016).
172. Tiedemann, F. gghalves: Compose Half-Half Plots Using Your Favourite Geoms. (2022).
173. Georgiou, G. & van Heeringen, S. J. fluff: exploratory analysis and visualization of high-throughput sequencing data. *PeerJ* (2016) doi:10.7717/peerj.2209.
174. Martin, M. Cutadapt removes adapter sequences from high-throughput sequencing reads. *EMBnet.journal* **17**, 10–12 (2011).
175. Langmead, B. & Salzberg, S. L. Fast gapped-read alignment with Bowtie 2. *Nat. Methods* **9**, 357–359 (2012).
176. Danecek, P. *et al.* Twelve years of SAMtools and BCFtools. *GigaScience* **10**, giab008 (2021).
177. Tarasov, A., Vilella, A. J., Cuppen, E., Nijman, I. J. & Prins, P. Sambamba: fast processing of NGS alignment formats. *Bioinformatics* **31**, 2032–2034 (2015).
178. Zhang, Y. *et al.* Model-based Analysis of ChIP-Seq (MACS). *Genome Biol.* **9**, R137 (2008).

179. Bolstad, B. preprocessCore: A collection of pre-processing functions. (2023).
180. Galle, E. *et al.* H3K18 lactylation marks tissue-specific active enhancers. *Genome Biol.* **23**, 207 (2022).
181. Meers, M. P., Tenenbaum, D. & Henikoff, S. Peak calling by Sparse Enrichment Analysis for CUT&RUN chromatin profiling. *Epigenetics Chromatin* **12**, 42 (2019).
182. Lawrence, M., Gentleman, R. & Carey, V. rtracklayer: an R package for interfacing with genome browsers. *Bioinformatics* **25**, 1841–1842 (2009).
183. Dobin, A. *et al.* STAR: ultrafast universal RNA-seq aligner. *Bioinformatics* **29**, 15–21 (2013).
184. Li, H. Seqtk: a fast and lightweight tool for processing FASTA or FASTQ sequences. (2013).
185. Neumann, T. *et al.* Quantification of experimentally induced nucleotide conversions in high-throughput sequencing datasets. *BMC Bioinformatics* **20**, 258 (2019).
186. Wachutka, L. & Demel, C. rCube: RNA Rates in R. (2017).

6. Tables

Table 1 | Primers for FKBP^{F36V}-mTOR cloning

Name	Sequence (5'-3')
Mtor_dTAG_sgRNA_FWD	CACCGTCAGGGCAAGATGCTTGGGA
Mtor_dTAG_sgRNA_REV	AAACTCCCAAGCATCTTGCCCTGAC
U6_seq_F	ATGGACTATCATATGCTTAC
PITCh-colony-FWD	GCCTTTTGCTGGCCTTTTGCTC
PITCh-colony-REV	CGGGCCATTTACCGTAAGTTATGTAACG
Mtor dTAG cassette-FWD	TATATGGAGTTCCGCGTTACATAGCATCGTACGCGTAC GTGTTTGGACCTCAGGGCAAGATGCTTGGCATGACCG AGTACAAGCCCAC
Mtor dTAG cassette-REV	TCAGCATTCTAGAGCATCGTACGCGTACGTGTTTGGG GCCACGGCAGGACCCGTCCCTAGAGATCCGCCGCCA C
dTAG-seq-FWD	TCGCCCTTAATTGTGAGCGGA
dTAG-seq-REV	GAAAGGACAGTGGGAGTGGCA
geno-Mtor-ex2-F1	GAGGGTCGAGCTACACCATA
geno-Mtor-ex2-F2	TTGATTCCTCCCGGGACAGA
geno-Mtor-ex2-R	TTGCTAGATGTGGCGGCACT
geno-seq-Mtor-dTAG-F	CCCGCAACCTCCCCTTCTACGA
geno-seq-Mtor-ex2-R	GCAATCTAAACCAGGGGCGGCA

Table 2 | Primers for ChIP-qPCR

Name	Sequence (5’-3’)
mTOR_neg1_fwd	TTGGCATTGATATTGGGGGTGGGAGCAACT
mTOR_neg1_rev	GACTTCTTACTTTGACGCTTTCCTCCATCG
Hoxb9 TSS_F	GCTGGCTACGGGGACAATAA
Hoxb9 TSS_R	TGTCCGCTTTATGGCCTCTC
Hoxb9 ex2_F	CTGTAACCTAGCCAGACGCC
Hoxb9 ex2_R	TGGATCAGGGCACAACCAAA
Pax9 TSS_F	GAATCTCGCAGCTCCAGTGT
Pax9 TSS_R	TTGCCTGCCTGGTACCAAAA
Pax9 int3_F	TCATAAAGCCGGGGCAAACT
Pax9 int3_R	GTCTGTCAGCCACTCGTCAA
Gata6 TSS_F	CCGAGTTATCACAGCGCCAA
Gata6 TSS_R	CGCTTAGGCTCATCGGAGAT

Table 3 | Antibody list

Name	Company, Cat. #	Application
mTOR Abcam	Abcam, ab32028	ChIP 1 mg/25μg chromatin
mTOR CST	Cell Signaling Technology, 2983	WB 1:1000
Vinculin	Sigma, V9131	WB 1:1000
β-actin	Abbkine, A01010	WB 1:2000
H2AT120ph	Active Motif, 39391	WB 1:1000, CUT&Tag 1:100
H2A	Cell Signaling Technology, 12349	WB 1:1000, CUT&Tag 1:100
pS6	Cell Signaling Technology, 4858	WB 1:1000
HA	Abcam, ab9110	WB 1:1000
Mouse anti-rabbit IgG	Jackson Immuno Research, 211-032-171	WB 1:2000
Goat anti-mouse IgG	Jackson Immuno Research, 115-035-174	WB 1:5000
H2AK119ub	Cell Signaling Technology, 8240	CUT&Tag 1:100
H3K27me3	Cell Signaling Technology, 9733	CUT&Tag 1:100
Rictor	Norvus Biologicals, NB100-612	CUT&Tag 1:50
Raptor	Thermo Fisher, 42-4000	CUT&Tag 1:50
Rabbit anti-mouse IgG	Abcam, ab46540	ChIP 1 mg/25μg chromatin, CUT&Tag (primary) 1:100
Guinea pig α-rabbit antibody	Antibodies online, ABIN101961	CUT&Tag (secondary) 1:100

7. List of figures

8. List of abbreviations

2i: MEK inhibitor PD0325901 and GSK3 inhibitor CHIR99021

4E-BP2: 4E-binding protein 2

4EBP1: 4E-binding protein 1

4sU: 4-thiouridine

AEBP2: Adenine E Box Binding Protein 2

Akt: Protein kinase B

AMPK: AMP-activated protein kinase

AR: Androgen receptor

BMP4: Bone morphogenetic protein 4

Bub1: BUB1 Mitotic Checkpoint Serine/Threonine Kinase

CASTOR: Colonization associated translocation regulator 1

CBX: Chromobox proteins

CCND1: Cyclin D1

Cdk9: Cyclin-dependent kinase 9

ChIP: chromatin immunoprecipitation

CHX: Cycloheximide

CPM normalisation: Counts per million normalisation

cPRC1: Canonical PRC1

Crm1: Chromosomal Maintenance 1

CUT&Tag: Cleavage Under Targets and Tagmentation

DEPTOR: DEP domain-containing mTOR-interacting protein

DMSO: Dimethyl sulfoxide

EED: Embryonic Ectodermal Derived

Eomes: T-box brain protein 2

EpiSCs: Epiblast stem cells

EPOP: Epithelial protein

ERRα: Estrogen-related receptor α

ESCs: Embryonic stem cells

EZH1/2: Enhancer of Zeste Homolog ½

FACS: Fluorescence-activated cell sorting

FGF4: Fibroblast growth factor 4

FKBP12: FK506 binding protein 12
FOXO1/3a: Forkhead box O1/3a
FRB domain: FKBP-rapamycin-binding domain
GAP: GTPase activating protein
GAPDH: Glyceraldehyde 3-phosphate dehydrogenase
GATA6: GATA binding protein 6
Gata6: GATA binding protein 6
GATOR2: GATOR complex protein 2
GRB10: Growth factor receptor-bound protein 10
GSK3β: Glycogen synthase kinase 3 beta
H2AK119ub: Histone H2A monoubiquitination at lysine 119
H2AT120ph: Histone H2A phosphorylation at threonine 120
H3K27me3: Histone H3 trimethylation at lysine 27
H3K4me3: Histone H3 trimethylation at lysine 4
Hoxb9: Homeobox B9
ICM: Inner cell mass
IGF-1: Insulin/insulin-like growth factor-1
IKK: IκB kinase
iPSCs: Induced pluripotent stem cells
IRS1: insulin receptor substrate 1
JARID2: Jumonji, AT rich interactive domain 2
KLF4: Kruppel-like factor 4
LIF: Leukaemia inhibitory factor
MEF: Mouse embryonic fibroblasts
MEK: Mitogen-activated protein kinase kinase
mESCs: Mouse embryonic stem cells
mLST8: Mammalian lethal with Sec13 protein 8-like
mTOR: Mechanistic target of rapamycin
mTORC: mTOR complex
NANOG: Nanog homeobox protein
NLS: Nuclear localisation signal
Oct1: Organic cation transporter 1
OCT4: Octamer-binding transcription factor 4
p300: Histone acetyltransferase p300

PALI1/2: Peptidyl arginine deiminase, type I/II

Pax9: Paired box gene 9

PCGF: Polycomb group RING finger

PCL: Polycomb-like proteins

PGC-1α: Peroxisome proliferator-activated receptor gamma coactivator-1α

PHC: Polyhomeotic subunit

PITCh: Precise Integration into target chromosome

PKA: Protein kinase A

PKC: Protein kinase C

PKG: Protein kinase G

PRC: Polycomb repressive complex

PSCs: Pluripotent stem cells

PTEN: Phosphatase and tensin homolog

PuroR: Puromycin resistant gene

Raptor: Regulatory associated protein of mTOR

RBBP4/7: Retinoblastoma Binding Protein 4/7

REDD1: Regulated in development and DNA damage response 1

REX1: C2H2 zinc-finger transcription factor

Rictor: Rapamycin-insensitive companion of mTOR

RING1A: RING finger protein 1A

RING1B: RING finger protein 1B

RYBP: YY1-binding protein

S6K: S6 kinase

SGK1: Serum- and glucocorticoid-inducible kinase 1

SMAD: Mothers Against Decapentaplegic protein

SOX2: SRY-box transcription factor 2

SREBP: Sterol-responsive element-binding protein

STAT3: Signal transducer and activator of transcription 3

SUZ12: Suppressor of Zeste 12 Homolog

TBC1D7: TBC1 domain family, member 7

TE: Trophectoderm,

Tfcp2l1: Transcription factor CP2-like 1

TFEB: transcription factor EB

TFs: Transcription factors

TNFα: Tumour necrosis factor alpha

TSC1: Tuberous sclerosis complex 1

TSC2: Tuberous sclerosis complex 2

TSS: Transcription start site

TT-seq: Transient transcriptome sequencing

ULK1: Unc-51-like kinase 1

vPRC1: variant PRC1

VRK1: VRK serine/threonine kinase 1

WNT: Wingless/Integrated

YAF2: YY1 Associated Factor 2

YY1: Yin Yang 1